Zur Erlangung des akademischen Grades Master of Science Global Change Geography
Influence of snowpack characteristics on winter soil temperatures (Qeqertarsuaq, Kalaallit Nunaat)
eingereicht von: Sofia Rosa Bauriedl
Gutachterinnen: Pr. Dr. Julia Boike Dr. Simone Maria Stuenzi
Eingereicht am Geographischen Institut der Humboldt-Universität zu Berlin am: $07.08.2025$

Masterarbeit

Master Thesis

Influence of snowpack characteristics on winter soil temperatures (Qeqertarsuaq, Kalaallit Nunaat)

Sofia Rosa Bauriedl

Supervisors:
Prof. Dr. Julia Boike
Dr. Simone Maria Stuenzi

Submitted to the Department of Geography, Humboldt-Universität zu Berlin

Berlin, August 7, 2025

Abstract

Seasonal snow cover plays a critical role in regulating Arctic soil temperatures, particularly in permafrost landscapes. Its insulating properties depend not only on snow depth but also on snow density and stratigraphy. However, these characteristics remain poorly understood in Arctic environments due to limited availability of high-resolution measurements. This thesis investigates how spatial variability in snow depth and snow density influences soil temperatures (6 cm) during late winter in a Low Arctic maritime tundra landscape on Qeqertarsuaq (Disko Island), Kalaallit Nunaat (Greenland). The study combines high-resolution snowpack data collected with the SnowMicroPen (SMP) in April 2024 with hourly soil temperature records from 14 temperature sensors.

Snow depths at the sensor locations ranged from $0.16\,\mathrm{m}$ to $1.10\,\mathrm{m}$ (mean: $0.56\,\mathrm{m}$), while snowpack densities varied between $247\,\mathrm{kg}\,\mathrm{m}^{-3}$ and $409\,\mathrm{kg}\,\mathrm{m}^{-3}$. Average soil temperatures from October 2023 to June 2024 spanned from $-4.67\,\mathrm{^{\circ}C}$ to $-0.23\,\mathrm{^{\circ}C}$ across the site.

To capture the relationship between snow cover characteristics and soil temperatures, and to assess spatial variability and uncertainty, I used Bayesian hierarchical modeling. The results show that snow depths greater than approximately 0.5 m effectively insulate the soil by dampening the impact of air temperature fluctuations, reinforcing the snowpack's role as a thermal buffer. I also observed a positive, though more uncertain, relationship between snow density and soil temperature, suggesting that denser snow may reduce insulating capacity. These findings indicate that snow density plays an important role in Arctic ground thermal regimes, but additional high-resolution observations and further model development are needed to better quantify its effects.

Contents

1	Intr	oducti	ion	1
2	Stu	dy area	a	3
3	Met	thodol	$\log \mathbf{y}$	5
	3.1	Data s	sets	5
	3.2	Chara	cterization of winter snowpack	6
	3.3	Cross	site comparison	7
	3.4	Statist	tical analysis	7
		3.4.1	Model parameters	7
		3.4.2	Bayesian linear regression models	8
		3.4.3	Bayesian hierarchical models	9
		3.4.4	Model comparison	11
4	Res	${ m ults}$		12
	4.1	Winter	r conditions	12
	4.2	Spatia	l variability	13
		4.2.1	Snow depth	13
		4.2.2	Snow density	13
		4.2.3	TMS temperatures	14
	4.3	Model	results	16
		4.3.1	Linear regression on snow depth	17
		4.3.2	Linear regression on relative snow density	
		4.3.3	Linear regression on snow temperature	
		4.3.4	Air-Soil Temperature model	19
		4.3.5	Snow-Soil Temperature model	
		4.3.6	Sensitivity analysis	23
5	Disc	cussion	1	24
	5.1	Spatia	l variability of snow characteristics and soil temperatures	24
	5.2	Model	outputs	26
		5.2.1	Modeling snow depth	26
		5.2.2	Modeling snow density	
		5.2.3	Influence of snow depth on temperature	
		5.2.4	Influence of relative density on temperature	
		5.2.5	Temperature propagation	
	5.3	Model	strengths, limitations, and opportunities for advancement	
6	Con	clusio	\mathbf{n}	32
A	cknov	wledge	ement	33
K	efere	nces		34

\mathbf{A}		ended methodology	42
	A.1	Data sets	42
		A.1.1 Snow measurements	42
		A.1.2 Temperature measurements	47
		A.1.3 Topography	47
		A.1.4 Vegetation	48
	A.2	Statistical analysis	51
В	Ext	ended results	54
	B.1	Winter conditions	54
	B.2	Spatial variability	56
	B.3	Bayesian linear regression models	59
	B.4	Bayesian hierarchical models	65

List of Figures

1	Location and dimensions of the study area	4
2	Assigning SMP profiles to TMS	6
3	Hierarchical model schemes	11
4	Winter conditions	13
5	Spatial variability of snow depth and snow density	14
6	Temperature time series per TMS	15
7	Averages TMS temperatures	16
8	LOO-CV model comparison	22
A.1	SMP derivative selection	14
A.2	Density deviations of SMP force signal	15
A.3	Snow depth comparison	16
A.4	Digital terrain model with TMS locations	18
A.5	Photos of vegetation at TMS (1)	19
A.6	Photos of vegetation at TMS (2)	50
A.7	Winter air temperature	54
A.8	Wind direction	55
A.9	Posterior predictive distributions for linear regression on snow depth 6	30
A.10	Posterior predictive distributions for linear regression on snow density 6	32
A.11	Posterior predictive distributions for linear regression on snow temperature 6	34
A.12	Posterior predictive distributions of Air-Soil Temperature model 6	66
A.13	Posterior predictive distributions of Snow-Soil Temperature model 6	38

List of Tables

1	Model parameters	8
A.1	Sensors used for field measurements	42
A.2	SMP derivatives statistics	44
A.3	Summary statistics of snow density deviations	46
A.4	Linear regression formulas and prior specifications	52
A.5	Air-Soil Temperature model formulas and prior specifications	53
A.6	Snow-Soil Temperature model formulas and prior specifications	53
A.7	SMP snow depth and density measurements across sampling locations $\ . \ .$.	56
A.8	Soil temperature and snow properties for each TMS	58
A.9	Posterior summary statistics for linear regressions on snow depth \dots	59
A.10	Posterior summary statistics for linear regressions on snow density	61
A.11	Posterior summary statistics for linear regressions on snow temperature $$. $$	63
A.12	Posterior summary statistics for Air-Soil Temperature model	65
A.13	Posterior summary statistics for Snow-Soil Temperature model	67

1 Introduction

Seasonal snow covers large parts of the Arctic for six to ten months of the year, reaching a maximum extent of approximately $47 \times 10^6 \,\mathrm{km^2}$ in the Northern Hemisphere between December and February (Estilow et al. 2015). However, long-term satellite records show a decline in arctic snow cover mass, with an average reduction of $-1.4\,\%$ per decade (Mudryk et al. 2022; Peng et al. 2024). This decline is primarily driven by anthropogenic climate warming. This warming also leads to more frequent and intense rain-on-snow events and mid-winter melt, which alter the physical structure and thermal behavior of snowpacks (Rantanen et al. 2022; Tan et al. 2022; Du et al. 2025).

The seasonal snowpack plays a crucial role in regulating the Arctic soil thermal regime. In autumn, the thin, fresh snow cover usually has a cooling effect because it reflects up to 90% of the incoming shortwave solar radiation (Pomeroy and Brun 2011). The proportion of reflected shortwave radiation is called albedo. As the snow ages, the surface albedo can drop as low as 50% (Pomeroy and Brun 2011). During winter, increasing snow depth and falling air temperatures cause snow to act as an insulating layer, slowing the transfer of heat from the relatively warmer soil to the colder atmosphere. This insulating effect is due to high air content and low thermal conductivity of snow (Pomeroy and Brun 2011; Huang et al. 2017; Pertermann 2017). Understanding the thermal behavior of snow and the properties that influence it is crucial for predicting subsurface temperatures in Arctic environments, which affect processes such as soil microbial activity, nutrient cycling, and permafrost dynamics.

Thermal conductivity is the key factor controlling snow's insulating capacity, as it governs the rate at which heat is transferred through the snowpack. Because of this relationship, snow with lower thermal conductivity insulates the ground more effectively. Thermal conductivity is primarily influenced by snow density, followed by temperature, microstructure (including grain size and bonding), moisture content, and anisotropy. Since direct field measurements of thermal conductivity are difficult, snow density is widely used as a practical and accessible proxy (Pertermann 2017; Macfarlane et al. 2023).

The relationship between density and thermal conductivity is non-linear (Macfarlane et al. 2023). Dry fresh snow and depth hoar (large, faceted crystals that typically form near the ground under strong temperature gradients) can have a density of less than $100\,\mathrm{kg}\,\mathrm{m}^{-3}$ with a thermal conductivity between $0.03\,\mathrm{W}\,\mathrm{m}^{-1}\,\mathrm{K}^{-1}$ to $0.11\,\mathrm{W}\,\mathrm{m}^{-1}\,\mathrm{K}^{-1}$ (Sturm and Johnson 1992), whereas melting snow and wind slab (dense, hard layers formed by wind compaction) can have a density above $600\,\mathrm{kg}\,\mathrm{m}^{-3}$ resulting in a thermal conductivity of $0.14\,\mathrm{W}\,\mathrm{m}^{-1}\,\mathrm{K}^{-1}$ to $0.35\,\mathrm{W}\,\mathrm{m}^{-1}\,\mathrm{K}^{-1}$ (Sturm and Johnson 1992; Pomeroy and Brun 2011; Pertermann 2017).

Variations in snow density within Arctic snowpacks arise from a combination of accumulation, transformation, and redistribution processes throughout the winter. For instance, snow deposition under cold conditions leads to low-density snow, while wind compaction and refreezing after melt events create denser, more cohesive layers (Meløysund et al. 2007; Lawrence and Slater 2010). Additionally, vertical temperature gradients within the snowpack drive metamorphic processes, which cause changes in the size, shape, and bonding of snow grains (Pomeroy and Brun 2011). Strong temperature gradients (1 °C cm⁻¹) favor the formation of depth hoar through constructive metamorphism, while weaker gradients promote destructive metamorphism and increased snow density (Bormann et al. 2013). As a result, Arctic snowpacks typically display a distinct stratification,

with dense, wind-compacted layers near the surface overlaying lower-density depth hoar (Larose et al. 2013). The complex vertical and horizontal structure of the snowpack plays a key role in determining its thermal properties (Schweizer et al. 2008; Pomeroy and Brun 2011; Bormann et al. 2013).

However, while the influence of snow depth on soil temperature is well established (Overduin et al. 2007; Krab et al. 2022; Pongracz et al. 2024; Grünberg et al. 2025), with deeper snow typically leading to warmer winter soils because of its stronger insulating effect, much less is known about the role of snow density. Snow density remains difficult to simulate accurately in physical snow models (Domine et al. 2021). Most multilayer snow-pack models, such as Crocus (Vionnet et al. 2012) and SNOWPACK (Bartelt and Lehning 2002), were developed for mid-latitude conditions and avalanche forecasting. These models often perform poorly in the Arctic, where dominant processes like wind redistribution and vapor flux are not well represented (Peng et al. 2024; Woolley et al. 2024). Consequently, model outputs frequently simulate vertical snow density profiles inverse to actual observations (Peng et al. 2024; Woolley et al. 2024). Although these models estimate snow depth reasonably, inaccuracies in simulating snow layering and thermal conductivity introduce errors in soil temperature predictions (Wever et al. 2023).

To address these shortcomings, this study adopts an alternative approach by applying a hierarchical Bayesian modeling framework to estimate how snow properties relate to soil temperatures. Statistical models offer several advantages in this context as they are flexible, data-driven, and capable of incorporating empirical snow measurements without relying on assumptions about the physical processes that govern snow evolution (Webb et al. 2010; Kruschke 2021).

Building on this framework, I apply Bayesian hierarchical modeling to snow profile and soil temperature data collected during a field campaign in April 2024 on Qeqertarsuaq (Disko Island), Kalaallit Nunaat (Greenland). The overarching research question guiding this study is: How does spatial variability in snow cover characteristics, particularly snow density, influence near-surface soil temperatures in a maritime permafrost setting? To address this, the analysis pursues three main objectives: First, I assess whether the snow profiles measured in April are representative of late-winter snowpack conditions. Second, I investigate the spatial variability of snow properties and near-surface soil temperatures across the study area. Third, I aim to quantify the relationship between snow density and soil temperatures during the late winter season.

2 Study area

The study area is located in the valley Kuup Ilua (Blæsedalen valley, $(69^{\circ}16'\text{N}, 53^{\circ}27'\text{W})$), on the southern-tip of Qeqertarsuaq, Kalaallit Nunaat (Figure 1). The glacially carved U-shaped valley lies within the zone of discontinuous permafrost and features a typical low-arctic climate with maritime influence. The research station *Arctic Station* just outside of Qeqertarsuaq operates multiple Automated Weather Stations (AWS), with records dating back to 1991. Between 1991 and 2018 the mean annual air temperature was $-2.8\,^{\circ}\text{C}$. The monthly mean air temperatures were highest in July $(7.9\,^{\circ}\text{C})$ and lowest in March $(-14.0\,^{\circ}\text{C})$ (Blok et al. 2016).

Annual precipitation averages $418 \,\mathrm{mm}$ (Zhang et al. 2019). Most precipitation (approximately $75\,\%$) occurs between June and December, driven by moist air masses advected from the south and southwest along the Davis Strait. The winter months are comparatively dry, dominated by cold, continental air masses descending from the Greenland Ice Sheet. Between $60\,\%$ to $70\,\%$ of the annual precipitation typically falls as snow, supporting the development of a continuous snowpack from late September through late May / June (Humlum 1998).

The soils in this valley originate from early Tertiary volcanic basalt and have weakly developed soil horizons due to limited weathering and pedogenesis over the past 10,000 years, following deglaciation. The soil is classified as Haplic Cryosol (Liu et al. 2023). The surface organic horizon is slightly acidic (5 pH to 6 pH), extends down to 0.25 m in depth, and contains 5 % to 15 % organic carbon, mostly derived from mosses, lichens, and dwarf shrub litter. Beneath this layer, the soil consists of coarse sediments, predominantly sand and gravel, with little organic matter and pH levels close to neutral. The mean annual soil temperature at a depth of 5 cm is 1.9 °C (Nielsen et al. 2017; Zhang et al. 2019). Frozen soil conditions last from October to May (Xu et al. 2021). The maximum active layer thickness depends on drainage conditions, and varies from 0.4 m in wet depressions up to 3 m on well-drained slopes (Rasmussen et al. 2022).

Located in Bio-climatic sub-zone D of the Arctic, vegetation cover is relatively high in comparison to other Arctic sub-zones. In the valley and on the slopes vegetation is dense and covers between 80% to 100% of the ground. On the flat mountaintops vegetation patches cover 5% to 50% of the ground (Hollesen et al. 2015; von Oppen et al. 2022). Vegetation diversity is relatively high as well. Deciduous dwarf shrubs (Betula nana, Salix glauca, and Vaccinium uliginosum), evergreen shrubs (Empetrum nigrum and Cassiope tetragona), and various mosses and lichens form the dominant well-drained mesic tundra heath ecosystem (Nielsen et al. 2017). Annual nitrogen deposition is low at $1 \text{ kg ha}^{-1} \text{ yr}^{-1}$, while the fixation of nitrogen supplies the ecosystem with between $1 \text{ kg ha}^{-1} \text{ yr}^{-1}$ to $2 \text{ kg ha}^{-1} \text{ yr}^{-1}$, with little (less than 10%) inter annual variation (Rasmussen et al. 2022).

Long-term data from the weather station near the Arctic Station (AWS1) reveal an annual increase in air temperature of 0.13 °C per year between 1991 and 2017. The highest increase in monthly air temperatures occurs from December to March, with strongest warming of 0.31 °C in February. In comparison to the period from 1991 to 2008, precipitation decreased by 25 % from 2008 to 2017, leading to shallow snow depths (Zhang et al. 2019). Additionally, warmer air temperatures have led to earlier snow melt that allows the soils to drain and warm more quickly (Hollesen et al. 2015). Zhang et al. (2019) recorded an increasing number of days with minimum soil temperatures above 0 °C (1991 to 2017)

which leads to a lengthening of the growing period. Consequently, the species composition is shifting as more shrubs are established, contributing to the widespread observed greening of the Arctic (Callaghan et al. 2011; Hollesen et al. 2015).

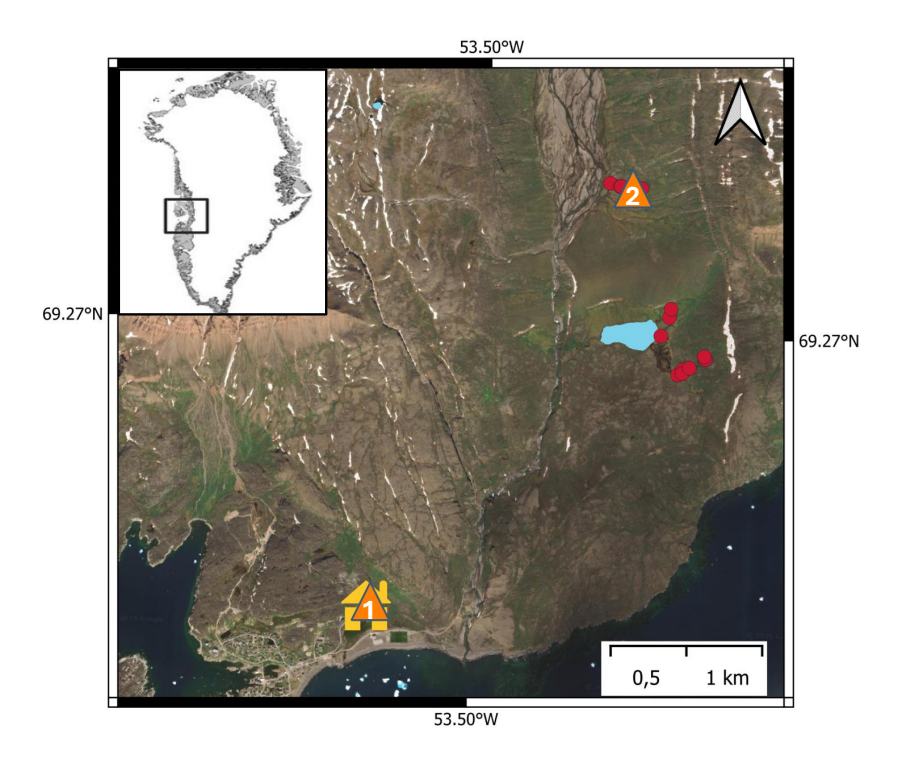


Figure 1: Overview of the study area and its location in the West of Kalaallit Nunaat. Arctic Station (house), automated weather stations (AWS1 and AWS2) (orange triangles) and Temperature-Moisture-Sensors (TMS) (red points) are highlighted. Hydrological features: von Oppen et al. (2022). Basemap: Google satellite.

3 Methodology

The following section outlines the methodological approach of my study. It describes the datasets, the assessment of snow cover conditions during winter 2023/24, the evaluation of spatial variability across the study area, and the modeling framework used to quantify the relationship between snowcover and soil temperature. Detailed information on data collection, processing steps, and sensor setup can be found in Appendix A.

3.1 Data sets

My datasets consisted of temperature and snow measurements, conducted during several field trips between 2022 and 2024, as part of the MOMENT project (Permafrost Research Towards Integrated Observation and Modeling of the Methane Budget of Ecosystems). The fieldwork involved vegetation and soil surveys, the installation of automated temperature sensors during the summers of 2022 and 2023, and snow measurements in April 2024 (Boike et al. 2024; Steffens et al. 2025).

For my analysis, I focused on the winter season of 2023/24, utilizing temperature data recorded at 15-minute intervals from 14 TOMST TMS-4 Temperature-Moisture Sensors (TMS). Each sensor measured temperatures at three distinct depths: 16 cm above the ground surface (representing snow temperature), directly at the ground surface (surface temperature), and 6 cm below the ground surface (soil temperature). After ice bath calibration, the sensors reached an accuracy of 0.3 °C (Appendix A.1.2).

To link snow properties with temperature conditions, I assigned snow profiles to each TMS based on data collected in April 2024. Snow density and depth profiles were measured using the SnowMicroPen (SMP), a high-resolution, portable penetrometer developed by Schneebeli et al. (1999). The SMP records the force required to penetrate the snowpack at high vertical resolution, with a force sensor resolution of 0.01 N and an estimated depth accuracy of 1 cm. From the force signal, I derived snow density profiles (Appendix A.1.1).

The SMP is limited to a maximum rod length of 1.20 m, which prevented measurement of deeper snowpacks. To account for this limitation, I used snow depth data from the MagnaProbe, a manual depth probe equipped with a GPS and digital depth sensor, collected at the same locations and on the same day. I matched MagnaProbe measurements to the closest SMP profiles to validate and complement depth estimates (Figure A.3). MagnaProbe readings confirmed that snow depths exceeded 2 m in some locations, beyond the reach of the SMP.

I then spatially matched the snow profiles to the TMS using drone orthophotos taken on the $10^{\rm th}$ and $11^{\rm th}$ of September 2023. For each sensor, I selected between two and twelve snow profiles (61 in total), based on proximity and similarity in surface characteristics (Figure 2, Table A.7). The distances between TMS and their assigned snow profiles ranged from $0.6\,\mathrm{m}$ to $43.8\,\mathrm{m}$, while the distances between the TMS themselves ranged from $7.5\,\mathrm{m}$ to $1337.5\,\mathrm{m}$.

In order to contextualize the field data, I used air temperature, precipitation and wind observations from an automated weather station (AWS2) at the study site, as well as long-term air temperature records from an automated weather station (AWS1) at the *Arctic Station* operated by the Greenland Ecosystem Monitoring Program (Greenland Ecosystem Monitoring 2020). Air temperature at AWS1 was measured at 9.5 m. At AWS2 air temperature was measured at 2.2 m and precipitation at 0.8 m with a precipitation

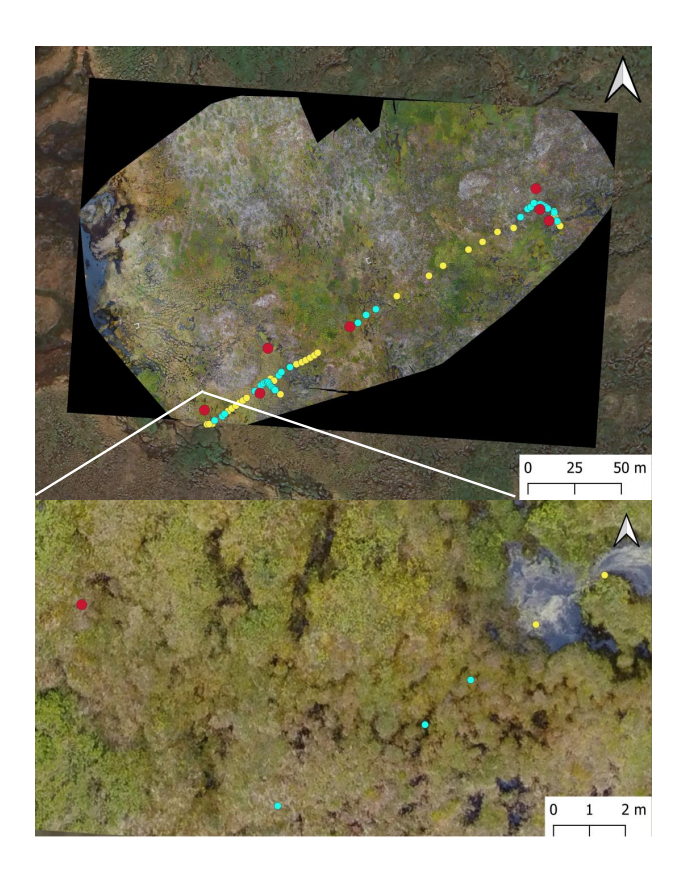


Figure 2: Assignment of SMP Profiles to TMS. An overview of the assignment process, showing TMS (red) and associated SMP profiles (blue) based on proximity and surface characteristics. Yellow points represent SMP profiles excluded from the analysis. The upper panel provides a broader view of several TMS, while the lower panel zooms in on TMS H and its corresponding SMP profiles.

gauge (Table A.1).

My analysis was further supported with topographic data derived from a high-resolution digital terrain model (DTM) provided by the Satellite-Based Crisis and Situation Service of the German Federal Agency for Cartography and Geodesy (BKG-SKD). From this DTM, I extracted elevation, slope, and aspect values for each TMS location. For previous analysis the DTM was also used by Becker (2024) to derive geomorphon types, following the method by Jasiewicz and Stepinski (2013), which classified terrain into distinct landform elements called geomorphons. Based on TMS locations, my data included the geomorphon types hollow/footslope, slope, and valley/depression (Appendix A.1.3).

To characterize vegetation around each TMS, I used an adjusted version of the Circumpolar Land Cover Map by Bartsch et al. (2024), modified by Gottuk et al. (2025), which classified the sites into three vegetation types: dry tundra, moist tundra, and wet tundra (Appendix A.1.4).

3.2 Characterization of winter snowpack

To evaluate the representativeness of the April 2024 SMP profiles for the full winter snow-pack, I analyzed the seasonal snow evolution for the snow covered season prior to April 2024 using AWS2 records. I examined hourly air temperatures, snow depths, rainfall

events, and wind conditions to determine the timing of snow accumulation and potential melt events. In particular, I identified thawing degree days, where air temperatures exceeded 0 °C, and corresponding rainfall events that could have influenced the formation of ice lenses or snow metamorphism.

3.3 Cross site comparison

I assessed the spatial variability of snow cover and temperature across the study area by linking multiple depth and density SMP profiles to each TMS (Table A.8). I computed the average snow depth and density for each sensor and calculated their local standard deviations in order to quantify small-scale heterogeneity (Figure 5). Additionally, I summarized the TMS temperature data over the winter season to identify spatial and temporal differences in the thermal regimes of the snow, surface, and soil (Figure 6 and 7). This cross-site comparison enabled an initial evaluation of the relationships between snowpack characteristics and soil temperatures at each location.

3.4 Statistical analysis

To investigate the relationship between snowpack properties and temperature conditions, I applied Bayesian hierarchical modeling. This approach is better suited than traditional frequentist methods because it handles unbalanced and sparse data more effectively, which is essential given the uneven number of observations across locations. Frequentist models typically struggle with partial pooling and often treat groups independently, leading to overfitting or unstable estimates when sample sizes are small (Webb et al. 2010). In contrast, the Bayesian framework allows for sharing information across groups, incorporation of prior knowledge, so called priors, and full uncertainty quantification through posterior distributions. Its hierarchical structure also captures both overall trends and site-level variability (Vehtari et al. 2017; Kruschke 2021).

The models were developed following the Bayesian workflow described by Gelman et al. (2020), which involves model building, inference, checking, and comparison. I implemented the models in Python (Version 3.13.2) (Python Software Foundation 2023) using the open-source libraries PyMC (version 5.22.0) (Patil et al. 2023) and Bambi (version 0.15.0) (Capretto et al. 2022) (Appendix A.2).

3.4.1 Model parameters

Before I set up my models, I scaled the predictor variables used in the analysis (Table 1). First, I converted the snow depth from centimeters to meters. To create a dimensionless variable, I then divided the snow density (in kg m⁻³) by the density of liquid water at 0 °C (1000 kg m⁻³). This transformation yields a relative density that expresses snow density as a fraction of water density, roughly corresponding to the snow's volumetric ice content. For a more detailed analysis, I split the relative density into bottom relative density, referring to the bottom 16 cm of the snowpack below the snow temperature sensor, and top relative density, representing the relative density of the snow above the temperature sensor. My temperature variables comprise daily mean values from April 10th 2024 where air temperature was measured at the AWS2 station, while snow, surface, and soil temperatures were obtained from each TMS. Regarding topography, I divided the slope values in degrees

by 10, converted the elevation from meters to kilometers, and decomposed the aspect into sine and cosine components.

Table 1: Overview of the variables used in the models, including their units, sample size, and value ranges. Snow depth and density were measured using the SnowMicroPen (SMP). Density refers to the mean density over the entire profile. Bottom density was calculated for the bottom 16 cm of the snowpack beneath the snow temperature sensor, while top density represents the density of the snowpack above the sensor. Temperature data (snow (16 cm above the surface), surface, and soil (in 6 cm depth)) were collected using temperature-moisture sensors (TMS). Air temperature was recorded by AWS2, an automated weather station equipped with various sensors, including air temperature and snow depth sensors. Topographic variables (elevation, aspect, and slope) were extracted from a digital elevation model (DEM). Additionally, geomorphon classes were derived from the DEM to represent landscape form. Vegetation classes are based on the classification from Bartsch et al. (2024), modified by Gottuk et al. (2025) to reflect local conditions.

Variable	Unit	N	Min	Mean	Max	Instrument
Snow variables						
Depth	m	61	0.16	0.57	1.10	SMP
Density	${\rm kg/m^3}$	61	247	297	409	SMP
Bottom density	${\rm kg/m^3}$	61	257	313	402	SMP
Top density	${\rm kg/m^3}$	61	51	286	411	SMP
Temperature variables						
Air temperature	$^{\circ}\mathrm{C}$	1	-10.3	-7.1	-3.1	AWS2
Snow temperature	$^{\circ}\mathrm{C}$	14	-5.2	-4.0	-0.6	TMS
Surface temperature	$^{\circ}\mathrm{C}$	14	-5.8	-3.6	-0.3	TMS
Soil temperature	$^{\circ}\mathrm{C}$	14	-5.9	-3.6	-0.6	TMS
Topographic variables						
Elevation	m a.s.l.	14	83.8	95.2	110.7	DEM
Aspect	degrees	14	4	213	321	DEM
Slope	degrees	14	0	5	20	DEM
Vegetation class	categorical	3	_	_	_	Gottuk et al. (2025)
Geomorphon class	categorical	3	_	_	_	derived from DEM

3.4.2 Bayesian linear regression models

As part of a Bayesian modeling workflow, I developed a series of regression models of increasing complexity to explore how topography, vegetation, and geomorphology influence snow depth, relative snow density, and snow temperature. The initial modeling stage used the Python library Bambi to construct and compare simple Bayesian regression models, which helped identify relevant predictors and informed the structure of more complex hierarchical models implemented in the second stage.

To assess the role of terrain, I included elevation, slope, and aspect as fixed effects in the models. In addition, I evaluated whether grouping observations by vegetation type or geomorphon class improved model performance by capturing additional variance in the response variables. Accordingly, I fitted three versions of all models: a pooled model (no grouping), a vegetation-group model, and a geomorphon-group model. The group models allowed for partial pooling using varying intercepts to account for group-level variation (Table A.4), enabling the models to borrow strength across categories while capturing local differences (Gelman et al. 2013).

I selected weakly informative priors based on prior predictive checks, which ensured that the priors produced plausible values within the range of the observed data. These checks helped me calibrate the priors to avoid extreme or unrealistic predictions while remaining agnostic about precise parameter values. Table A.4 provides the full list of priors.

I fit all models using the No-U-Turn Sampler (NUTS) (Hoffman and Gelman 2011), running each chain with 2000 warm-up steps. The sampler automatically discarded these warm-up iterations before drawing samples from the posterior.

Linear regression on snow depth

To investigate the influence of topographic and categorical predictors on snow depth, I fitted a Bayesian Gamma regression model with a log link function. I chose the Gamma likelihood, since snow depth is a positive, continuous variable with a skewed distribution. The log link ensured that predictions remained positive and allowed for multiplicative relationships between predictors and the response.

Linear regression on relative snow density

To model relative snow density I used a Beta regression with a logit link. This approach is well suited for continuous, bounded outcomes. The logit link function converts values between 0 and 1 into an unbounded scale, enabling additive effects of predictors. All three models included a precision parameter kappa (κ), controlling the dispersion of the Beta distribution, allowing the models to adjust the width of the predicted relative density interval.

Linear regression on snow temperature

To model snow temperature, I used Gaussian regression with an identity link function, which is suitable for unbounded continuous variables such as temperature (in °C).

I chose the priors on the regression intercept and standard deviation based on observed air temperatures and prior predictive checks. A sensitivity analysis compared the original pooled model with domain-informed priors to a version using wide reference priors (Normal($\mu = 0, \sigma = 100$)). This comparison evaluated the influence of prior assumptions on posterior inferences.

3.4.3 Bayesian hierarchical models

In the second stage, I used the information distilled from the first stage to construct hierarchical models in PyMC. As previously, each model was configured in three different versions, one pooled, one grouped by vegetation, and one grouped by geomorphons.

Air-Soil Temperature model

The first model was a three-level hierarchical Bayesian model (Air-Soil Temperature model) (Figure 3). It estimated snow, surface and soil temperatures at the TMS on a single day (Table A.5). The model included linear effects between adjacent layers, so that temperatures at deeper levels depend on those above. All temperatures were constrained below 0°C using truncated normal distributions to reflect the physical limits. The first level of the model predicted snow temperatures from air temperature, slope, aspect, snow depth and relative snow density. Since the snow temperature sensor was installed 16 cm above the ground, I subtracted 16 cm from the total snow depth and averaged relative density above the sensor. The second level used the snow temperatures from level 1 and the bottom layer relative density (between the snow and the surface temperature sensor) to predict surface temperature (level 2). This surface temperature was then used as a linear predictor for soil temperatures on the third level.

To assess the influence of prior assumptions on model behavior, I performed a sensitivity analysis on the pooled model, comparing the initial version with a second version that used reference priors (Normal(mu = 0, $\sigma = 100$)).

Snow-Soil Temperature model

The second hierarchical model (Snow-Soil Temperature Model) omitted topographic predictors and treated snow temperature as a known input. This model directly estimated surface and soil temperatures from snow temperature and bottom-layer relative density (Table A.6).

To fit the hierarchical models, I utilized the NUTS approach again, running four chains with 1,000 tuning steps and 1,000 posterior draws per chain. I increased the target acceptance rate to 0.95 to ensure stable and efficient sampling.

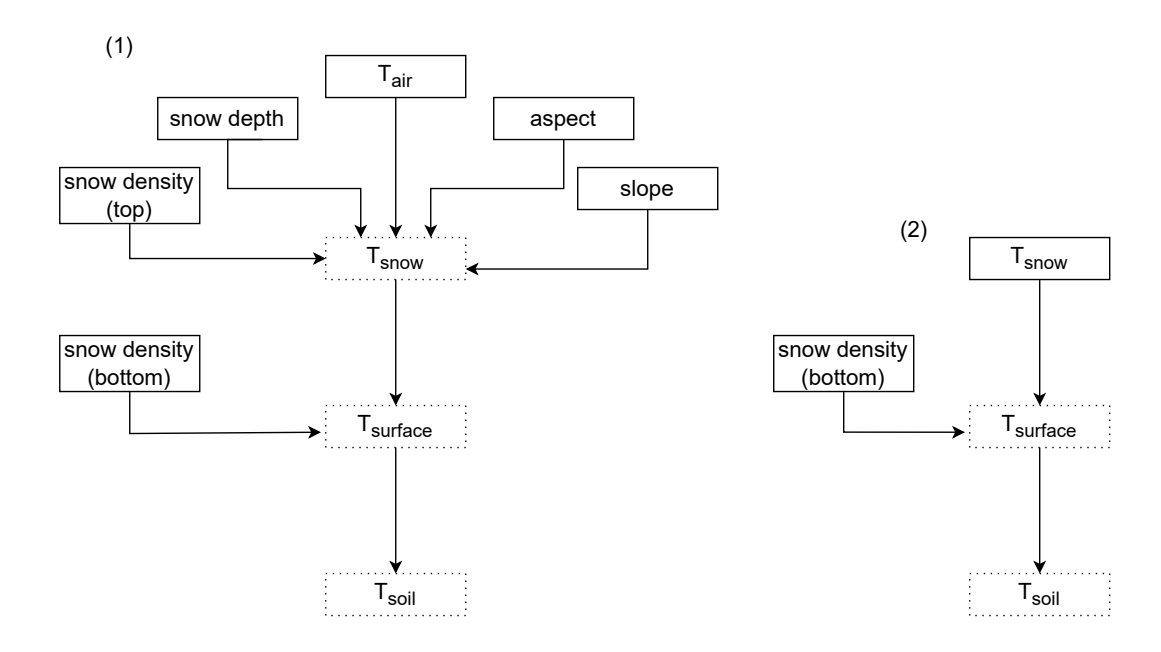


Figure 3: Model schemes of hierarchical models for soil temperature. Arrows indicate linear effects. Solid-line boxes represent observed input variables, while dashed-line boxes represent modeled variables. Model (1) corresponds to the Air-Soil Temperature model, Model (2) corresponds to the Snow-Soil Temperature model.

3.4.4 Model comparison

To compare the models and assess the importance of grouping, I used the Leave-one-out cross-validation (LOO) method to evaluate each model's predictive performance. LOO estimates the model's out-of-sample prediction accuracy by removing one observation at a time and computing its log-likelihood based on the remaining data. I used Pareto-smoothed importance sampling, as implemented in the ArviZ Python package, and reported the expected log pointwise predictive relative density (ELPD) and the effective number of parameters p_{loo} for each model. Higher ELPD corresponds to better predictive fit, while p_{loo} provides an estimate of model complexity, with higher values indicating greater flexibility but also a higher risk of overfitting if not accompanied by improved predictive performance. While other information criteria exist, such as the widely applicable or Watanabe-Akaike information criterion, I selected the LOO criterion because it is more robust for small datasets, weak priors, or when some observations have a high influence (Vehtari et al. 2017). In addition, I consulted the Pareto k diagnostics to assess the reliability of the estimates, with values below 0.7 being considered trustworthy.

4 Results

In the following sections, I present the winter climate conditions, the spatial variability of snow properties and snow temperature, and the findings from the statistical analyses. Decimal precision in the reported values reflects either the measurement accuracy of the respective sensors (Table A.1) or the limited relevance of finer detail for interpreting specific variables.

4.1 Winter conditions

I chose my study period to align with the snow cover duration of the winter 2023/24 season, measured at the AWS2, which spanned from October 1st, 2023, marked by the first snowfall, to June 20^{th} , 2024, when the snow cover had completely melted (Figure 4). During this interval, the mean daily air temperature measured at 2 m at AWS2 was $-6.7\,^{\circ}$ C, ranging from a minimum of $-25.5\,^{\circ}$ C to a maximum of $9.8\,^{\circ}$ C. During the long-term period from 1991 to 2018, the average air temperature from October to June measured at AWS1 was slightly warmer at $-6.5\,^{\circ}$ C, with March typically being the coldest month with a mean temperature of $-13.3\,^{\circ}$ C. Compared to this historical record, the winter of 2023/24 exhibited slightly warmer monthly mean temperatures in November, March, and April, and below-average values in the other months (October, December, January, February, May, June), but all remained within one standard deviation of the historical variability (Figure A.7).

During this period (October to June), winds at AWS2 predominantly originated from the north to northeast sector. Most recorded wind speeds ranged between $0.1\,\mathrm{m\,s^{-1}}$ and $4.8\,\mathrm{m\,s^{-1}}$, with fewer observations in the higher wind speed classes above $6.3\,\mathrm{m\,s^{-1}}$ (Figure A.8).

Snow accumulation recorded at AWS2 showed an average depth of 0.32 m between October and June with a maximum snow depth of 0.53 m by mid-February, which was followed by a dry period.

Between October and April, 178 days had daily average temperatures below 0 °C, while only 17 days experienced thawing conditions, two of which (March 24^{th} and 25^{th}) took place about two weeks before the snow profile measurements. On each thawing day, precipitation – either rain or the melting of old snow in the rain gauge – was recorded by the AWS2, which could both have led to the formation of ice lenses in the snowpack. Despite these thawing events, major snow melt had not begun by April, and snowpack temperatures remained relatively stable, ranging between -5 °C and -10 °C.

Given these conditions, the April snow profiles were a reliable representation of the winter snow cover, reflecting advanced metamorphism, with most layers well developed and little fresh snow remaining untransformed. Furthermore, the spatial distribution of the SMP profiles across varying aspects, elevations, and vegetation types supported their representativeness of the broader winter snow conditions. Nonetheless, considerable local variability existed in snowpack structure and thermal dynamics, which will be detailed in the following section.

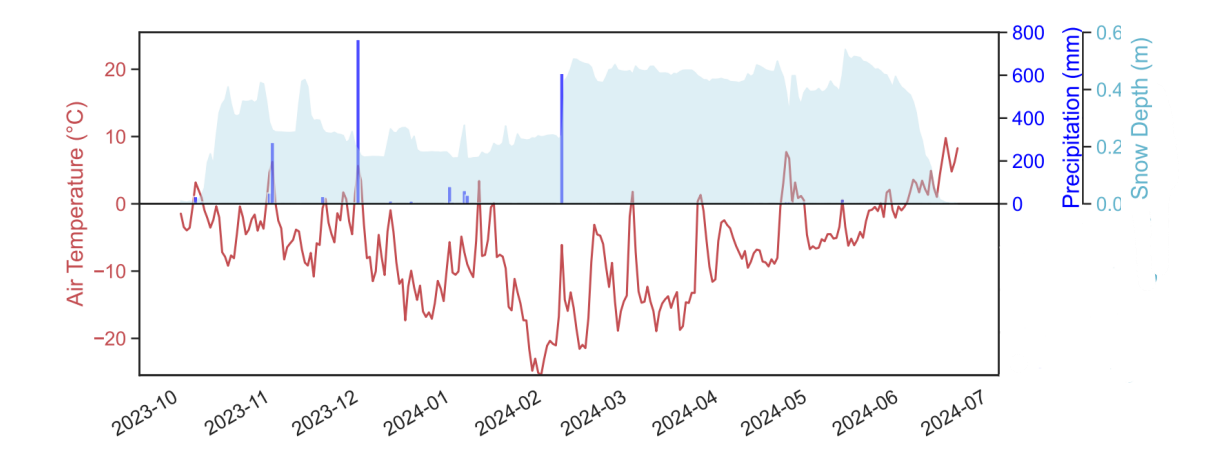


Figure 4: Winter conditions 2023/2024. Air temperature at 2m, snow cover, and precipitation during the winter of 2023/2024, measured at AWS2.

4.2 Spatial variability

The spatial variability of the snow cover across the study area was evident not only in the structural properties of the snowpack but also in the duration of the snow cover. I observed pronounced differences between sites regarding the timing of snowmelt. At four of the 14 locations (sensors A, B, C, and I), the snow cover lasted until June 2024, similar to the AWS2 site. In contrast, the remaining sites showed earlier melt, with consistently positive snow sensor temperatures by the end of April, indicating snow-free conditions. One site in particular (sensor E) recorded only a shallow snowpack which had already disappeared by early March.

4.2.1 Snow depth

The snow depths of the 61 SMP profiles ranged from 0.16 m to 1.10 m (Table A.7). However, MagnaProbe measurements across the site indicate that snow depths exceeded 2 m in some areas. These deeper snowpacks could not be captured by the SMP, as it is limited to a maximum rod length of 1.20 m. The mean SMP snow depth across all 14 TMS was 0.56 m with a standard deviation (SD) of 0.13 m. The highest mean was observed at sensor D (0.96 m, SD: 0.29 m), and the lowest at sensor F at 0.20 m (SD: 0.06 m). The largest SD was 0.35 m (sensor M) at a mean depth of 0.50 m (Table A.8).

4.2.2 Snow density

The average snow densities per profile varied from $247\,\mathrm{kg\,m^{-3}}$ to $409\,\mathrm{kg\,m^{-3}}$ (Figure 5). The average snow density of all SMP profiles was $297\,\mathrm{kg\,m^{-3}}$ (SD: $13\,\mathrm{kg\,m^{-3}}$). Local averages of the SMP profiles per TMS ranged from $273\,\mathrm{kg\,m^{-3}}$ (SD: $21\,\mathrm{kg\,m^{-3}}$) to $343\,\mathrm{kg\,m^{-3}}$ (SD: $55\,\mathrm{kg\,m^{-3}}$). The greatest SD was $55\,\mathrm{kg\,m^{-3}}$. Local SD was lower at six sensors (B, G, H, K, L, N) compared to the overall SD (Table A.8).

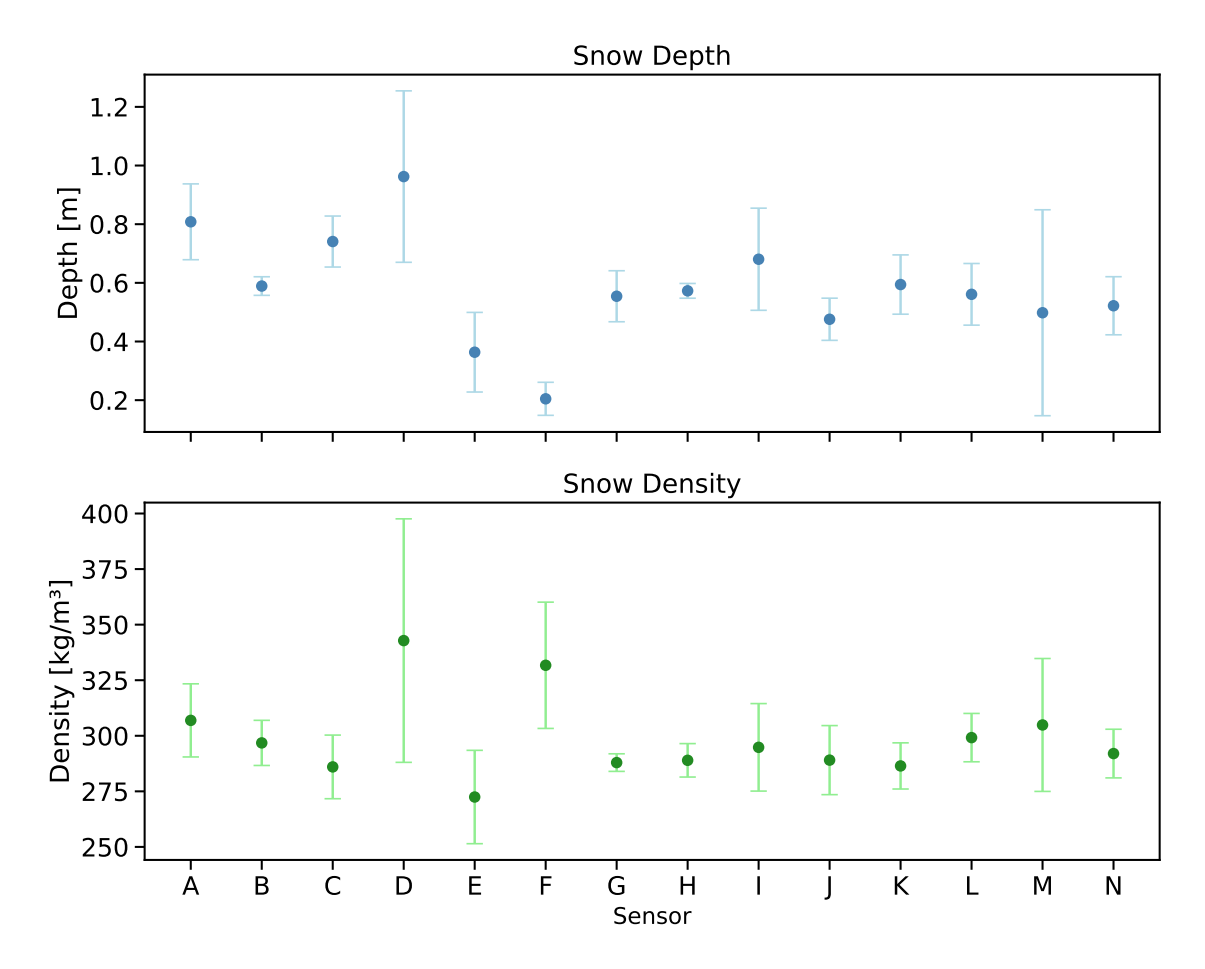


Figure 5: Spatial variability of snow depth and snow density measured in April 2024 at the Disko Study site. Averages of SMP profile measurements around their respective TMS. Bars represent the standard deviation.

4.2.3 TMS temperatures

The thermal conditions measured by the TMS revealed substantial spatial variability across the study area. Snow temperature was recorded 16 cm above the ground surface, representing the temperature within the lower snowpack. Surface temperature was measured directly at the ground surface, while soil temperature was recorded 6 cm below the surface. The complete winter temperature time series (Figure 6) illustrates the evolution of these three temperature layers from snow onset in early October to snowmelt in late spring.

Across the study area, the mean snow temperature was $-4.2\,^{\circ}\text{C}$ (SD: $3.4\,^{\circ}\text{C}$), the mean surface temperature was $-2.0\,^{\circ}\text{C}$ (SD: $2.9\,^{\circ}\text{C}$), and the mean soil temperature was $-1.8\,^{\circ}\text{C}$ (SD: $2.4\,^{\circ}\text{C}$). Starting in October, the time series shows that some sensors (e.g., A, G) exhibited large diurnal fluctuations in snow and surface temperatures around $0\,^{\circ}\text{C}$. At other sensors, no such amplitudes were observed as all three temperature measurements (snow, surface, soil) started near $0\,^{\circ}\text{C}$ and then dropped steadily as winter conditions established. The snow temperature generally showed the strongest and earliest cooling. The coldest snow temperature was recorded on February 1^{st} , 2024, at sensor E ($-22.8\,^{\circ}\text{C}$). The surface temperatures ranged from $-14.0\,^{\circ}\text{C}$ (sensor E) to $17.5\,^{\circ}\text{C}$ (sensor I), with the largest amplitude observed at sensor E ($31.1\,^{\circ}\text{C}$). The smallest surface temperature range

occurred at sensor D (3.9 °C; range -2.2 °C to 1.7 °C). Soil temperatures varied between -12.4 °C (sensor E) and 11.3 °C (sensor I), again with sensor E showing the largest soil temperature range (21.1 °C), and sensor D the smallest (1.9 °C). Mean soil temperatures across sensors ranged from -3.8 °C (sensor F) to -0.3 °C (sensor D).

At several sensors (e.g., D, H), once the snow cover was fully established, soil temperatures plateaued close to 0 °C during January before dropping further during February and March. This plateau is a classic example of the zero-curtain effect, where latent heat released during soil moisture refreezing, maintains temperatures near the freezing point over extended periods. Most soils froze at the beginning of October and remained below 0°C over the whole study period. The last sensor that froze was sensor K at the beginning of November 2023. Mid-winter marks the coldest and most thermally stable period. Snow temperatures during this phase show the greatest amplitude and site-to-site variability, ranging from about -5 °C to -15 °C at most sensors. Surface temperatures consistently remained 1 °C to 3 °C warmer than snow temperatures. The timing and magnitude of spring warming also varied across the network. Some sensors began to show a gradual increase in snow and soil temperatures by March or April, whereas others remained near freezing until May (Figure 6). In early spring, daily temperature amplitudes, particularly at the surface, increased again. Overall, the data revealed a consistent thermal gradient from the snow (coldest), through the snow / soil interface, to the underlying soil (warmest), with a clear damping of both daily and overall temperature amplitude with depth.

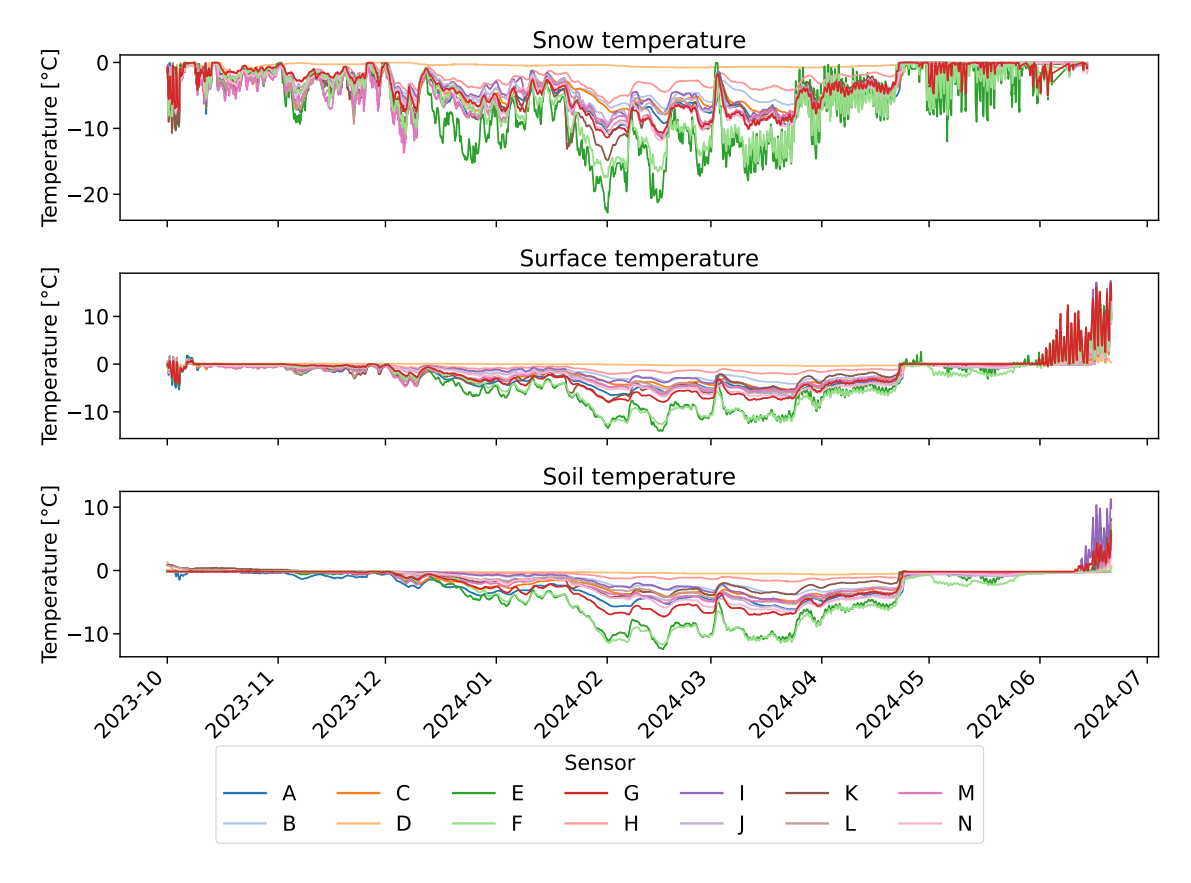


Figure 6: Time series of temperatures measured at the TMS. Hourly time series of snow, surface, and soil temperatures from October 2023 to June 2024 for each TMS. Snow temperature data are filtered to include only subzero value.

An initial inspection of the data indicated that thicker snow cover was associated with warmer winter soil temperatures. For example, Sensor D, which had the deepest snowpack $(0.96\,\mathrm{m})$, also recorded the highest mean soil temperature $-0.3\,^\circ\mathrm{C}$ (Figure 7). In contrast, sensors E and F, with the shallowest average snow depths $(0.36\,\mathrm{m}$ and $0.20\,\mathrm{m}$, respectively), recorded the coldest winter soil temperatures $(-3.6\,^\circ\mathrm{C})$ and $-3.8\,^\circ\mathrm{C}$. To better understand the local variability in snow depth, snow density, and soil temperatures and to explore the relationships among them, I used Bayesian hierarchical modeling. The following section presents these results and explores how snow cover properties influence (sub)surface thermal conditions.

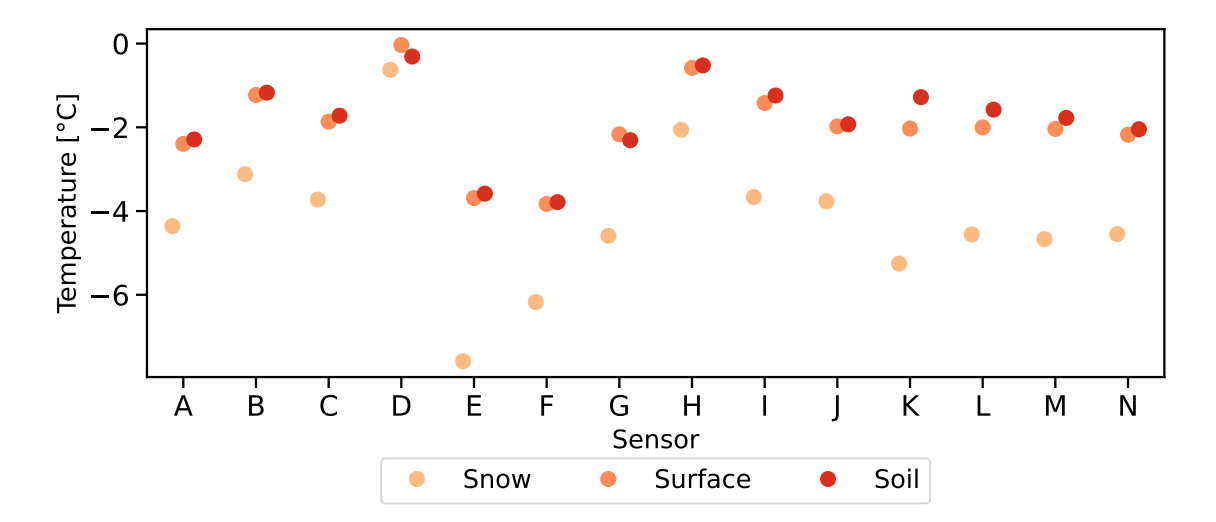


Figure 7: Average snow, surface and soil temperatures for each TMS between October 2023 and June 2024. Surface and soil temperatures represent full-period averages, while snow temperatures include only values below 0 °C, reflecting a simplified representation of subzero snow cover.

4.3 Model results

In the first stage of my modeling approach, I used Bayesian multivariate linear regression models to identify relevant predictors for snow depth, relative snow density, and snow temperature. These results informed the development of more complex hierarchical models in the second stage.

Unless otherwise noted, all models showed satisfactory convergence diagnostics, with $\hat{R} < 1.05$ and effective sample sizes (ESS) typically exceeding 400. Monte Carlo standard errors remained below 1% of the posterior standard deviations, indicating that posterior means and standard deviations were estimated with high precision (Figures A.9, A.10, A.11). Prior predictive checks confirmed that the chosen priors generated temperature and snow property values that were physically plausible and consistent with observed ranges, supporting the appropriateness of the prior distributions given domain knowledge.

To summarize uncertainty in the posterior estimates I report 94% highest density intervals (HDIs). These intervals represent the most credible values for a parameter, bounded between the 3rd and 97th percentiles of the posterior distribution. While HDI width reflects uncertainty, it also depends on the scale of the parameter being estimated, thus wider intervals do not always imply higher uncertainty.

4.3.1 Linear regression on snow depth

To predict snow depth across all sites, I fitted a Gamma regression with a log link using slope, elevation, and aspect as predictors. The Gamma distribution is characterized by the shape parameter alpha (α) , which controls the skewness of the distribution. Higher values of α indicate a more symmetric (less skewed) distribution (Table A.4). The pooled model estimated moderate residual variability in snow depth across all sites (α , mean: 6.9, HDI: 1.8 to 12.6). The intercept, reflecting expected snow depth at mean slope, elevation, and aspect, was -0.1 (HDI: -0.7 to 0.5) (Table A.9). Among the fixed effects, snow depth increases by approximately 15% per unit increase in slope (slope scaled between 0 and 2; mean: 0.14, HDI: -0.2 to 0.5). However, the probability that this effect is truly positive is only 68%, indicating weak support. The effect of elevation is small and uncertain (mean: -6.9, HDI: -31.0 to 17.1). Given the limited elevation range across the study area (85 m to $110 \,\mathrm{m}$), this corresponds to an approximate snow depth change of $\pm 17 \,\%$, but with no clear trend. Aspect shows similarly weak patterns where west-facing slopes (sine of aspect) have slightly lower snow depths (mean: -0.18, HDI: -0.9 to 0.6), while northsouth oriented slopes (cosine of aspect) had no systematic influence (mean: 0.04, HDI: -0.6 to 0.6).

The vegetation-group model estimates greater heterogeneity in snow depth across sites, with more right-skewed residuals than in the pooled model (α , mean: 2.9, HDI: 1.4 to 4.7). Snow depth varies modestly across vegetation types, with a standard deviation of group-level intercepts (mean: 0.1, HDI: 0.0 to 0.2). Dry tundra has a slightly lower snow depth (mean: -0.1, HDI: -0.4 to 0.2), moist tundra is similarly reduced (mean: -0.1, HDI: -0.4 to 0.2), and wet tundra shows little difference (mean: 0.04, HDI: -0.3 to 0.2). These correspond to expected decreases of approximately 9%, 8%, and 4%, respectively, compared to the baseline. However, the uncertainty intervals for all three, indicate weak and uncertain vegetation effects.

The geomorphon-group model yields broadly similar fixed effects. Slope again shows a weak positive association with snow depth (mean: 0.1, HDI: -0.4 to 0.6), suggesting a potential increase of about $10\,\%$ in snow depth per unit increase in slope, though with substantial uncertainty. There is no evidence for systematic control of snow depth by elevation or aspect. The standard deviation of group-level intercepts indicate small differences between geomorphon classes (mean: 0.08, HDI: 0.00 to 0.18). Expected snow depths are slightly higher in hollows and footslopes (mean: 0.03, HDI: -0.2 to 0.3), and slightly lower on slopes (mean: -0.01, HDI: -0.2 to 0.2) and in valleys or depressions (mean: -0.01, HDI: -0.2 to 0.2). All differences are distributed closely around zero and thus highly uncertain. Overall, terrain types appear to have little influence on snow accumulation in this landscape.

Based on LOO, the pooled model has the best predictive fit, with an ELPD of -1.4 and a $p_{\rm loo}$ of 4.9. However, it also has one influential data point identified by a high Pareto-k diagnostic, suggesting that this observation had a disproportionate influence on the model fit. The vegetation-group model performed slightly worse (ELPD: -4.3, $p_{\rm loo}$: 0.7), as did the geomorphon-group model (ELPD: -3.5, $p_{\rm loo}$: 1.5). Both group models had lower complexity and showed good diagnostic values (all Pareto-k < 0.7). Although the pooled model has the highest predictive score, the differences in ELPD across models are small. Thus, there is no strong evidence that one model substantially outperforms the others.

4.3.2 Linear regression on relative snow density

I also modeled relative snow density as a function of slope, aspect, and elevation using a beta distribution, where the dispersion parameter is denoted by κ (Table A.4). The pooled model estimated a κ of 939 (HDI: 195 to 1817; Table A.10). The posterior mean of the intercept is -0.9 (HDI: -1.3 to -0.5). Among the fixed effects, slope has the strongest influence: for every unit increase in slope, relative density increases by about 11% (mean: 0.1, HDI: 0.0 to 0.2), with a 99% posterior probability of a positive effect. Elevation contributes little explanatory power to the model (mean: -0.3, HDI: -4.5 to 4.0). For aspect, northeast-facing slopes (cosine of aspect) were associated with slightly denser snow (mean: 0.1, HDI: 0.0 to 0.2), while east- or west-facing slopes (sine of aspect) had no clear effect (mean: 0.0, HDI: -0.1 to 0.1).

The vegetation-group model, yields a κ of 862 (HDI: 155 to 1693), lower than the pooled model. The standard deviation of the group-level intercepts, indicates no variability in relative density across vegetation types (mean: 0.0, HDI: 0.0 to 0.1). Fixed effects in this model were nearly identical to the pooled model. In contrast, the geomorphon-group model estimated a much lower κ of 2.8, implying a higher residual variance in the predicted relative densities. Unlike the other two models, terrain variables had no clear effect in this model. The standard deviation of geomorphon-level intercepts (mean: 0.08, HDI: 0.00 to 0.18), points to slight differences among terrain types. However, group-level intercepts don't reveal systematic variation in relative snow density by geomorphon class. Looking at LOO the geomorphon-group model has a much lower predictive performance (ELPD: 3.3) compared to the pooled (ELPD: 36.4) and the vegetation-group model (ELPD: 35.3). This might be due to the fact, that it is too simple (p_{loo} : 0.3) compared to the vegetation-group model (p_{loo} : 4.7) and the pooled model (p_{loo} : 4.1).

In summary, the relative snow density is weakly influenced by slope, with steeper slopes associated with denser snow. However, this relationship is only evident in the pooled and vegetation-group models, as the geomorphon-group model performs poorly. Elevation, aspect, and vegetation type show minimal influence on density, and differences among geomorphons are small and not systematically related to relative snow density.

4.3.3 Linear regression on snow temperature

The third model examines snow temperature as a response to slope, elevation and aspect (Table A.4). In the pooled model, the estimated baseline snow temperature is highly uncertain (intercept, mean: -1.2, HDI: -7.6 to 4.8; Table A.11). The residual standard deviation (σ) is 1.1 (HDI: -0.5 to 0.8), indicating unexplained variability between observed and predicted snow temperatures. The model provides evidence for a positive effect of slope (mean: 1.1, HDI: 0.1 to 2.1), suggesting that snow temperature increases with steeper terrain. Elevation has a large negative effect (mean: -37.9, HDI: -105.9 to 31.4) though the wide interval reflects high uncertainty. Despite this, the trend suggests that snow temperatures tend to decrease with elevation. Aspect effects were weak and uncertain.

In the vegetation-group model, uncertainty of the intercept increases (mean: -2.44, HDI -9.5 to 4.0). The residual standard deviation as well as the fixed effects remain similar to the pooled model. Snow temperature varies slightly between vegetation types (group-level standard deviation, mean: 1.0, HDI: 0.0 to 2.4), where dry tundra is colder (mean: -0.3, HDI: -1.8 to 1.0), and moist and wet tundra are warmer (mean: 0.6, HDI: -0.7 to 2.2, and mean: 0.3, HDI: -1.1 to 1.9, respectively).

The geomorphon-group model yields similar findings, with a positive slope effect, a negative elevation effect and little support for aspect, as in the previous models. Snow temperatures vary slightly by terrain type, with a group-level standard deviation of 1.06 (HDI: 0.00 to 2.39). Warmer snow temperatures are likely in hollows and footslopes (mean: 0.8, HDI: -0.3 to 3.5), while slope (mean: 0.2, HDI: -1.5 to 2.1) and valley/depression (mean: 0.0, HDI: -1.8 to 2.1) show no consistent effects. This model shows signs of mild convergence issues, with some \hat{R} values above 1.05 and low effective sample sizes for several group-level parameters, likely due to small sample sizes within some geomorphon categories, suggesting caution in interpreting the group effects.

According to LOO the vegetation-group model performs best (ELPD: -23.2) though there are minor differences to the pooled (ELPD: -24.4) and the geomorphon-group model (ELPD: -25.2). The geomorphon-group model has the highest complexity (p_{loo} : 6.5), suggesting potential overfitting. All models show Pareto k values slightly above the recommended threshold (k > 0.7), for two observations indicating moderate influence and reduced stability of the LOO estimate for those points. This implies that the models may not fully capture the structure of those specific cases, though overall LOO scores remain interpretable.

In summary, the first part of my analysis suggests that slope is a weak positive predictor for snow depth and snow temperature and possibly for relative density. The effects of elevation and aspect remain uncertain, although north-facing slopes show some indication of a positive effect on relative density, as suggested by the positive HDIs. Groupings allow for model flexibility and add slight explanatory power to the models for snow depth and snow temperature, but remain inconclusive. Based on LOO, models grouped by vegetation improve predictive performance for predicting snow temperature, while grouping by geomorphon offers no predictive advantage. In two out of three cases, the pooled models perform best, suggesting that snow and temperature responses are generally consistent across sites and may not require additional grouping for prediction. However, this finding is limited by very small sample sizes within some groups – sometimes as low as a single observation – which reduces the power of hierarchical models to detect group-level differences.

4.3.4 Air-Soil Temperature model

Based on my findings, I set up a hierarchical model that predicts the daily averaged temperature at the snow, surface and soil sensor of each TMS based on the observed average daily air temperature using linear effects of slope and cosine aspect (Figure 3). Across all models, relationships between predictors and temperature are largely consistent, with only subtle differences in coefficient strength and uncertainty.

In the pooled model, snow temperature increases as air temperature rises. On average, a 1 °C increase in air temperature leads to a 0.7 °C increase in snow temperature (Table A.12). Snow depth also helps insulate snow temperature, with deeper snow associated with warmer snow temperatures. Specifically, each additional meter of snow reduces the gap between air and snow temperature by about 1.8 °C, supporting its insulating role. The density of the snow layers plays a more complex role. Top-layer relative density has a negative effect (mean: -2.0, HDI -16.5 to 12.5), but the wide uncertainty range suggests that this relationship is not well supported by the data. Alternatively, this uncertainty may also reflect limitations in the model's ability to capture the true effect.

In contrast, relative density of the bottom layer shows a more robust positive effect on snow temperature estimated at 3.98° C (HDI -2.4 to 11.0). The uncertainty interval for this estimate mostly includes positive values, indicating moderate evidence that denser bottom layers provide less insulation. Terrain features such as slope and aspect have only weak effects on snow temperature in this model (mean: 0.8, HDI -0.3 to 1.8 and mean: 0.4, HDI: -0.5 to 1.3, respectively). The temperature coupling from the snow layer to the surface sensor is strong and positive (mean: 1.3, HDI: 0.9 to 1.6). Similarly, surface temperature strongly influences soil temperature with an effect of 1.0 (HDI: 1.0 to 1.2), suggesting direct and reliable propagation of heat through the snowpack. The model also includes offset values for surface (mean: 0.3) and soil temperatures (mean: 0.2), which help account for any systematic differences not explained by the main predictors. These offsets adjust the temperature baseline at each level to better match observed data. While the surface offset shows higher variability and a wider HDI (-1.5 to 2.0), suggesting greater uncertainty, soil offset has a smaller mean and tighter HDI (-0.2 to 0.6), suggesting less unexplained variation at this depth. Temperature variation also decreases with depth. The estimated standard deviations decrease from snow (σ : 1.1) to surface (σ : 0.7) to soil (σ : 0.3) temperatures, which indicates that the model explains a larger share of the variance at greater depths, consistent with fewer external influences on soil temperature.

Comparing the pooled model to the two grouped models, all models confirm the positive influence of snow depth, which is especially pronounced in the vegetation model (mean: 2.7, HDI 0.3 to 4.9). Likewise, the effect of bottom relative density is similar across the models, showing a moderately uncertain positive effect. In contrast, all models show a negative effect of top relative density, counter to the prior. As in the pooled model, both vegetation and geomorphon models find a moderate positive effect for slope (both 1.0), but only the geomorphon-group model detects an influence of aspect (mean: 0.4, HDI -0.4 to 1.4). Additionally, both models confirm the strong temperature propagation from snow to surface and soil, evident already in the pooled model. In the vegetation-group model, differences between vegetation types show up as varying baseline temperatures. Dry tundra is associated with lower temperatures (mean: -0.8, HDI -2.0 to 0.5), whereas wet tundra is associated with higher temperatures (mean: 0.6, HDI -0.7 to 1.9). Moist tundra shows no clear effect (mean: 0.1, HDI -1.3 to 1.3). In the geomorphon-group model footslopes have slightly higher temperatures (mean: 0.5, HDI -0.9 to 1.9), and slopes and valleys/depressions slightly lower temperatures (mean: 0.3, HDI -1.6 to 1.1 and mean: 0.3, HDI: -1.9 to 1.3, respectively). However, all posterior means have high standard deviations and distribute around zero, suggesting uncertainty in these group effects. Thus, while the inclusion of group-level intercepts helps to adjust for some variability, most of the predictive power comes from snow properties and temperature coupling across the layers.

Model comparison using LOO supports these findings (Figure 8). For snow temperature, the vegetation-group model performs best (ELPD: -20.6), followed by the pooled model (ELPD: -24.3) and the geomorphon-group model (ELPD: -24.5). The vegetation-group model also has the highest model complexity (p_{loo} : 6.7), suggesting a better fit at the cost of added complexity. For surface temperature, all models perform similarly, with negligible differences in ELPD and p_{loo} . However, the vegetation-group model has the highest ELPD (-13.6) and the lowest p_{loo} (2.4), indicating a slightly better and more efficient fit. For soil temperature, the geomorphon-group model shows the best performance (ELPD: -2.0, p_{loo} : 3.9), followed by the pooled and vegetation-group models, though the

differences are minor. Overall, these comparisons suggest that the hierarchical structure improves predictions for snow and soil temperatures, particularly when grouping by vegetation. However, most of the model's predictive performance is driven by the physical covariates (such as snow depth and relative density) and the way temperatures at different depths are linked within the model.

In summary and as expected, increasing air temperature shows a consistent positive effect on snow temperature across all models. The insulation effect of snow depth on snow temperatures is also evident in all three models. While increased top relative density shows a cooling effect on snow temperatures, and thus more insulation, across all models, higher bottom relative density provide less insulation. Terrain effects from slope and aspect are subtle but present. The strongest and most consistent finding across all models is the clear and direct propagation of temperature down through the snowpack. Including vegetation and geomorphon group-level intercepts improves model fit modestly but most predictive power still comes from snow properties and thermal coupling.

4.3.5 Snow-Soil Temperature model

In the second hierarchical model, I excluded snow depth, air temperature, aspect and slope from the previous model to only investigate the effect of the bottom relative density of the snowpack on surface temperatures (Figure 3). Thus, I treated snow temperatures as a given variable, assuming that the effects of the excluded predictors are included in the snow temperatures. The pooled model reveals a strong positive effect of snow temperature on surface temperature (mean: 1.7, HDI: 0.9 to 1.6), and likewise between surface and soil temperature (mean: 1.0, HDI 0.9 to 1.1; Table A.13). The effect of bottom relative density has a positive posterior mean (4.4), and a mostly positive HDI (-2.6 to 11.6), that shifted substantially from its diffuse prior (mean: 0.6, HDI: -20.4 to 19.7), indicating the data contribute evidence for a positive, though uncertain, effect. Residual variance is low – especially for soil temperature (σ : 0.3 °C) – suggesting that the model explains a substantial portion of the observed variability.

The vegetation-group model modestly strengthens the snow-to-surface temperature relationship (mean: 1.3, HDI 0.9 to 1.8), while the surface-to-soil effect remains nearly identical (mean: 1.0, HDI 0.9 to 1.1). The bottom relative density effect increases slightly (mean: 5.2, HDI -2.7 to 11.5). The varying intercepts by vegetation class are weak and uncertain, with all HDIs centered around zero, indicating little evidence for systematic vegetation effects.

The geomorphon-group model introduces weak differentiation across terrain types. The hollow/footslope type shows a possible positive effect (mean: 0.4, HDI -0.8 to 1.5), while the valley/depression type suggests a negative effect (mean: -0.6, HDI -1.9 to 0.8). However, all geomorphon-specific intercepts remain highly uncertain. The snow-to-surface temperature effect slightly weakens (mean: 1.2, HDI 0.8 to 1.6), while the surface-to-soil relationship remains robust (mean: 1.0, HDI 1.0 to 1.1). The model also exhibits a slightly lower surface temperature residual variance (σ : 0.6 °C), compared to the pooled and vegetation models (both 0.7 °C), suggesting geomorphon grouping may marginally improve model fit for surface temperatures. Together, these models show that snow and surface temperatures are strong predictors of soil temperature, and that bottom relative density may have a positive albeit uncertain effect on heat transfer through the snowpack. Although vegetation-based grouping does not yield clearly interpretable

intercepts, it marginally improves predictive performance for soil temperature, as shown by leave-one-out cross-validation.

For surface temperatures, the pooled model achieves the highest ELPD (-13.7) with the lowest effective number of parameters $(p_{loo}\ 2.5)$, indicating the most efficient and accurate fit. Vegetation and geomorphon grouped models have slightly lower predictive accuracy (ELPD: -15.6 and -14.6, respectively) and increased complexity $(p_{loo}: 4.0$ and 4.5, respectively). This suggests that including group-level effects does not substantially improve predictions of surface temperature and may slightly reduce model efficiency. In contrast, for soil temperatures, the vegetation-group model performs best, with the highest ELPD (-1.9) and lowest p_{loo} (4.0), suggesting it captures relevant structure with minimal added complexity (Figure 8). The pooled model performs similarly (ELPD: -2.1, p_{loo} : 4.0), while the geomorphon-group model has slightly lower predictive accuracy and higher complexity (ELPD: -2.2, p_{loo} : 4.2). These results indicate once more that vegetation grouping may offer marginal improvements for soil temperature prediction, while geomorphon-based grouping does not consistently enhance model performance.

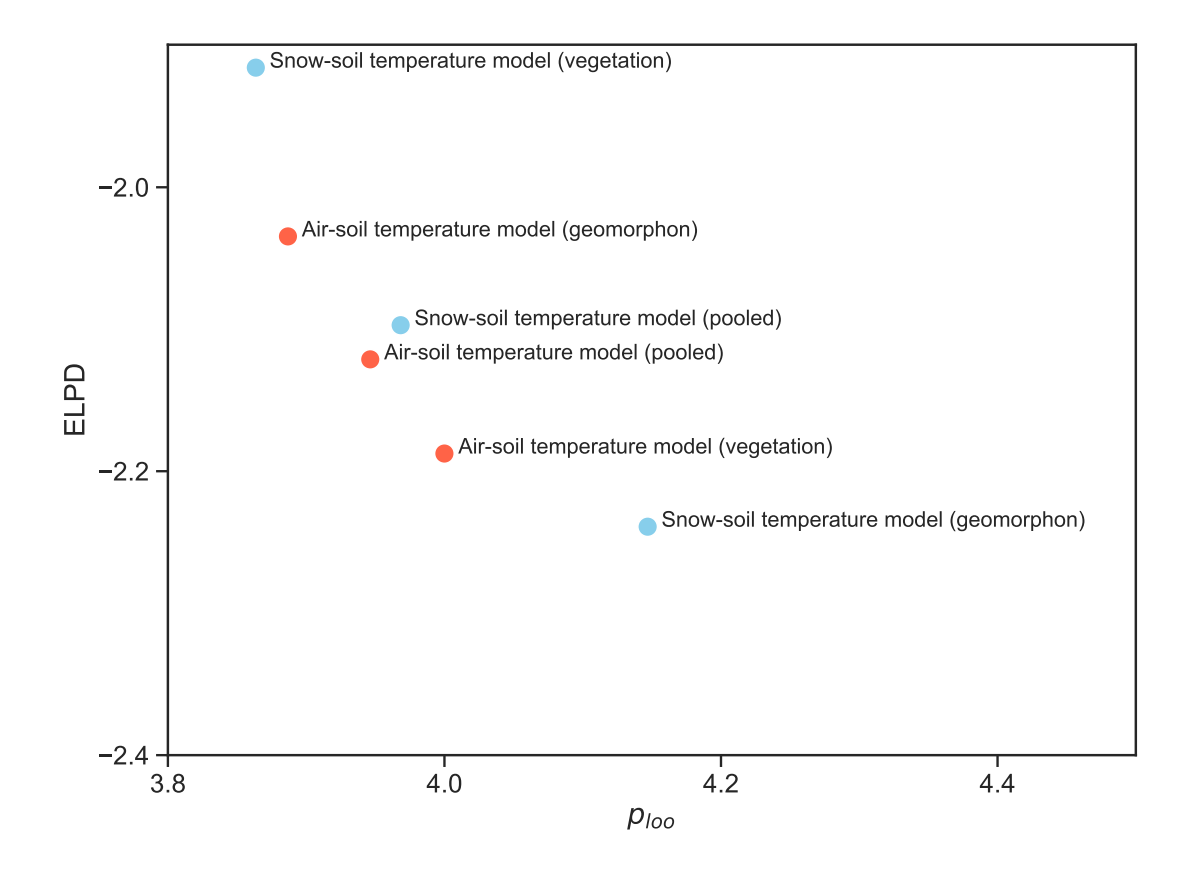


Figure 8: Comparison of expected log pointwise predictive density (ELPD) and effective number of parameters (p_{loo}) for hierarchical models on soil temperature. Snow-Soil Temperature models (blue) predict soil temperature using snow temperature as an input; Air-Soil Temperature models (red) include air temperature as an additional hierarchical level. Higher ELPD values indicate better predictive performance while higher p_{loo} values indicate more complex models.

4.3.6 Sensitivity analysis

To assess the influence of prior assumptions on model behavior, I compared two versions of the pooled linear regression model on snow temperatures, one using informative priors and the other using reference priors. The model with reference priors generates a greater number of extreme outliers, with predictions ranging from approximately $-500\,^{\circ}$ C to $700\,^{\circ}$ C, far beyond any physically meaningful range. In contrast, the informative-prior model produces predictions within a more plausible range, between $-23.8\,^{\circ}$ C to $-7.5\,^{\circ}$ C. Despite these differences at the extremes, the central tendency and overall spread of the predictions were similar across both models. The reference model shows substantially wider posterior intervals and larger effect estimates, while the informed model constrains parameter estimates to more realistic ranges and avoids implausible extrapolations. Consistent with this, the informative-prior model achieves a slightly higher ELPD (-24.4) compared to the reference model (ELPD: -25.2). Both models have similar moderate effective complexity, with estimated effective parameters (p_{loo}) of 4.9 and 5.7.

I performed a second sensitivity analysis for the Air-Soil Temperature model that predicts snow, surface and soil temperatures. The results show that the core temperature relationships remain stable in both models, indicating that these parameters are well supported by the data. Some coefficients, such as those for snow depth, relative snow density and the surface temperature, are more sensitive to the choice of the prior. These parameters shift in posterior means and increase in width of their uncertainty intervals under vague priors. The effect of bottom relative density even changes direction from positive to negative.

5 Discussion

In the following, I will first discuss the spatial variability of snow cover and surface and soil temperatures at my study site, contextualizing these patterns with observations from comparable Arctic environments. Next, I evaluate how my models captured key relationships between snow properties and soil temperatures, and consider how different predictors and modeling choices influenced the results. Finally, I reflect on the main strengths and limitations of the study, including data constraints and methodological assumptions, and suggest directions for future research.

5.1 Spatial variability of snow characteristics and soil temperatures

The snow depth in April exhibited considerable spatial heterogeneity across the study area, ranging from 0.15 m to 1.10 m, with a mean of 0.56 m and a standard deviation of 0.13 m based on SMP profile data. This reflects typical small-scale variation in Arctic tundra snow cover, where wind redistribution and microtopographic controls lead to uneven accumulation (Sturm et al. 1995). Comparable snow depth ranges were observed by Van Tatenhove and Olesen (1994) near Sisimiut in Western Greenland, who reported mean maximum depths of 0.55 m over a 12-year period (1968–1980), with individual winters spanning from only 0.10 m to 0.90 m. In contrast, spatial variability was highlighted by Grünberg et al. (2025), who used data from 13 spatially distributed temperature loggers in the Trail Valley Creek (TVC) catchment, Northwest Territories, Canada, to examine snow and soil temperature dynamics. They recorded snow depths ranging from 0 m to 1.7 m, demonstrating the potential for extreme spatial variation. Similarly, Shirley et al. (2025) examined snow cover across the Seward Peninsula, Alaska, using snow depth data collected in both 2019 (mean: 1.0 m) and 2022 (mean: 0.59 m). They found that approximately 80% of snow depth variability occurred at small scales (less than 90 m), emphasizing the dominant role of microtopography in governing snow distribution. Earlier modeling work by Liston and Sturm (1998) further supports these observations, showing that snow depths can vary by a factor of ten or more over short distances in Arctic terrain due to wind and topographic influences. In my study area, terrain elevation ranges from 80 m to 112 m, with slope angles between 0° to 20°. These variations, together with prevailing winds from the north to northeast, likely shaped the observed snow depth patterns through localized drift formation and wind scour.

Average snow density at the TMS sites also displayed spatial variability, ranging from $247\,\mathrm{kg\,m^{-3}}$ to $409\,\mathrm{kg\,m^{-3}}$, with a mean of $297\,\mathrm{kg\,m^{-3}}$ and a standard deviation of $13\,\mathrm{kg\,m^{-3}}$. Mean densities per TMS ranged from $273\,\mathrm{kg\,m^{-3}}$ to $343\,\mathrm{kg\,m^{-3}}$. These values are higher than many reported Arctic tundra snowpack densities, which typically fall within the $150\,\mathrm{kg\,m^{-3}}$ to $300\,\mathrm{kg\,m^{-3}}$ range (Damseaux et al. 2025). For example, Bormann et al. (2013) measured snow density at twelve sites in the Siberian tundra and reported a spring mean of $219\,\mathrm{kg\,m^{-3}}$, indicating a lighter snowpack under colder continental conditions. In contrast, higher pre-melt densities were observed in central Northeast Greenland, where Hollesen et al. (2011) documented snow densities of $386\pm56\,\mathrm{kg\,m^{-3}}$. A recent large-scale synthesis by Zhao et al. (2023) found an average tundra snow density of $225\,\mathrm{kg\,m^{-3}}$ across Arctic sites, placing the results from my study at the upper end of the observed distribution. The relatively high densities measured on Disko Island likely reflect

the effects of wind packing and enhanced snow metamorphism. In particular, prevailing winds from the north to northeast sector and frequent wind speeds above $5\,\mathrm{m\,s^{-1}}$ suggest strong redistribution and compaction of snow in the valley. This aligns with the site's English name, Windy Valley, and supports the interpretation that wind-driven processes contributed to the denser snow structure observed at the TMS sites.

Temperature patterns across the study area mirrored the spatial heterogeneity observed in snow depth and density. The snowpack exhibited a clear dampening effect on ground thermal conditions. Snow temperatures measured 16 cm above the ground were the coldest, averaging $-4.2\,^{\circ}\text{C}$ (SD: $3.4\,^{\circ}\text{C}$). Surface temperatures at the ground-snow interface were milder at $-2.0\,^{\circ}\text{C}$ (SD: $2.9\,^{\circ}\text{C}$), and soil temperatures at 6 cm depth were the warmest, averaging $-1.8\,^{\circ}\text{C}$ (SD: $2.4\,^{\circ}\text{C}$). This vertical gradient highlights the snowpack's insulating role, reducing heat loss from the ground and buffering subnivean conditions from atmospheric impacts.

The minimum winter soil temperatures occurred at sensor E, where April snow depth only reached $0.4\,\mathrm{m}$ and the minimum temperature reached $-12.4\,^{\circ}\mathrm{C}$, while the warmest soil conditions were observed at sensor D with a snow depth of $1.0\,\mathrm{m}$ and a minimum temperature of $-0.6\,^{\circ}\mathrm{C}$. While the range of minimum winter soil temperatures in my study was relatively moderate, greater variability was observed by Grünberg et al. (2025), who recorded winter minima from $-31.0\,^{\circ}\mathrm{C}$ to $-4.0\,^{\circ}\mathrm{C}$ across 13 temperature loggers in TVC in 2022/23. Mirroring the patterns observed at my study site, the coldest soil temperatures occurred at locations with little or no snow, while warmer soils were consistently found beneath thicker snowpacks, reinforcing the critical role of snow insulation in Arctic tundra systems

This insulating effect was also evident at the snow-ground interface. Winter average surface temperatures across my study area ranged from $-3.8\,^{\circ}$ C to $-0.03\,^{\circ}$ C, further reflecting the high degree of spatial variability typical of Arctic tundra environments. Although the range I observed was smaller, it aligns with results from four tundra sites in Alaska where Sturm and Holmgren (1994) recorded spatial surface temperature ranges of up to 7.0°C over transects only 1.5 m long during the 1989-1990 winter, primarily driven by microtopographic contrasts between cold-exposed tussocks and better-insulated hollows during cold spells with air temperatures dropping below -30.0 °C. My average winter surface temperature of $-2.0\,^{\circ}\text{C}$ (SD: $2.9\,^{\circ}\text{C}$) was also markedly warmer than the mean air temperature (-6.7 °C) over the same period, underscoring the moderating influence of snow. A similar offset was observed in the Kuparuk Basin in Arctic Alaska, where Taras et al. (2002) found that snow-ground interface temperatures averaged 7.5 °C higher than air temperatures. They also noted that interface temperatures varied on much finer spatial scales than air temperature and were more closely influenced by snow properties. Moreover, temperature amplitudes attenuated progressively from air to snow surface to soil, highlighting the layered dampening imposed by the snowpack, which was also evident at my study site. This attenuation depends strongly on snow depth. In my April records, soil temperatures at sensor H (0.60 m snow) and sensor D (1.00 m) showed virtually no trace of concurrent air-temperature fluctuations, whereas sensors E (0.40 m) and F (0.20 m) still exhibited clear oscillations. These observations suggest a local threshold of roughly 0.50 m (Figure 6). At a broader regional scale, Goncharova et al. (2019) employed vertical iButton arrays to monitor ground-surface temperatures in West Siberia over an eight-month winter. They found that snow thicker than 0.80 m on lower, forested terrain produced the strongest insulation, but even 0.20 m of snow was enough to generate notable reduction in

soil cooling. The timing of when a site first accumulated $\geq 20\,\mathrm{cm}$ of snow exerted the dominant control on seasonal soil-temperature trajectories, underlining the importance of both depth and duration. A different depth threshold emerged from the hemispheric analysis by Slater et al. (2017), who used six-month continuous records (October-March) to examine how snow controls the seasonal amplitude of soil temperature. Their results showed the expected exponential decay in soil-temperature variability with increasing snow depth and demonstrated that the marginal effect of insulation diminishes beyond approximately 0.5 m. Although my study is based on discrete snow surveys and TMS data, it captures the same physical pattern.

However, the limited spatial variability in my dataset and the snapshot nature of the snow surveys posed challenges for fully resolving complex snow-soil interactions using traditional modeling approaches. These constraints motivated the development of a flexible Bayesian framework that explicitly incorporates uncertainty and hierarchical structure.

5.2 Model outputs

5.2.1 Modeling snow depth

In the first model, I set up a simple linear regression on snow depth. This model only found minimal differences in snow depth between vegetation and geomorphon groups. These effects appeared negligible, which is likely due to the limited variability in vegetation types and terrain features at the study site. The relatively homogeneous conditions may not have provided sufficient contrast to detect such differences that are well-documented in more heterogeneous environments. For instance, Grünberg et al. (2020) reported substantial snow accumulation beneath tall shrubs (up to 2 m) at TVC, compared to areas with short or sparse vegetation. Their findings illustrate how vegetation height and structure enhance snow trapping and reduce wind erosion. These mechanisms were less evident in my study due to the prevalence of low-lying tundra vegetation (less than 20 cm).

Despite the overall weak grouping effect, all three models indicated a minor positive influence of slope on snow depth, eventhough this effect was likely limited, due to the gentle topography of the site. Other studies such as by Borges (2024) demonstrate more pronounced effects of topography and vegetation on snow distribution. The high-resolution LiDAR-based snow depth mapping within an area of 127 km² in TVC revealed deeper snow in micro- and macrotopographic lows, leeward slopes, and densely vegetated areas. Snow depths were highest on northeast- to southeast-facing slopes, consistent with dominant wind directions (west and northwest) that facilitate snow transport and deposition. The importance of wind redistribution and its interaction with topography and vegetation which are widely reported (König and Sturm 1998; Liston and Sturm 1998; Taras et al. 2002; Domine et al. 2015; Shirley et al. 2025) were less evident in this study because the measurements were situated in relatively flat areas, with limited variation in vegetation cover and a relatively small number of sampling points.

5.2.2 Modeling snow density

I also examined potential landscape controls on snow density. In the linear regression models, cosine aspect showed a weak but positive effect on relative density (mean: 0.1, HDI: 0.0 to 0.2), suggesting slightly higher densities on north-facing slopes. This pattern may reflect wind slab formation caused by frequent strong winds (above $8\,\mathrm{m\,s^{-1}}$) from the

north-northeast, which likely enhance compaction and densification of the snowpack on leeward-facing slopes. Elevation and sine aspect had no meaningful influence on relative density, and models including group-level effects such as geomorphon classification were not supported by the data and tended to overfit. These results align with expectations, given that the models did not incorporate major climatological drivers of snow densification, namely precipitation amount, air temperature, wind exposure, and snow duration. Large-scale analyses, such as by Bormann et al. (2013), which used over 1,700 snow density records across the United States, Australia, and the former Soviet Union, have shown that these climate variables are the primary controls on snow density development over time. However, the primary aim of this study was not to predict snow density under varying climate conditions, but rather to understand how small-scale spatial variations in density may influence near-surface soil temperatures.

5.2.3 Influence of snow depth on temperature

The hierarchical models used in the second part of the analysis revealed consistent positive effects of snow depth on winter soil temperature across all model structures. This effect was most pronounced in the vegetation model, where a 1.0 m increase in snow depth was associated with a 2.7 °C increase in snow temperature (HDI: 0.3 to 4.9). While this estimate reflects the modeled slope, it should not be interpreted as a linear relationship that holds across the entire range of snow depths. In fact, the observed data suggest a much stronger insulation effect at shallow depths. As shown in Figure 7, temperature differences between the snow and surface sensors ranged from 2°C to 4°C, even though the vertical distance between these sensors is just 16 cm, which would imply a much steeper local gradient than the modeled slope. This discrepancy highlights the limits of interpreting the modeled slope at face value: the model estimates an average effect over the entire snow depth range, while in reality the relationship is nonlinear. The intercept may include part of the initial insulation effect already present at low snow depths, flattening the estimated slope. Much of the insulation effect likely occurs at low snow depths and then diminishes, as also reported by earlier findings from Slater et al. (2017), who showed that around 0.5 m of snow is often sufficient to decouple soil from air temperature.

While vegetation heterogeneity at the study site was limited, vegetation types still contributed to measurable differences in winter soil temperatures. Dry tundra sites had the lowest average soil temperatures (-0.8 °C), while wet tundra sites were notably warmer (0.6°C), likely due to higher initial soil moisture content and associated latent heat buffering during freeze-up. Moist tundra showed no clear thermal signature (0.1 °C). These modest differences suggest that even subtle variations in vegetation and soil moisture can influence ground thermal regimes, especially in shallow, variably insulated snowpacks. In more heterogeneous environments, vegetation-related contrasts in soil temperatures are more pronounced. Grünberg et al. (2020) found that tall shrub patches accumulated deeper snow and had markedly warmer soils, while dwarf shrub and lichen tundra – associated with sparse snow – exhibited colder and more variable ground temperatures. Similarly, Van Tatenhove and Olesen (1994) documented substantial vegetation-driven differences in West Greenland, attributing warmer soils to deeper and more stable snow cover. Both studies highlight how vegetation primarily modifies soil thermal regimes via its effect on snow accumulation and retention, often exerting stronger control than regional air temperature. These snow-soil-vegetation interactions have important implications in

the context of Arctic greening. Long-term records from western Greenland show that Betula nana expansion correlates with warmer soils and earlier meltout in spring (Hollesen et al. 2015). Increasing shrub cover can trap more snow, reduce its compaction, and enhance thermal insulation, raising winter soil temperatures by several degrees (Sturm et al. 2001; Domine et al. 2015; Paradis et al. 2016; Rixen et al. 2022). Although vegetation effects at my study site were less pronounced due to the limited range of types, the observed temperature patterns still align with these broader dynamics and underscore the importance of vegetation-snow interactions in shaping soil thermal conditions.

In the geomorphon-group model, the geomorphon-level intercepts reveal subtle topographic ordering. Hollows/footslopes tend to be warmest, followed by slopes, whereas valley/depression sites tend to be coolest. Although all highest-density intervals distribute around zero, the relative ranking of the posterior distributions echoes the snow-depth results: micro-relief is too subdued for consistent thermal offsets to emerge. Hollows are marginally warmer because they hold slightly deeper, denser snow; valleys and gentle slopes lack enough depth contrast to sustain a systematic temperature advantage. This muted hierarchy contrasts with stronger-relief tundra, where deeper snow in leeward hollows and depressions yields 4 °C to 8 °C warmer winter soils than wind-scoured ridges (Sturm and Holmgren 1994; Van Tatenhove and Olesen 1994). Recent LiDAR surveys at TVC show more than 0.5 m of additional snow accumulation in leeward hollows, corresponding to soil temperatures up to 6 °C warmer than those on exposed slopes (Borges 2024).

5.2.4 Influence of relative density on temperature

I assessed how vertical snow density structure affects thermal coupling from the atmosphere through the snowpack to the soil. My hierarchical models showed that denser snow in the bottom 16 cm of the snowpack (i.e., between the snow and surface temperature sensors) exerts a positive effect on surface and soil temperatures. Denser snow at the base of the pack implies higher thermal conductivity, reduced insulation and stronger thermal coupling between the surface and the soil. On April 9, air temperatures were around -6°C, colder than the snowpack (about -4°C), which was itself colder than the surface and soil temperatures (about -2° C). These conditions, might in principle promote soil heat loss toward the colder snowpack and atmosphere. But since the air temperature measured at AWS2 during the first days of April was higher than most of the snow temperatures at that time, soil temperatures measured on April 9 may have been influenced by these warmer air temperatures resulting in downward heat flux where the stronger thermal coupling due to denser snow has a positive effect on soil temperatures. The denser snowpack may also have allowed the soil to track the diurnal cycles in early spring where solar input is increasing more closely. The daily averages might hide the actual daytime heat transfer, which is more complicated than a single-direction flux.

The negative effect of denser snow near the surface is likely less reliable, as my initial model predicting snow temperature from air temperature performed poorly, limiting confidence in this result. If the effect is meaningful, however, it is also physically difficult to interpret; one possible explanation is that denser upper layers inhibit energy transfer from the air into the snowpack, potentially forming crusts or compact layers that delay surface warming.

Integrating density into soil temperature models is not merely a refinement but is

essential for correct soil-temperature prediction as my results suggest that differentiating only two layers might already capture thermal contrasts. Other studies support the importance of accurate snow density profiles for modeling soil thermal dynamics. For instance, Marchand et al. (2018) used satellite microwave polarization ratios to optimize simulated snow density in a land surface model. Incorporating more accurate density profiles led to better estimates of soil temperature, showing that denser snow increases thermal conductivity, thereby reducing snow insulation and leading to cooler soils beneath. Their results from a site near TVC, demonstrated that underestimated snow densities led to overly warm soil simulations due to excessive insulation. In their study they use snow density to derive the thermal conductivity of snowpacks, where higher densities generally lead to increased conductivity and reduced insulation, which aligns with my observations of bottom snow density.

5.2.5 Temperature propagation

All models consistently indicated strong temperature propagation from snow to the surface and ultimately to the soil. This directional patter highlights the insulating role of the snowpack in winter. The modulation of the temperature signal by snow depth and snow density underscores the conclusions of Zhang (2005) and Slater et al. (1998), who both demonstrated that snow properties strongly influence the thermal regime of tundra soils. Their models and observations revealed that even small changes in snow depth or density could shift soil freezing dynamics, highlighting snow's insulating role in Arctic energy balance. Collectively, the models presented here align with these earlier studies in showing that, even in relatively uniform terrain, snowpack structure and depth exert primary control over winter soil temperatures – more so than terrain or vegetation alone.

5.3 Model strengths, limitations, and opportunities for advancement

The Bayesian models developed for this study successfully captured the principal relationships between snow cover and ground-surface temperature, with snow depth consistently emerging as the dominant predictor. The hierarchical structure of the model enabled partial pooling across sites, which was especially valuable given the limited dataset (14 TMS and a single-day mean of observations from April 9th, 2024). This structure allowed the model to incorporate group-level predictors, such as vegetation type and geomorphon class, even when some categories were sparsely represented. For instance, the weak estimated effects of vegetation and geomorphon likely reflect small sample sizes rather than a true absence of influence. By sharing statistical strength across groups, the model reduces overfitting while preserving variation that may emerge more clearly in larger datasets.

A key strength of the Bayesian framework lies in its ability to integrate diverse sources of information including field observations, expert knowledge, and physical understanding while explicitly accounting for uncertainty in both predictor effects and measurement variability (Berliner et al. 2003; Ekici et al. 2014). This capacity is particularly important in Arctic research, where logistical constraints limit data collection and environmental heterogeneity is high. Incorporating informative priors proved essential for ensuring physically realistic model behavior. When vague or reference priors were used, the model occasionally produced implausible predictions such as soil temperatures hundreds of degrees outside

the physical range highlighting the danger of overfitting and nonphysical extrapolation in the absence of prior constraints. Informative priors, by contrast, anchored model estimates within meaningful geophysical bounds and improved predictive performance, even though the central tendencies remained similar between models. This sensitivity to prior specification was especially evident in the effect of snow density. A particularly notable case involved bottom relative density, whose association with soil temperature reversed direction depending on the priors used. Under vague priors, denser basal snow layers appeared to increase insulation (a negative association), whereas under informative priors they were linked to reduced insulation (a positive association). This instability suggests that the model cannot reliably estimate the influence of snow density on soil temperature without being guided by physically grounded prior knowledge.

Compared to physically based snow models, which simulate energy and mass exchange through mechanistic equations, the Bayesian statistical approach offers several advantages under Arctic field conditions. Physical models often struggle to represent key processes such as wind redistribution of snow, vapor flux, and fine-scale heterogeneity in snow layering and vegetation cover. These limitations can lead to large simulation errors, particularly when model parameters are poorly constrained by local observations. In contrast, Bayesian models estimate probabilistic relationships directly from observed data, while incorporating physical understanding through priors. They do not aim to simulate every process explicitly but instead focus on producing robust inference under uncertainty. This makes Bayesian methods especially well suited for Arctic environments where full process representation is infeasible. Lastly, the Bayesian models provided full posterior distributions for all parameters, supporting more nuanced inference and explicit uncertainty quantification (Figures A.12, A.13). Unlike traditional statistical approaches that rely on point estimates and strict assumptions, Bayesian methods can adapt flexibly to the structure and limitations of the available data, further enhancing model transparency and interpretability (Webb et al. 2010; Kruschke 2021).

Despite these strengths, several limitations should be acknowledged. Most fundamentally, the models are based on a single-day snapshot of snow and temperature conditions, which constrains inference about seasonal dynamics or cumulative effects. The limited number of TMS (14) also restricted the complexity of the model and reduced statistical power, particularly for categorical predictors such as vegetation and geomorphon class. As a result, some potentially meaningful differences may remain undetected. To advance beyond this limitation, future work should shift toward time series modeling that captures the evolution of snow insulation and soil thermal dynamics over the entire season. The current focus on a single day in April limits inference about temporal variation, yet snow-soil interactions unfold across months. Hierarchical Bayesian models are particularly suited for temporal extensions, as they can incorporate autocorrelation structures and model latent states developing through time (Gregory 2005).

Furthermore, model assumptions such as normality in the response distributions may be too restrictive. For instance, the soil temperature response to snow depth may flatten under deep snow due to insulation saturation, leading to nonlinear behavior that is not well captured by linear-normal models. Replacing the Gaussian likelihood with non-Gaussian models could better capture skewed or nonlinear responses in snow and soil temperatures, such as thresholds beyond which insulation effects plateau. This shift would help address cases where snow insulation effects are not linear but saturate or intensify abruptly. Similarly, the linear modeling framework complicates the interpretation of certain results,

particularly the effect of snow density. Including snow density as an additive linear predictor fails to capture the conditional nature of thermal conduction, where the effect of snow density depends on the direction of the temperature gradient. That is, the same density profile may either enhance or suppress warming depending on whether the soil is losing (winter) or gaining (spring) heat. Future models should address this by allowing snow density to modulate the strength of the coupling between air, snow, and soil temperatures. For example, snow density could interact with temperature gradients or be incorporated as a scaling factor on the regression coefficients linking air, snow, and surface temperatures. This would better reflect the nonlinear and state-dependent role of snow structure in controlling subsurface thermal dynamics. Another important modeling challenge is collinearity among predictors such as elevation, slope, aspect, and geomorphon class. While Bayesian shrinkage helps to regularize estimates, collinearity can still inflate uncertainty and obscure the effects of individual predictors (Webb et al. 2010).

Furthermore, spatial mismatch between snow and soil measurements limited the resolution of the models. SMP profiles were assigned to TMS sensors based on proximity, with distances ranging from less than a meter to over 40 m. This introduced spatial noise that likely weakened the ability to detect precise relationships between snow properties and soil temperatures. Reducing this mismatch through closer spatial alignment between snow and soil measurements would improve model sensitivity. However, co-locating snow and soil measurements is challenging in practice, as invasive snow profiling can disturb the snowpack directly above the temperature sensors. More precise placement, e.g. using tools like DGPS or clearly marked reference points along transects, could help minimize offsets without compromising the integrity of the snow or soil measurements. Furthermore, strategic sensor placement should also target diverse microtopographic settings (e.g., ridges, slopes, depressions) and vegetation types (e.g., shrub, grass, bare ground) to better capture landscape heterogeneity. Complementing this, expanding sensor coverage along elevational gradients and different slopes and aspects will help disentangle climatic and topographic influences on snowpack structure and soil thermal behavior. Increasing the frequency of snow measurements through automated profiling or repeated manual sampling would enable the resolution of temporal dynamics. These enhancements would improve the models abilities to quantify the respective roles of snow properties, vegetation, and topography in mediating soil temperatures.

Meteorological variables such as incoming radiation, wind speed, and precipitation are also key drivers of snowpack development and energy exchange at the snow-soil interface, which have not been included in the presented models. Their future inclusion could substantially enhance predictive accuracy, especially given their projected changes under climate warming. For example, rain-on-snow events – expected to increase by up to 40 % by the end of the century – can alter snow hardness and melt dynamics (Putkonen and Roe 2003). Climate projections for Disko Island suggest winter snowfall may increase, but this is unlikely to offset enhanced ablation due to warming (Bonsoms et al. 2024). At the same time, increased atmospheric moisture could lead to thicker snowpacks that delay ground freeze-up and intensify soil insulation in mid-winter (Pongracz et al. 2024).

Overall, while the models robustly capture the primary snow insulation effect and demonstrate the value of Bayesian approaches for small, uncertain datasets, future studies would benefit from expanded temporal coverage, increased sensor density, and improved spatial alignment of measurements to better resolve the drivers of snow-soil interactions.

6 Conclusion

This thesis investigated the interactions between snow depth and snow density and near-surface soil temperatures in a coastal Arctic tundra environment on Qeqertarsuaq, Kalaal-lit Nunaat. By combining SMP profiles, TMS temperature data, and detailed topographic and vegetation information with a Bayesian modeling framework, the study aimed to identify key controls on snowpack structure and its insulating effects during the late winter period of 2023/24.

The first objective was to determine whether the April snow profiles accurately reflected late-winter snowpack conditions. Given the relatively stable weather and minimal melting observed throughout the winter, the snowpack measured in April was deemed representative of the seasonal snow conditions.

The second objective focused on assessing the spatial variability of snow properties and near-surface soil temperatures. Results revealed substantial heterogeneity in both snow depth and density, as well as in soil temperatures, even across a landscape that appears relatively uniform in terms of topography and vegetation variability.

For the third objective of quantifying the relationship between snow density and soil temperatures, the two- and three-level Bayesian hierarchical models effectively captured broad patterns in temperature behavior and provided evidence that denser bottom layers were associated with reduced insulation of soil temperatures. This supports the hypothesis that snow density, not just depth, play a critical role in regulating soil thermal regimes.

In summary, these findings highlight the critical, yet underrepresented, role of snow density in controlling soil thermal regimes in Arctic environments. While current physical snow models often perform poorly in Arctic conditions due to inadequate representation of key processes such as wind-driven snow redistribution and vapor fluxes, this study demonstrates that Bayesian statistical approaches offer a promising alternative for understanding snow-soil thermal interactions. By building probabilistic, data-informed models that explicitly incorporate uncertainty and complexity, the Bayesian framework developed here provides a foundation for future modeling efforts.

Acknowledgement

This study would not have come together without the support of Julia Boike, Simone Stünzi, Bill Cable, and Ephraim Erkens. Our weekly meetings gave structure to my work, and I learned so much from each of you also beyond permafrost-related topics. Thank you for sharing your knowledge so generously.

I owe endless gratitude and respect to Brian Groenke, who I secretly called Brain Brian. He introduced me to Bayesian hierarchical modeling, guided me through its twists and turns, and somehow managed to stay incredibly patient and responsive no matter how chaotic I got. Thank you for always being available.

Lars Mewes wasn't always available, but when we did talk, his feedback led to major breakthroughs, thank you.

I'm also really grateful to Moritz, Jennika and Jannika for their help with feedback and QGIS issues.

And a special thanks to Jael Maenke: your thoughtful input, honesty, and shared moments of frustration helped me feel less lost more than once.

Moreover, I'm deeply thankful to the whole SPARC group at the Alfred Wegener Institute in Potsdam for welcoming me so warmly. Your passion and curiosity about the Arctic are genuinely inspiring. Thank you also to Tobias Sauter, who I think made my path to AWI easier.

This study also stands on the shoulders of many others. I want to acknowledge the scientists and staff at the Arctic Station (University of Copenhagen) in Qeqertarsuaq (arktiskstation.ku.dk) for their kind support during fieldwork. And to everyone whose field data and efforts built the foundation of this research, thank you.

All in all, I would like to sincerely thank everyone who supported me throughout this thesis. Your patience, understanding, and encouragement, especially during the uncertainty of my diagnosis, meant a lot to me. I am deeply grateful for the unique opportunity to work on this project and to prepare for a research stay in Greenland. As I write this today, I am still hopeful that I will have the chance to go. No matter the outcome, this experience has been invaluable, and I thank everyone who made it possible.

References

- Bartelt, P. and Lehning, M.: A Physical SNOWPACK Model for the Swiss Avalanche Warning: Part I: Numerical Model, Cold Regions Science and Technology, 35, 123–145, https://doi.org/10.1016/S0165-232X(02)00074-5, 2002.
- Bartsch, A., Efimova, A., Widhalm, B., Muri, X., von Baeckmann, C., Bergstedt, H., Ermokhina, K., Hugelius, G., Heim, B., and Leibman, M.: Circumarctic Land Cover Diversity Considering Wetness Gradients, Hydrology and Earth System Sciences, 28, 2421–2481, https://doi.org/10.5194/hess-28-2421-2024, 2024.
- Becker, L.: Analysis of micro-climate variation and feedbacks in an Arctic tundra land-scape on Disko Island, Western Greenland, 2024.
- Bellaire, S., Pielmeier, C., Schneebeli, M., and Schweizer, J.: Stability Algorithm for Snow Micro-Penetrometer Measurements, Journal of Glaciology, 55, 805–813, https://doi.org/10.3189/002214309790152582, 2009.
- Berliner, L. M., Milliff, R. F., and Wikle, C. K.: Bayesian Hierarchical Modeling of Air-Sea Interaction, Journal of Geophysical Research: Oceans, 108, https://doi.org/10.1029/2002JC001413, 2003.
- Blok, D., Elberling, B., and Michelsen, A.: Initial Stages of Tundra Shrub Litter Decomposition May Be Accelerated by Deeper Winter Snow But Slowed Down by Spring Warming, Ecosystems, 19, 155–169, https://doi.org/10.1007/s10021-015-9924-3, 2016.
- Boike, J., Chadburn, S., Martin, J., Zwieback, S., Althuizen, I. H., Anselm, N., Cai, L., Coulombe, S., Lee, H., Liljedahl, A. K., Schneebeli, M., Sjöberg, Y., Smith, N., Smith, S. L., Streletskiy, D. A., Stuenzi, S. M., Westermann, S., and Wilcox, E. J.: Standardized Monitoring of Permafrost Thaw: A User-Friendly, Multiparameter Protocol, Arctic Science, 8, 153–182, https://doi.org/10.1139/as-2021-0007, 2022.
- Boike, J., Stünzi, S. M., Gottuk, J., Bornemann, N., and Groenke, B.: Arctic Land Expeditions in Permafrost Research. The MOMENT Project: Expedition to the Arctic Station, Qeqertarsuaq, Disko Island and Ilulissat, West Greenland in 2022, https://doi.org/10.57738/BzPM_0782_2024, 2024.
- Bonsoms, J., Oliva, M., Alonso-González, E., Revuelto, J., and López-Moreno, J. I.: Impact of Climate Change on Snowpack Dynamics in Coastal Central-Western Greenland, Science of The Total Environment, 913, 169616, https://doi.org/10.1016/j.scitotenv. 2023.169616, 2024.
- Borges, D. H.: Snow accumulation patterns from 2023 Airborne Laser Scanning data in Trail Valley Creek, Western Canadian Arctic, 2024.
- Bormann, K. J., Westra, S., Evans, J. P., and McCabe, M. F.: Spatial and Temporal Variability in Seasonal Snow Density, Journal of Hydrology, 484, 63–73, https://doi.org/10.1016/j.jhydrol.2013.01.032, 2013.
- Callaghan, T., Christensen, T. R., and Jantze, E.: Plant and Vegetation Dynamics on Disko Island, West Greenland: Snapshots Separated by Over 40 Years, Ambio, 40, 624–37, https://doi.org/10.1007/s13280-011-0169-x, 2011.

- Calonne, N., Richter, B., Löwe, H., Cetti, C., ter Schure, J., Van Herwijnen, A., Fierz, C., Jaggi, M., and Schneebeli, M.: The RHOSSA Campaign: Multi-Resolution Monitoring of the Seasonal Evolution of the Structure and Mechanical Stability of an Alpine Snowpack, The Cryosphere, 14, 1829–1848, https://doi.org/10.5194/tc-14-1829-2020, 2020.
- Capretto, T., Piho, C., Kumar, R., Westfall, J., Yarkoni, T., and Martin, O. A.: Bambi: A Simple Interface for Fitting Bayesian Linear Models in Python, Journal of Statistical Software, 103, 1–29, https://doi.org/10.18637/jss.v103.i15, 2022.
- Damseaux, A., Matthes, H., Dutch, V. R., Wake, L., and Rutter, N.: Impact of Snow Thermal Conductivity Schemes on Pan-Arctic Permafrost Dynamics in the Community Land Model Version 5.0, The Cryosphere, 19, 1539–1558, https://doi.org/10.5194/tc-19-1539-2025, 2025.
- Domine, F., Barrere, M., Sarrazin, D., Morin, S., and Arnaud, L.: Automatic Monitoring of the Effective Thermal Conductivity of Snow in a Low-Arctic Shrub Tundra, The Cryosphere, 9, 1265–1276, https://doi.org/10.5194/tc-9-1265-2015, 2015.
- Domine, F., Lackner, G., Sarrazin, D., Poirier, M., and Belke-Brea, M.: Meteorological, Snow and Soil Data (2013–2019) from a Herb Tundra Permafrost Site at Bylot Island, Canadian High Arctic, for Driving and Testing Snow and Land Surface Models, Earth System Science Data, 13, 4331–4348, https://doi.org/10.5194/essd-13-4331-2021, 2021.
- Du, J., Kirchner, P. B., Pan, C. G., Watts, J. D., and Kimball, J. S.: Assessing Rain-on-Snow Event Dynamics over Alaska Using 30 Year Satellite Microwave Observations, Environmental Research Letters, 20, 034 048, https://doi.org/10.1088/1748-9326/adb9ff, 2025.
- Ekici, A., Chadburn, S., Chaudhary, N., Hajdu, L., Marmy, A., Peng, S., Boike, J., Burke, E., Friend, A., Hauck, C., Krinner, G., Langer, M., Miller, P., and Beer, C.: Sitelevel model intercomparison of high latitude and high altitude soil thermal dynamics in tundra and barren landscapes, The Cryosphere Discussions, 8, https://doi.org/10.5194/tcd-8-4959-2014, 2014.
- Estilow, T. W., Young, A. H., and Robinson, D. A.: A Long-Term Northern Hemisphere Snow Cover Extent Data Record for Climate Studies and Monitoring, Earth System Science Data, 7, 137–142, https://doi.org/10.5194/essd-7-137-2015, 2015.
- Gelman, A., Carlin, J. B., Stern, H. S., Dunson, D. B., Vehtari, A., and Rubin, D. B.: Bayesian Data Analysis, Chapman and Hall/CRC, 3 edn., https://doi.org/10.1201/b16018, 2013.
- Gelman, A., Vehtari, A., Simpson, D., Margossian, C. C., Carpenter, B., Yao, Y., Kennedy, L., Gabry, J., Bürkner, P.-C., and Modrák, M.: Bayesian Workflow, https://arxiv. org/abs/2011.01808, 2020.
- Goncharova, O. Y., Matyshak, G. V., Epstein, H. E., Sefilian, A. R., and Bobrik, A. A.: Influence of Snow Cover on Soil Temperatures: Meso- and Micro-Scale Topographic Effects (a Case Study from the Northern West Siberia Discontinuous Permafrost Zone), CATENA, 183, 104 224, https://doi.org/10.1016/j.catena.2019.104224, 2019.

- Gottuk, B., Stuenzi, M., Runge, T., and Boike, J.: Influence of Vegetation and Wetness on Arctic Snow-Free Albedo: Comparative Analysis of HLS, MODIS, and Weather Station Data Across Diverse Tundra Sites and Land Cover Types, Science of Remote Sensing, in review, 2025.
- Greenland Ecosystem Monitoring: GeoBasis Disko Meteorology AWS1-Meteorology, https://doi.org/10.17897/A22W-9Z72, accessed: 2025-07-01, 2020.
- Gregory, P.: Bayesian Logical Data Analysis for the Physical Sciences: A Comparative Approach with Mathematica® Support, Cambridge University Press, Cambridge, ISBN 9780521841504, 2005.
- Grünberg, I., Wilcox, E. J., Zwieback, S., Marsh, P., and Boike, J.: Linking Tundra Vegetation, Snow, Soil Temperature, and Permafrost, Biogeosciences, 17, 4261–4279, https://doi.org/10.5194/bg-17-4261-2020, 2020.
- Grünberg, I., Hollenbach Borges, D., Hammar, J., Rutter, N., Marsh, P., and Boike, J.: Snow on Permafrost: The Effect of Spatial Snow Variability on Soil Temperature in Trail Valley Creek, NWT, Canada, https://doi.org/10.5194/egusphere-egu24-17057, 2025.
- Hagenmuller, P. and Pilloix, T.: A New Method for Comparing and Matching Snow Profiles, Application for Profiles Measured by Penetrometers, Frontiers in Earth Science, 4, https://doi.org/10.3389/feart.2016.00052, 2016.
- Hagenmuller, P., Van Herwijnen, A., Pielmeier, C., and Marshall, H.-P.: Evaluation of the Snow Penetrometer Avatech SP2, Cold Regions Science and Technology, 149, 83–94, https://doi.org/10.1016/j.coldregions.2018.02.006, 2018.
- Hoffman, M. D. and Gelman, A.: The No-U-Turn Sampler: Adaptively Setting Path Lengths in Hamiltonian Monte Carlo, https://arxiv.org/abs/1111.4246, 2011.
- Hollesen, J., Elberling, B., and Jansson, P. E.: Future Active Layer Dynamics and Carbon Dioxide Production from Thawing Permafrost Layers in Northeast Greenland, Global Change Biology, 17, 911–926, https://doi.org/10.1111/j.1365-2486.2010.02256.x, 2011.
- Hollesen, J., Buchwal, A., Rachlewicz, G., Hansen, B. U., Hansen, M. O., Stecher, O., and Elberling, B.: Winter Warming as an Important Co-Driver for Betula Nana Growth in Western Greenland during the Past Century, Global Change Biology, 21, 2410–2423, https://doi.org/10.1111/gcb.12913, 2015.
- Huang, Y., Jiang, J., Ma, S., Ricciuto, D., Hanson, P. J., and Luo, Y.: Soil Thermal Dynamics, Snow Cover, and Frozen Depth under Five Temperature Treatments in an Ombrotrophic Bog: Constrained Forecast with Data Assimilation, Journal of Geophysical Research: Biogeosciences, 122, 2046–2063, https://doi.org/10.1002/2016JG003725, 2017.
- Humlum, O.: Active Layer Thermal Regime 1991–1996 at Qeqertarsuaq, Disko Island, Central West Greenland, Arctic and Alpine Research, 30, 295–305, https://doi.org/10.1080/00040851.1998.12002903, 1998.

- Jasiewicz, J. and Stepinski, T. F.: Geomorphons—a Pattern Recognition Approach to Classification and Mapping of Landforms, Geomorphology, 182, 147–156, 2013.
- Kaltenborn, J., Macfarlane, A. R., Clay, V., and Schneebeli, M.: Automatic Snow Type Classification of Snow Micropenetrometer Profiles with Machine Learning Algorithms, Geoscientific Model Development, 16, 4521–4550, https://doi.org/10.5194/ gmd-16-4521-2023, 2023.
- King, J., Howell, S., Brady, M., Toose, P., Derksen, C., Haas, C., and Beckers, J.: Local-Scale Variability of Snow Density on Arctic Sea Ice, The Cryosphere, 14, 4323–4339, https://doi.org/10.5194/tc-14-4323-2020, 2020.
- Krab, E. J., Lundin, E. J., Coulson, S. J., Dorrepaal, E., and Cooper, E. J.: Experimentally Increased Snow Depth Affects High Arctic Microarthropods Inconsistently over Two Consecutive Winters, Scientific Reports, 12, 18049, https://doi.org/10.1038/s41598-022-22591-5, 2022.
- Kruschke, J.: Bayesian Analysis Reporting Guidelines, Nature Human Behaviour, 5, 1282–1291, https://doi.org/10.1038/s41562-021-01177-7, 2021.
- König, M. and Sturm, M.: Mapping Snow Distribution in the Alaskan Arctic Using Aerial Photography and Topographic Relationships, Water Resources Research, 34, 3471–3483, https://doi.org/10.1029/98WR02514, 1998.
- Larose, C., Dommergue, A., and Vogel, T. M.: The Dynamic Arctic Snow Pack: An Unexplored Environment for Microbial Diversity and Activity, Biology, 2, 317–330, https://doi.org/10.3390/biology2010317, 2013.
- Lawrence, D. M. and Slater, A. G.: The Contribution of Snow Condition Trends to Future Ground Climate, Climate Dynamics, 34, 969–981, https://doi.org/10.1007/s00382-009-0537-4, 2010.
- Liston, G. and Sturm, M.: A snow-transport model for complex terrain, Journal of Glaciology, 44, 498–516, https://doi.org/10.3189/s0022143000002021, 1998.
- Liu, Y., Hansen, B. U., Elberling, B., and Westergaard-Nielsen, A.: Snow Depth and the Associated Offset in Ground Temperatures in a Landscape Manipulated with Snow-Fences, Geoderma, 438, 116632, https://doi.org/10.1016/j.geoderma.2023.116632, 2023.
- Macfarlane, A. R., Löwe, H., Gimenes, L., Wagner, D. N., Dadic, R., Ottersberg, R., Hämmerle, S., and Schneebeli, M.: Temporospatial Variability of Snow's Thermal Conductivity on Arctic Sea Ice, The Cryosphere, 17, 5417–5434, https://doi.org/10.5194/tc-17-5417-2023, 2023.
- Marchand, N., Royer, A., Krinner, G., Roy, A., Langlois, A., and Vargel, C.: Snow-Covered Soil Temperature Retrieval in Canadian Arctic Permafrost Areas, Using a Land Surface Scheme Informed with Satellite Remote Sensing Data, Remote Sensing, 10, 1703, https://doi.org/10.3390/rs10111703, 2018.

- Meløysund, V., Leira, B., Høiseth, K. V., and Lisø, K. R.: Predicting Snow Density Using Meteorological Data, Meteorological Applications, 14, 413–423, https://doi.org/10.1002/met.40, 2007.
- Mewes, L.: Snow density and SSA measurements on Disko Island using the SnowMicroPen (Gen5), unpublished metadata document, April 2024, Swiss Federal Institute for Forest, Snow and Landscape Research (SLF), 2024.
- Mudryk, L., Elias Chereque, A., Derksen, C., Luojus, K., and Decharme, B.: Terrestrial Snow Cover, NOAA Arctic Report Card: Update for 2022, https://www.arctic.noaa.gov/report-card/report-card-2022/terrestrial-snow-cover/, accessed: 2025-07-08, 2022.
- Nielsen, C. S., Michelsen, A., Strobel, B. W., Wulff, K., Banyasz, I., and Elberling, B.: Correlations between Substrate Availability, Dissolved CH4, and CH4 Emissions in an Arctic Wetland Subject to Warming and Plant Removal, Journal of Geophysical Research: Biogeosciences, 122, 645–660, https://doi.org/10.1002/2016JG003511, 2017.
- Overduin, P. P., Boike, J., Kane, D. L., and Westermann, S.: Soil Temperatures Under a Range of Organic and Snow Covers, in: EPIC3American Geophysical Union Fall Meeting, December 10-14, 2007, San Francisco, CA, USA, 2007.
- Paradis, M., Lévesque, E., and Boudreau, S.: Greater Effect of Increasing Shrub Height on Winter versus Summer Soil Temperature, Environmental Research Letters, 11, 085 005, https://doi.org/10.1088/1748-9326/11/8/085005, 2016.
- Patil, A., Carpenter, B., Gelman, A., Salvatier, J., Wiecki, T. V., Fonnesbeck, C., and Martin, O.: PyMC: Probabilistic Programming in Python, https://www.pymc.io/, 2023.
- Peng, X., Frauenfeld, O. W., Huang, Y., Chen, G., Wei, G., Li, X., Tian, W., Yang, G., Zhao, Y., and Mu, C.: The Thermal Effect of Snow Cover on Ground Surface Temperature in the Northern Hemisphere, Environmental Research Letters, 19, 044 015, https://doi.org/10.1088/1748-9326/ad30a5, 2024.
- Pertermann, I.: Comparison of Formulae Heat Conductivity and Density of Snow, Miscellaneous Topics from the Background Report for the Review of EN 13031: Greenhouses, 2017.
- Pomeroy, J. W. and Brun, E.: Physical Properties of Snow, in: SpringerReference, Springer-Verlag, Berlin/Heidelberg, https://doi.org/10.1007/SpringerReference_225906, 2011.
- Pongracz, A., Wårlind, D., Miller, P. A., Gustafson, A., Rabin, S. S., and Parmentier, F.-J. W.: Warming-Induced Contrasts in Snow Depth Drive the Future Trajectory of Soil Carbon Loss across the Arctic-Boreal Region, Communications Earth & Environment, 5, 1–7, https://doi.org/10.1038/s43247-024-01838-1, 2024.
- Proksch, M., Löwe, H., and Schneebeli, M.: Density, Specific Surface Area, and Correlation Length of Snow Measured by High-Resolution Penetrometry, Journal of Geophysical Research: Earth Surface, 120, 346–362, https://doi.org/10.1002/2014JF003266, 2015.

- Putkonen, J. and Roe, G.: Rain-on-Snow Events Impact Soil Temperatures and Affect Ungulate Survival, Geophysical Research Letters, 30, https://doi.org/10.1029/2002GL016326, 2003.
- Python Software Foundation: Python, https://www.python.org/, 2023.
- QGIS Development Team: QGIS Geographic Information System, https://qgis.org, version 3.6, Open Source Geospatial Foundation, 2019.
- Rantanen, M., Karpechko, A. Y., Lipponen, A., Nordling, K., Hyvärinen, O., Ruosteenoja, K., Vihma, T., and Laaksonen, A.: The Arctic Has Warmed Nearly Four Times Faster than the Globe since 1979, Communications Earth & Environment, 3, 1–10, https://doi.org/10.1038/s43247-022-00498-3, 2022.
- Rasmussen, L. H., Zhang, W., Ambus, P., Michelsen, A., Jansson, P.-E., Kitzler, B., and Elberling, B.: Nitrogen Transport in a Tundra Landscape: The Effects of Early and Late Growing Season Lateral N Inputs on Arctic Soil and Plant N Pools and N2O Fluxes, Biogeochemistry, 157, 69–84, https://doi.org/10.1007/s10533-021-00855-y, 2022.
- Rixen, C., Høye, T. T., Macek, P., Aerts, R., Alatalo, J. M., Anderson, J. T., Arnold, P. A., Barrio, I. C., Bjerke, J. W., Björkman, M. P., Blok, D., Blume-Werry, G., Boike, J., Bokhorst, S., Carbognani, M., Christiansen, C. T., Convey, P., Cooper, E. J., Cornelissen, J. H. C., Coulson, S. J., Dorrepaal, E., Elberling, B., Elmendorf, S. C., Elphinstone, C., Forte, T. G., Frei, E. R., Geange, S. R., Gehrmann, F., Gibson, C., Grogan, P., Halbritter, A. H., Harte, J., Henry, G. H., Inouye, D. W., Irwin, R. E., Jespersen, G., Jónsdóttir, I. S., Jung, J. Y., Klinges, D. H., Kudo, G., Lämsä, J., Lee, H., Lembrechts, J. J., Lett, S., Lynn, J. S., Mann, H. M., Mastepanov, M., Morse, J., Myers-Smith, I. H., Olofsson, J., Paavola, R., Petraglia, A., Phoenix, G. K., Semenchuk, P., Siewert, M. B., Slatyer, R., Spasojevic, M. J., Suding, K., Sullivan, P., Thompson, K. L., Väisänen, M., Vandvik, V., Venn, S., Walz, J., Way, R., Welker, J. M., Wipf, S., and Zong, S.: Winters Are Changing: Snow Effects on Arctic and Alpine Tundra Ecosystems, Arctic Science, 8, 572–608, https://doi.org/10.1139/as-2020-0058, 2022.
- Schneebeli, M., Pielmeier, C., and Johnson, J. B.: Measuring Snow Microstructure and Hardness Using a High Resolution Penetrometer, Cold Regions Science and Technology, 30, 101–114, https://doi.org/10.1016/S0165-232X(99)00030-0, 1999.
- Schweizer, J., Kronholm, K., Jamieson, J. B., and Birkeland, K. W.: Review of Spatial Variability of Snowpack Properties and Its Importance for Avalanche Formation, Cold Regions Science and Technology, 51, 253–272, https://doi.org/10.1016/j.coldregions. 2007.04.009, 2008.
- Shirley, I., Uhlemann, S., Peterson, J., Bennett, K., Hubbard, S. S., and Dafflon, B.: Disentangling the Impacts of Microtopography and Shrub Distribution on Snow Depth in a Subarctic Watershed: Toward a Predictive Understanding of Snow Spatial Variability, Journal of Geophysical Research: Biogeosciences, 130, e2024JG008604, https://doi.org/10.1029/2024JG008604, 2025.
- Slater, A. G., Pitman, A. J., and Desborough, C. E.: The Validation of a Snow Parameterization Designed for Use in General Circulation Models, International Journal of

- Climatology, 18, 595–617, https://doi.org/10.1002/(SICI)1097-0088(199805)18:6 \langle 595:: AID-JOC275 \rangle 3.0.CO;2-O, 1998.
- Slater, A. G., Lawrence, D. M., and Koven, C. D.: Process-Level Model Evaluation: A Snow and Heat Transfer Metric, The Cryosphere, 11, 989–996, https://doi.org/10.5194/tc-11-989-2017, 2017.
- Steffens, C., Beer, C., and Kutzbach, L.: Expedition Report 2023 of the Projects MO-MENT and CLICCS A1, https://doi.org/10.5281/zenodo.15720240, zenodo, 2025.
- Sturm, M. and Holmgren, J.: Effects of microtopography on texture, temperature and heat flow in Arctic and sub-Arctic snow, Annals of Glaciology, 19, 63–68, https://doi.org/10.3189/1994aog19-1-63-68, 1994.
- Sturm, M. and Johnson, J. B.: Thermal Conductivity Measurements of Depth Hoar, Journal of Geophysical Research: Solid Earth, 97, 2129–2139, https://doi.org/10.1029/91JB02685, 1992.
- Sturm, M., Holmgren, J., and Liston, G. E.: A Seasonal Snow Cover Classification System for Local to Global Applications, Journal of Climate, 8, 1261–1283, https://doi.org/10.1175/1520-0442(1995)008(1261:ASSCCS)2.0.CO;2, 1995.
- Sturm, M., Holmgren, J., McFadden, J. P., Liston, G. E., Chapin, F. S., and Racine, C. H.: Snow—Shrub Interactions in Arctic Tundra: A Hypothesis with Climatic Implications, Journal of Climate, 14, 336–344, https://doi.org/10.1175/1520-0442(2001)014\langle0336: SSIIAT\langle2.0.CO;2, 2001.
- Tan, X., Luo, S., Li, H., Hao, X., Wang, J., Dong, Q., and Chen, Z.: Investigating the Effects of Snow Cover and Vegetation on Soil Temperature Using Remote Sensing Indicators in the Three River Source Region, China, Remote Sensing, 14, 4114, https://doi.org/10.3390/rs14164114, 2022.
- Taras, B., Sturm, M., and Liston, G. E.: Snow–Ground Interface Temperatures in the Kuparuk River Basin, Arctic Alaska: Measurements and Model, Journal of Hydrometeorology, 3, 377–394, https://doi.org/10.1175/1525-7541(2002)003\(0377:SGITIT\)2.0.CO;2, 2002.
- Van Tatenhove, F. G. M. and Olesen, O. B.: Ground temperature and related permafrost characteristics in west greenland, Permafrost and Periglacial Processes, 5, 199–215, https://doi.org/https://doi.org/10.1002/ppp.3430050402, 1994.
- Vehtari, A., Gelman, A., and Gabry, J.: Practical Bayesian Model Evaluation Using Leave-One-out Cross-Validation and WAIC, Statistics and Computing, 27, 1413–1432, https://doi.org/10.1007/s11222-016-9696-4, 2017.
- Vionnet, V., Brun, E., Morin, S., Boone, A., Faroux, S., Le Moigne, P., Martin, E., and Willemet, J.-M.: The Detailed Snowpack Scheme Crocus and Its Implementation in SURFEX v7.2, Geoscientific Model Development, 5, 773–791, https://doi.org/10.5194/ gmd-5-773-2012, 2012.

- von Oppen, J., Assmann, J. J., Bjorkman, A. D., Treier, U. A., Elberling, B., Nabe-Nielsen, J., and Normand, S.: Cross-Scale Regulation of Seasonal Microclimate by Vegetation and Snow in the Arctic Tundra, Global Change Biology, 28, 7296–7312, https://doi.org/10.1111/gcb.16426, 2022.
- Webb, J. A., Stewardson, M. J., and Koster, W. M.: Detecting ecological responses to flow variation using Bayesian hierarchical models, Freshwater Biology, 55, 108–126, https://doi.org/https://doi.org/10.1111/j.1365-2427.2009.02205.x, 2010.
- Wever, N., Keenan, E., Amory, C., Lehning, M., Sigmund, A., Huwald, H., and Lenaerts, J. T. M.: Observations and Simulations of New Snow Density in the Drifting Snow-Dominated Environment of Antarctica, Journal of Glaciology, 69, 823–840, https://doi.org/10.1017/jog.2022.102, 2023.
- Wild, J., Kopecký, M., Macek, M., Šanda, M., Jankovec, J., and Haase, T.: Climate at Ecologically Relevant Scales: A New Temperature and Soil Moisture Logger for Long-Term Microclimate Measurement, Agricultural and Forest Meteorology, 268, 40–47, https://doi.org/10.1016/j.agrformet.2018.12.018, 2019.
- Woolley, G. J., Rutter, N., Wake, L., Vionnet, V., Derksen, C., Essery, R., Marsh, P., Tutton, R., Walker, B., Lafaysse, M., and Pritchard, D.: Multi-Physics Ensemble Modelling of Arctic Tundra Snowpack Properties, The Cryosphere, 18, 5685–5711, https://doi.org/10.5194/tc-18-5685-2024, 2024.
- WSL Institute for Snow and Avalanche Research SLF: SnowMicroPen® 5 User Manual, URL: https://www.slf.ch/fileadmin/user_upload/SLF/Services_Produkte/Forschungsgeraete/SMP5/SMP5_UserManual_v5-0.pdf, accessed: 2025-05-12, 2023.
- Xu, W., Prieme, A., Cooper, E. J., Mörsdorf, M. A., Semenchuk, P., Elberling, B., Grogan, P., and Ambus, P. L.: Deepened Snow Enhances Gross Nitrogen Cycling among Pan-Arctic Tundra Soils during Both Winter and Summer, Soil Biology and Biochemistry, 160, 108 356, https://doi.org/10.1016/j.soilbio.2021.108356, 2021.
- Zhang, T.: Influence of the Seasonal Snow Cover on the Ground Thermal Regime: An Overview, Reviews of Geophysics, 43, https://doi.org/10.1029/2004RG000157, 2005.
- Zhang, W., Jansson, P.-E., Sigsgaard, C., McConnell, A., Jammet, M. M., Westergaard-Nielsen, A., Lund, M., Friborg, T., Michelsen, A., and Elberling, B.: Model-Data Fusion to Assess Year-Round CO2 Fluxes for an Arctic Heath Ecosystem in West Greenland (69°N), Agricultural and Forest Meteorology, 272–273, 176–186, https://doi.org/10.1016/j.agrformet.2019.02.021, 2019.
- Zhao, W., Mu, C., Wu, X., Zhong, X., Peng, X., Liu, Y., Sun, Y., Liang, B., and Zhang, T.: Spatio-Temporal Characteristics and Differences in Snow Density between the Tibet Plateau and the Arctic, Remote Sensing, 15, https://doi.org/10.3390/rs15163976, 2023.

A Extended methodology

The following section provides a detailed description of the data sets, data collection, processing, and analysis.

A.1 Data sets

Table A.1: Sensors used for field measurements. AWS2 refers to the automatic weather station installed at the study site, which recorded meteorological data during the field campaign.

Sensor	Brand / Model	Measurement	Accuracy	
Air Temperature (AWS2)	Vaisala HMP115A	Air temperature	$\pm (0.226$ - $0.0028 \times \text{temperature})^{\circ}\text{C}$ (-80 to $+20^{\circ}\text{C}$)	
Precipitation (AWS2)	RM Young 52203	Liquid precipitation (unheated tipping bucket)	2% up to 25 mm/h; $3%$ up to 50 mm/h	
Wind speed and direction (AWS2)	RM Young 05108-45	Wind speed and direction	Speed: ± 0.3 m/s or 1% of reading; Direction: $\pm 3^{\circ}$	
TMS sensor	TOMST, TMS-4	Soil, surface, and snow temperature at 3 depths	$\pm 0.5 ^{\circ}\text{C} (-40 \text{to} 60 ^{\circ}\text{C})$ (MAX31850 sensor)	
Snow Micro Pen (SMP)	WSL, SMP5	Penetration resistance profile	Resolution: 0.3 mm; Force: 0.01 N (0-50 N)	
MagnaProbe	SnowHydro, Mag- naProbe	Snow depth	±1 cm	

A.1.1 Snow measurements

Snow density can be derived from snow hardness which can be obtained from manual measurements or penetrometers (Hagenmuller and Pilloix 2016). Manual measurements from snow pits are operator biased and time consuming (Kaltenborn et al. 2023). In contrast, the SnowMicroPen (SMP), a portable high resolution penetrometer, developed by Schneebeli et al. (1999) measures snow stratigraphy of a meter profile in less than a minute (Proksch et al. 2015). The SMP determines the bond strength between snow grains within the snowpack. The bond strength can be obtained from the penetration resistance and is directly influenced by the micro-structural properties of snow, such as density and surface area. For example, high-density snow has a higher bond strength and consequently a higher penetration resistance than low-density snow (Kaltenborn et al. 2023). Hence, the force signal can be used to infer snow structural parameters such as density or specific surface area. The device consists of a conic measurement tip with a 60° included angle which is connected to a force transducer in a drive cone. The force transducer ranges from 0 N to 52 N (WSL Institute for Snow and Avalanche Research SLF 2023). A rotary motor drives the rod up to 1.2 m into the snowpack at a constant penetration velocity of 20 mm s⁻¹. The motor is fixed above the snow surface by ski poles (Schneebeli et al. 1999; Hagenmuller et al. 2018). The penetrometer acquires a force measurement every 4 µm (i.e., 250 mm⁻¹) (Schneebeli et al. 1999). Each SMP profile consists of the penetration force signal at the measurement tip in Newtons along its depth signal (Kaltenborn et al. 2023). The force sensor's resolution is 0.01 N, and the depth accuracy is estimated to be $1\,\mathrm{cm}$.

During a field campaign in April 2024, 224 snow profiles were conducted across three transects in Kuup Ilua (Blæsedalen valley), using the fifth generation SnowMicroPen. For each profile, an additional GNSS measurement was performed using Emild GNSS. An Emlid Reach M+ was used as a rover and connected to the SMP. It received real-time kinematic corrected position information from the base, an Emlid RS2+. Thereby, the position estimates of the profiles were improved from 2 m to 3 m accuracy to a few centimeters accuracy during post-processing. Another essential post-processing step involved the combination of multiple SMP signals into complete profiles. This was necessary as there were layers within the snowpack (likely ice layers) that could not be penetrated by the SMP due to their hardness. At these points, the snow profile measurement was continued after carefully breaking the hard layer with an avalanche probe. During post-processing, the individual measurements were stitched into one profile. This leads to the following implications: 1) Some layers of the SMP profile are missing (NAs), 2) the properties of these layers, specifically their density and height are unknown, 3) by breaking hard layers with an avalanche probe, snow properties directly below might have been altered. I decided to keep the missing values in the profiles, since treating the resulting sequence of missing values as ice layers with a respective density of $917 \,\mathrm{kg}\,\mathrm{m}^{-3}$ was not adequate because of their different length. Ice layer thickness would have likely ranged between 1 cm to 2 cm; however, there were longer sequences (up to 8 cm) of NAs within the profiles.

Lastly, I converted the penetration force signal into density using algorithms provided by the SnowMicroPyn software (Mewes 2024). As there are different algorithms to derive snow properties from the penetration force signal, I compared deviations from Proksch et al. (2015), Calonne et al. (2020) and King et al. (2020) with manual measurements from five snow pits to choose the best fitting algorithm and validated the data (Figure A.1). I selected the closest SMP profile to each snow pit and averaged its density for the depth interval of each sample in the snow pit. Then, I compared the density estimations of the derivatives to the manual measurements and calculated R² and SD of each derivative (Table A.2).

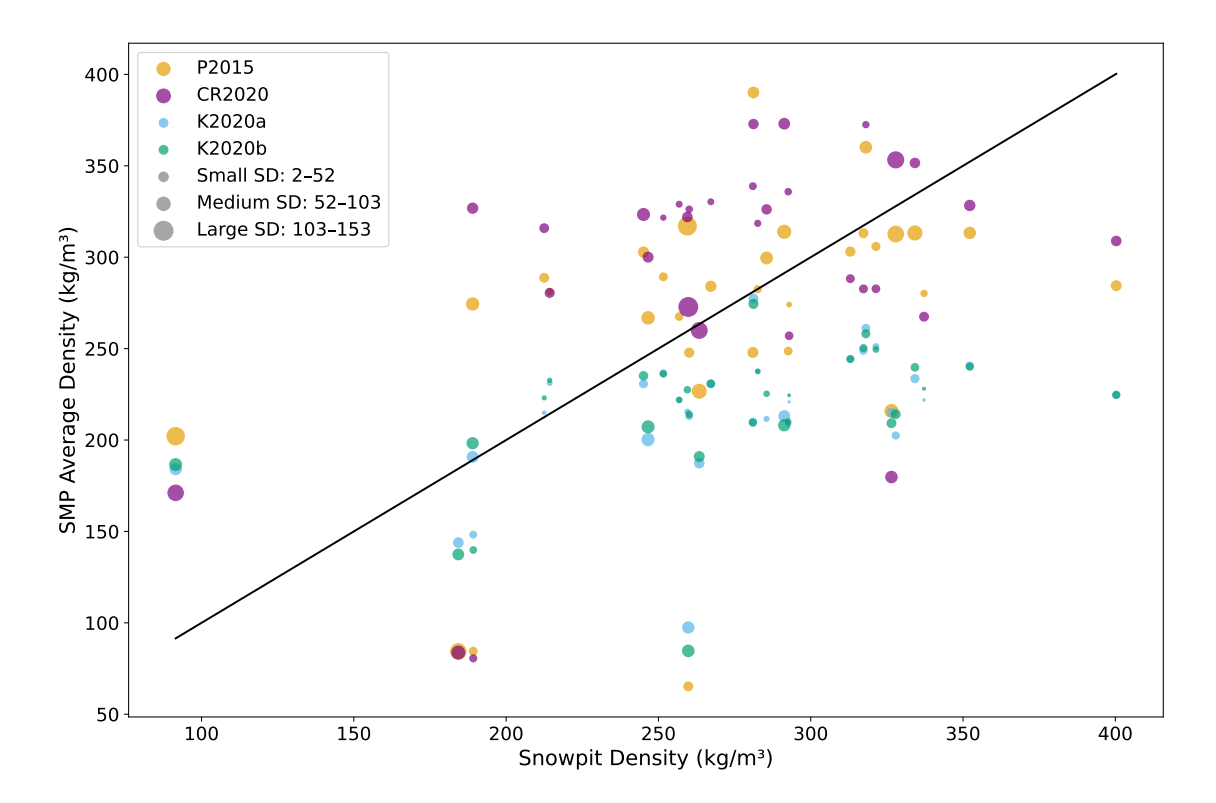


Figure A.1: Selection of Derivative. Comparison of snow pit density and SnowMicroPen (SMP) average density for density estimation algorithms by Proksch et al. (2015), Calonne et al. (2020) and King et al. (2020). Point size represents the standard deviation of SMP density within each snow pit depth interval, categorized into small, medium, and large SD ranges. The black diagonal line indicates a 1:1 relationship between snow pit and SMP densities.

Table A.2: SMP derivatives statistics. Coefficient of determination (R^2) quantifies the linear relationship between SMP and snow pit densities. Standard deviation (SD) reflects the variability in SMP-derived densities within each snow pit depth interval.

Derivative	\mathbb{R}^2	$SD (kg/m^3)$	Publication
P2015	-0.341	52	Proksch et al. (2015)
CR2020	-0.456	43	Calonne et al. (2020)
K2020a	-0.781	24	King et al. (2020)
K2020b	-0.773	26	King et al. (2020)

Based on my results, I used densities obtained from the algorithm of Proksch et al. (2015). The statistical model developed in this approach was calibrated by combining SMP data with 3D micro structural data from micro computed tomography from alpine, arctic and antarctic snow profiles. The density derived from the SMP had a mean relative error of 10.6 %. Within the derived data, I recognized invalid density values outside the possible physical range. These values can stem from errors in the force signal. For instance, large temperature changes during the measurements may cause signal drift (Bellaire et al. 2009). Furthermore, the piezoelectric force sensor captures not only compression but also tensile forces. Negative peaks result from sudden changes of snow hardness from soft to hard snow, where the sensor is exposed to compression forces and shear forces. Other reasons leading to negative force signals can be a bent or broken tooth of the cogwheel or movement of the rod during the measurement (WSL Institute for Snow and Avalanche Research SLF 2023).

However, I also obtained invalid density values for profiles in which the force signal was not negative / erroneous, in other words, where the deviation methods yielded wrong values. Different derivation methods applied to the raw force signal produce markedly different results, especially at force peaks where small variations in the calculation approach lead to large discrepancies in estimated densities (Figure A.2).

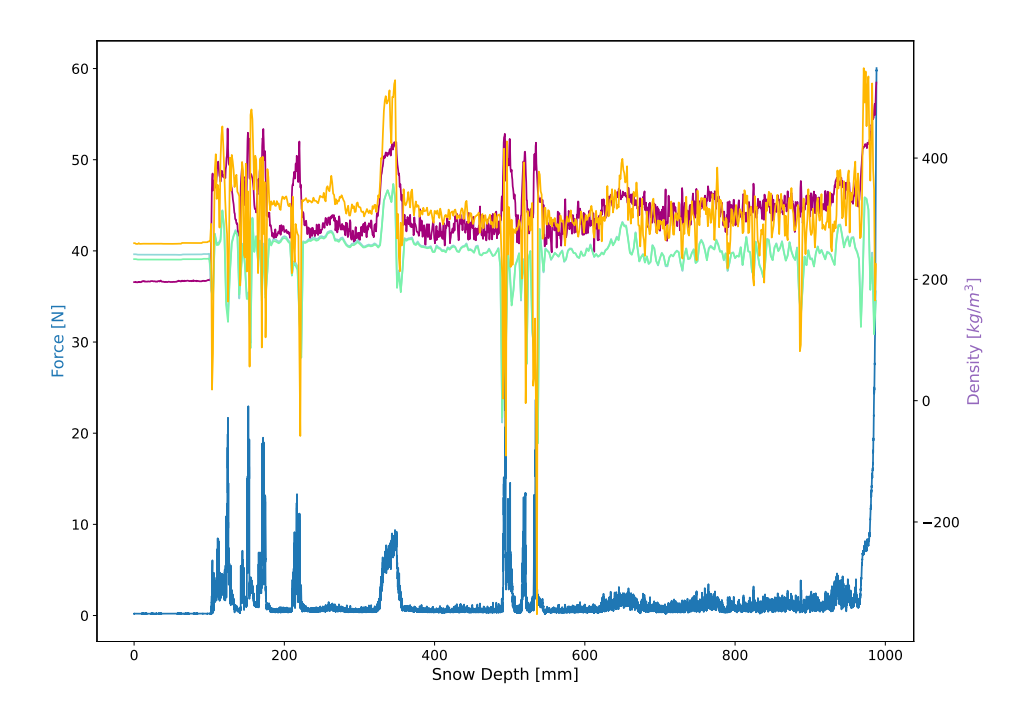


Figure A.2: Comparison of snow density derivations from different deviation algorithms. Density profiles derived from the force signal (blue) using calculation methods after Proksch et al. (2015) P2015 (orange), Calonne et al. (2020) CR2020 (purple), King et al. (2020) K2020a (light blue), K2020b (light green). Substantial differences at force peaks lead to discrepancies in both peak magnitude and profile shape, influencing the interpretation of snow density.

As all four deviation methods included invalid density estimations, I adhered to the Proksch et al. (2015) algorithm, since its density distribution aligned best with the observed density values from the snow pits (Table A.3). I handled invalid values within the derived data by removing all densities outside $0\,\mathrm{kg}\,\mathrm{m}^{-3}$ to $917\,\mathrm{kg}\,\mathrm{m}^{-3}$. It is important to note that the derived data were analyzed in a relative context rather than an absolute one. Absolute values are not suitable for direct comparisons between different sites, due to the mentioned differences between the derivation methods.

Table A.3: Summary statistics of snow density derivation methods. Mean, standard deviation (SD), and percentiles (25%, 50%, 75%) for snowpit and SMP-derived snow densities $[kg/m^3]$.

Statistic	Snowpit	P2015	CR2020	K2020a	K2020b
Mean	272	299	318	228	230
SD	57	125	83	89	101
25%	246	264	289	211	215
50%	281	286	321	226	229
75%	314	336	354	252	252

To validate snow depth data, I compared the measurements of the SMP to MagnaProbe measurements, which were taken on the same days along the same transects. Based on their coordinates, I paired the closest SMP and MagnaProbe measurements, to compare their recorded snow depths (Figure A.3). Overall, the measurements aligned well. However, because the SMP rod is limited to a maximum length of 1.20 m and was positioned approximately 10 cm above the snow surface, the effective measurement range was approximately 1.10 m. As a result, large deviations occurred in deeper snowpacks, where MagnaProbe recorded snow depths up to 2.43 m.

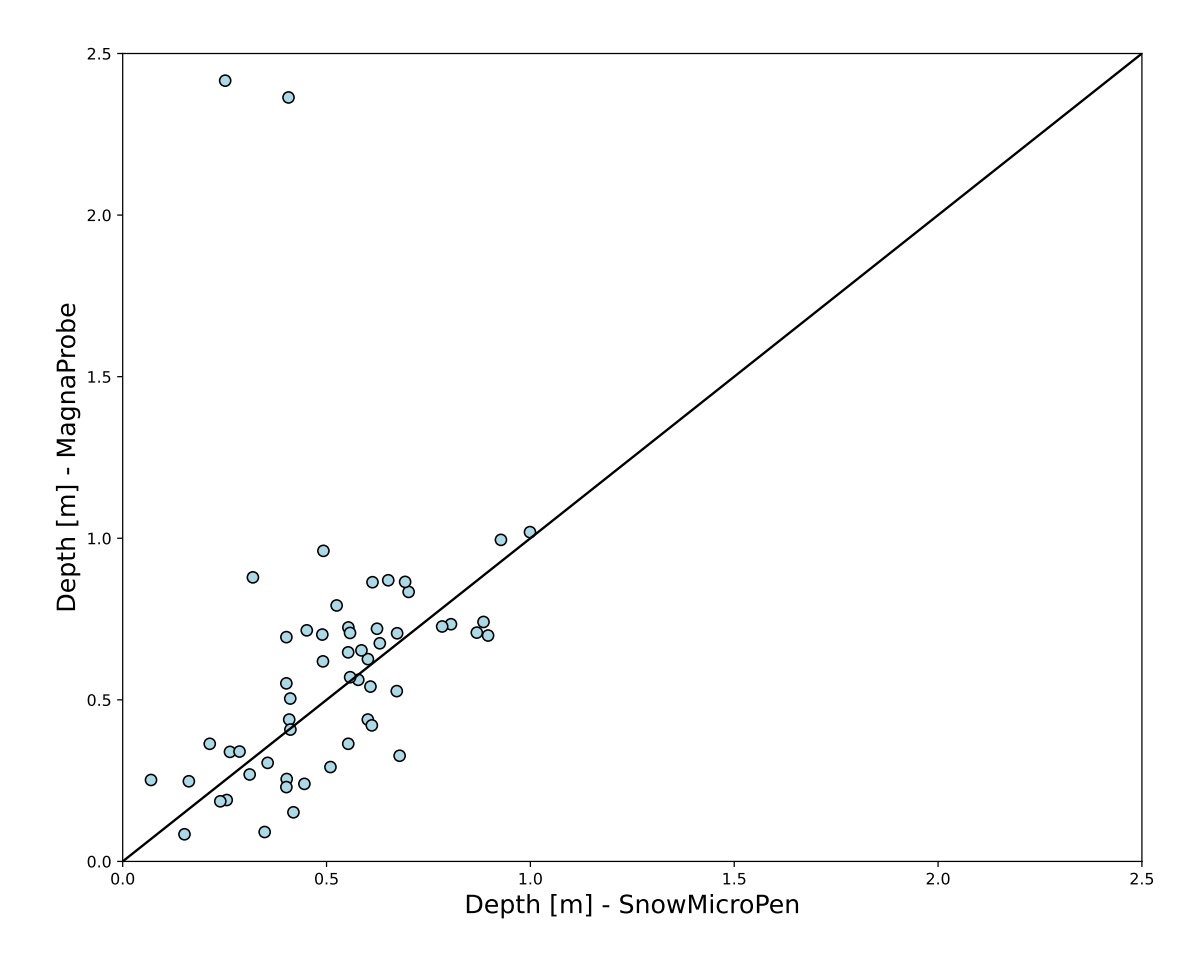


Figure A.3: Snow depth comparison. Comparison of snow depth measured by the MagnaProbe (x-axis) and SnowMicroPen (y-axis). The black line indicates a 1:1 relationship between the two measurement methods.

A.1.2 Temperature measurements

Snow, soil surface, and subsurface soil temperatures were recorded using TOMST TMS-4 temperature and moisture sensors (Wild et al. 2019). Each sensor contains three digital thermometers (DS7505U+; www.maximintegrated.com) and is designed to mimic the structure of a small herbaceous plant. The sensors recorded temperatures at 15-minute intervals at three positions: 16 cm above the surface (snow layer), directly at the surface (snow / soil interface), and 6 cm below the surface (soil temperature). According to the manufacturer, the sensors have a resolution of 0.0625 °C and an accuracy of ± 0.5 °C. To improve accuracy, all sensors were calibrated in an ice-bath before installation. Each sensor was placed in a 0 °C ice-bath until its readings stabilized. The difference between the observed and expected value (0 °C) was recorded as the sensor's individual measurement error. These offsets were then subtracted from the raw data to produce a calibrated temperature time series, which was used for all further analyses.

A.1.3 Topography

I used a digital terrain model (DTM, GRL_Qeqertarsuaq_0m50_L1_DTM_001_EGM96.tif © 2024 Maxar Technologies) provided by the German Federal Agency for Cartography and Geodesy's Satellite Based Crisis and Situation Service (Bundesamt für Kartographie und Geodäsie (BKG), Satellitengestützter Krisen- und Lagedienst (SKD)). The DTM has a horizontal resolution of 0.5 m, and was derived from WorldView-3 optical satellite imagery in stereo configuration using the Semi-Global Matching photogrammetric algorithm developed by the German Aerospace Center (Deutsches Zentrum für Luft- und Raumfahrt). To improve the relative alignment, image geometry was refined with 243 tie points. According to the provider, the native accuracy of the WorldView-3 data is less than 3.5 m vertically and less than 5 m horizontally. The final DTM was created by applying ground-point masks to exclude surface features such as vegetation and buildings. Additionally, I calculated the slope using the terrain analysis tool included in QGIS (QGIS Development Team 2019). The DEM has previously been used to classify the terrain into topographic landforms, termed Geomorphons (Jasiewicz and Stepinski 2013). For the detailed description and application of the method, see Becker (2024). The TMS sites cover the geomorphon types: hollow/footslope, slope, and valley/depression (Figure A.4).

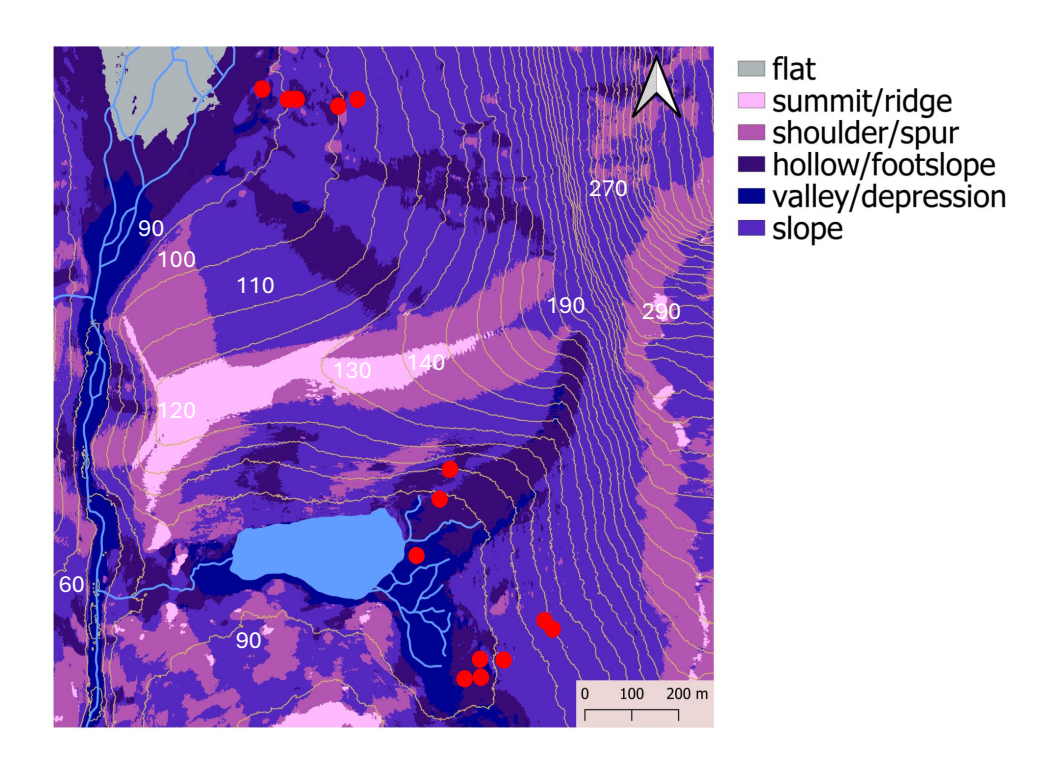


Figure A.4: Digital Terrain Model of the Study Area. Topographic overview of Blæsedalen in the south of Disko Island, showing TMS locations (red points) overlaid on geomorphon landform classifications and 10 m elevation contour lines. Hydrological features: von Oppen et al. (2022). DTM License: Based on material by Maxar Products. GRL_Qeqertarsuaq_0m50_L1_DTM_001_EGM96.tif © 2024 Maxar Technologies, including material by AW3D Enhanced, AW3D Metro, AW3D Standard and AW3D Telecom Products. GRL_Qeqertarsuaq_0m50_L1_DTM_001_EGM96.tif © 2024 NTT Data Corporation and by Ecopia Building Footprints Powered by Maxar. Ecopia Building Footprints © 2024 Ecopia Tech Corporation. Imagery © 2024 Maxar Technologies, provided by BKG and BMI, all rights reserved.

A.1.4 Vegetation

I used an adjusted version of the circumpolar land cover unit map by Bartsch et al. (2024) to categorize the vegetation around each TMS. The initial map provides three types of wetland and 14 terrestrial tundra units based on shrub physiognomy and soil moisture, at a resolution of $10 \times 10 \,\mathrm{m}$. For previous studies, Gottuk et al. (2025) aggregated and validated the vegetation units using vegetation records from September 2023, where vegetation cover was assessed in a $1 \times 1 \,\mathrm{m}$ plot around each TMS (Boike et al. 2024) (Figure A.5 and Figure A.6). Within each plot, vegetation heights ranging from $1.5 \,\mathrm{cm}$ to $20 \,\mathrm{cm}$ (mean $8.1 \,\mathrm{cm}$, SD $3.3 \,\mathrm{cm}$) were recorded at four points according to the standardized permafrost monitoring protocol (Boike et al. 2022). In summary, the TMS locations feature three different vegetation classes: dry tundra, moist tundra and wet tundra.

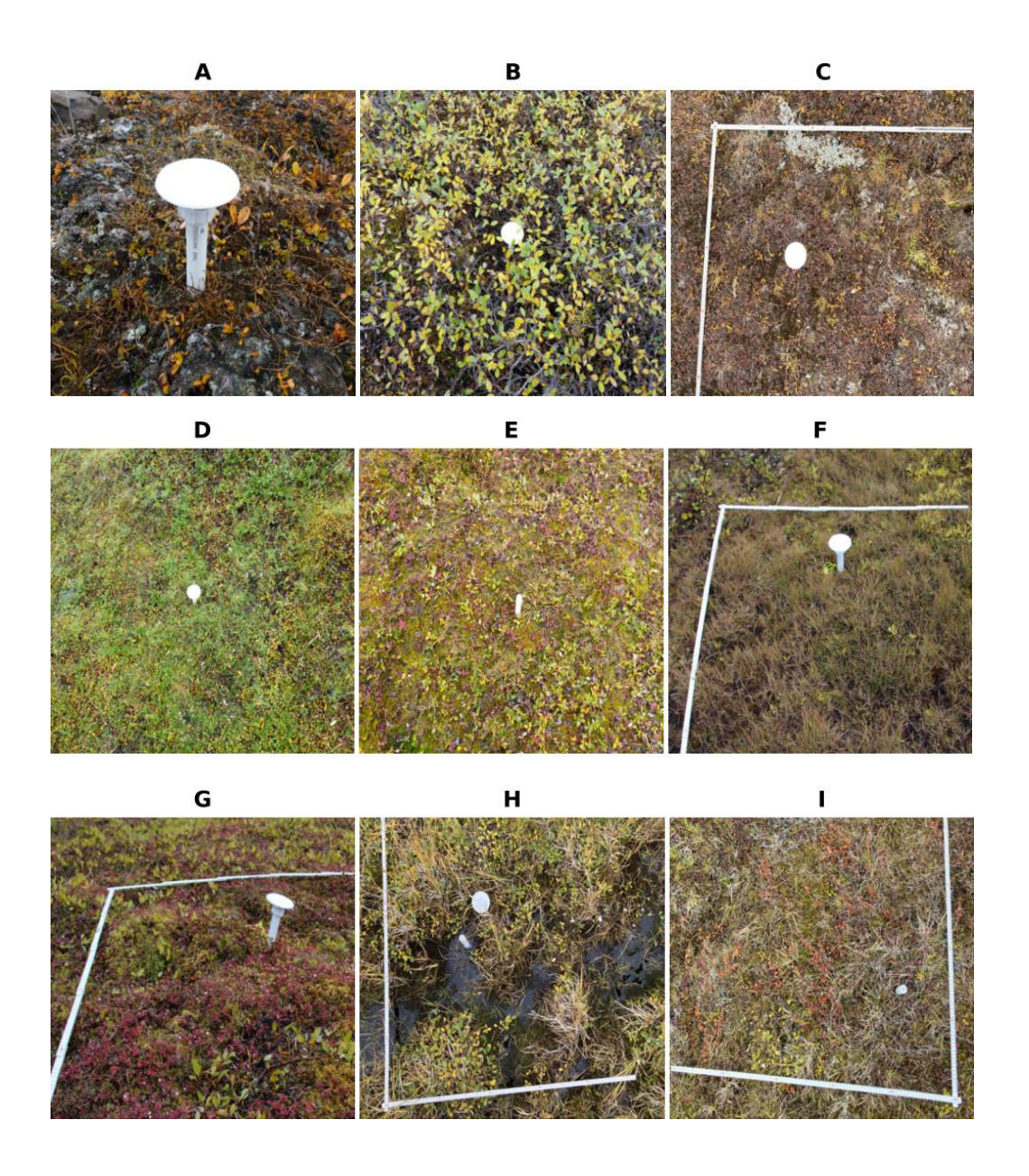


Figure A.5: TMS plots vegetation. TMS sensor locations (A–I) with site-specific vegetation. Photos taken by Simone Stuenzi and Jannika Gottuk in August 2022 and 2023.

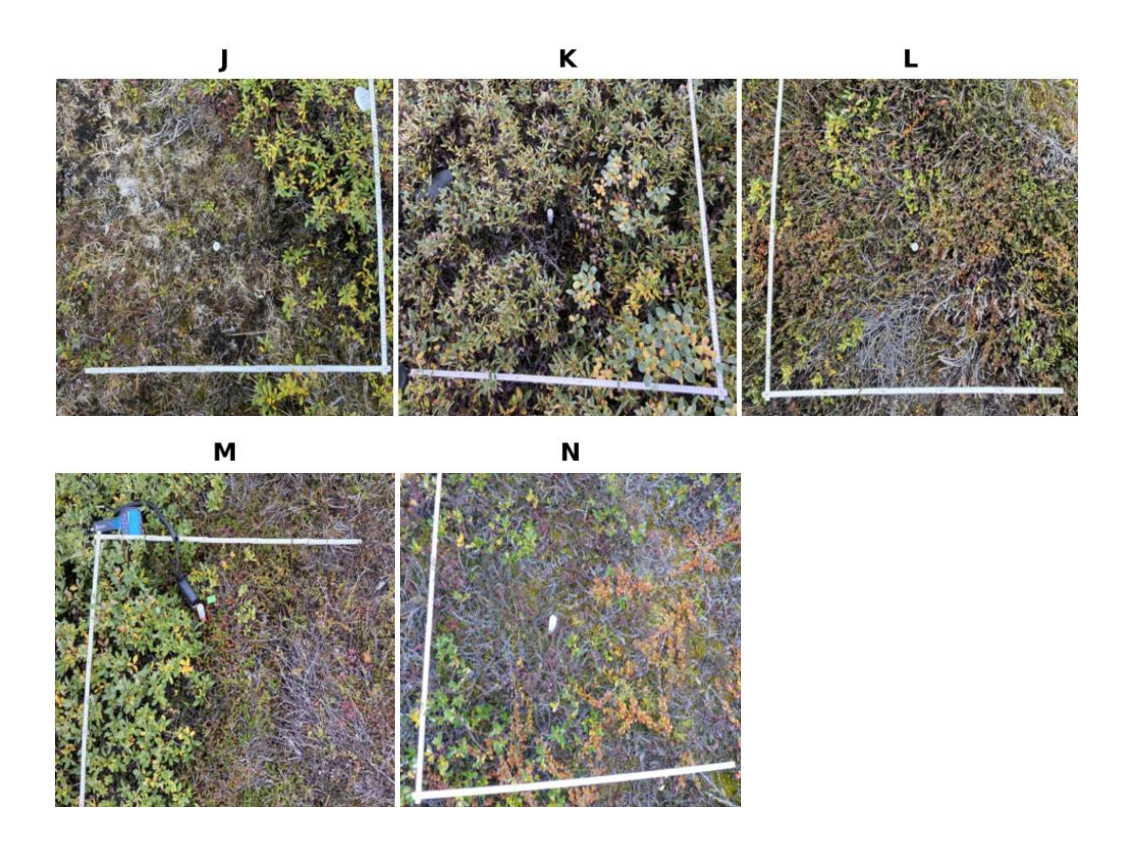


Figure A.6: TMS plots vegetation. TMS sensor locations (J-N) with site-specific vegetation. Photos taken by Simone Stuenzi and Jannika Gottuk in August 2022 and 2023.

A.2 Statistical analysis

I followed the Bayesian workflow outlined by Gelman et al. (2020), which includes model building, inference, model checking, and model comparison. I began by selecting an initial model. Bayesian models can be viewed as consisting of modules that are adjusted as necessary throughout the process. I incorporated prior information through both the prior distributions, ranging from non-informative to highly informative, and the likelihood function, which reflects assumptions about the data-generating process (Gelman et al. 2020). When using strongly informative priors or small datasets, the posterior distribution can be strongly dependent on the prior distribution. To ensure appropriate prior choices, I performed prior predictive checks and sensitivity analyses. Prior predictive checks display the data that is being simulated from the parameter values in the prior distribution. A sensitivity analysis investigates how much the posterior distribution changes when the prior is changed (Kruschke 2021).

After checking the prior predictive distribution, I fit the model using the No-U-Turn Sampler (NUTS), an efficient Markov Chain Monte Carlo (MCMC) algorithm implemented in PyMC (Hoffman and Gelman 2011). For this, the MCMC explores the parameter space randomly, tending to explore the high-probability regions more often than low-probability regions. The resulting sequence of samples formed Markov chains that, in the limit of infinite samples, approximated the posterior distribution. To ensure that the chains explored the parameter space sufficiently and thus generated a representative posterior distribution, I ran at least three chains and verified their convergence using the potential scale reduction factor (R). I also monitored the stability of the MCMC estimates by evaluating the effective sample size (ESS). For all key parameters, I ensured an ESS greater than 400, which indicates sufficient chain length and reliable estimation (Kruschke 2021). I used the Monte Carlo Standard Error (MCSE) to assess the precision of the parameter estimates. Low MCSE values indicate that the estimated means and standard deviations from the MCMC draws are stable. PyMC reports both the mean and standard deviation for each parameter, which helped to quantify uncertainty due to the finite number of posterior samples (Gelman et al. 2020).

Next, I performed posterior predictive checks by comparing simulated data from the posterior distributions to the actual observations (Gelman et al. 2020; Kruschke 2021). These checks helped me evaluate the model's fit to the data. After validating model fit, I reported the parameters by summarizing their central tendency and credible intervals (e.g., highest density intervals, HDI).

As recommended in the Bayesian workflow, I fit and compared several models to address the same problem. I concluded the process with model comparison, results reporting, and, where necessary, further model refinement or reassessment (Gelman et al. 2020).

Table A.4: Linear regression formulas and prior specifications

Model Formula	All Priors
snow_depth \sim slope + elevation + aspect	Intercept $\sim \text{Normal}(-0.69, 1.1)$ slope $\sim \text{Normal}(0, 0.4)$ elevation $\sim \text{Normal}(0, 20)$ aspect_sin $\sim \text{Normal}(0, 0.6)$ aspect_cos $\sim \text{Normal}(0, 0.5)$ alpha $\sim \text{HalfCauchy}(1.0)$
snow_depth $\sim 0 + (1$ —vegetation)	1—vegetation $\sim \text{Normal}(\sigma: \text{HalfNormal}(0.1))$ alpha $\sim \text{HalfNormal}(2.0)$
snow_depth \sim (1—geomorphon) + slope + elevation + aspect	Intercept \sim Normal(-0.693, 1.1) slope \sim Normal(0, 0.4) elevation \sim Normal(0, 10) aspect_sin \sim Normal(0, 0.6) aspect_cos \sim Normal(0, 0.5) 1—geomorphon \sim Normal(σ : HalfNormal(0.1)) alpha \sim HalfNormal(1.0)
snow_density \sim slope + elevation + aspect	Intercept $\sim \text{Normal}(0, 0.5)$ slope $\sim \text{Normal}(0, 0.15)$ elevation $\sim \text{Normal}(0, 3)$ aspect_sin $\sim \text{Normal}(0, 0.3)$ aspect_cos $\sim \text{Normal}(0, 0.3)$ kappa $\sim \text{HalfCauchy}(1.0)$
snow_density \sim (1—vegetation) + slope + elevation + aspect	Intercept $\sim \text{Normal}(0, 0.5)$ slope $\sim \text{Normal}(0, 0.15)$ elevation $\sim \text{Normal}(0, 3)$ aspect_sin $\sim \text{Normal}(0, 0.3)$ aspect_cos $\sim \text{Normal}(0, 0.3)$ 1—vegetation $\sim \text{Normal}(\sigma: \text{HalfNormal}(0.1))$ kappa $\sim \text{HalfCauchy}(1.0)$
snow_density \sim (1—geomorphon) + slope + elevation + aspect	Intercept \sim Normal(-0.8, 0.3) slope \sim Normal(0, 0.15) elevation \sim Normal(0, 3) aspect_sin \sim Normal(0, 0.3) aspect_cos \sim Normal(0, 0.3) 1—geomorphon \sim Normal(σ : HalfNormal(0.1)) kappa \sim HalfNormal(1.0)
T_snow \sim slope + elevation + aspect	Intercept $\sim \text{Normal}(-6.09, 2.0)$ slope $\sim \text{Normal}(0, 1.0)$ elevation $\sim \text{Normal}(0, 70)$ aspect_sin $\sim \text{Normal}(0, 0.5)$ aspect_cos $\sim \text{Normal}(0, 0.5)$ $\sigma \sim \text{HalfStudentT}(4.0, 1.20)$
T_snow \sim (1—vegetation) + slope + elevation + aspect	Intercept \sim Normal(-6.09, 2.0) slope \sim Normal(0, 1.0) elevation \sim Normal(0, 70) aspect_sin \sim Normal(0, 0.5) aspect_cos \sim Normal(0, 0.5) 1—vegetation \sim Normal(mu: 0.0, σ : HalfNormal(2.0)) $\sigma \sim$ HalfStudentT(4.0, 1.20)
T_snow \sim (1—geomorphon) + slope + elevation + aspect	Intercept \sim Normal(-6.09, 2.0) slope \sim Normal(0, 1.0) elevation \sim Normal(0, 70) aspect_sin \sim Normal(0, 0.5) aspect_cos \sim Normal(0, 0.5) 1—geomorphon \sim Normal(mu: 0.0, σ : HalfNormal(2.0)) $\sigma \sim$ HalfStudentT(4.0, 1.20)

Table A.5: Air-Soil Temperature model formulas and prior specifications. This table shows the structure and priors for the pooled model, which does not include group-level effects. In the vegetation and geomorphon models, additional varying intercepts are added to account for hierarchical structure, allowing either vegetation type or geomorphon class to influence the intercepts of the temperature models.

Level	Priors
$T_snow \sim \beta_{air} \cdot T_air$ $+ \beta_{depth} \cdot snow_depth_adj$ $+ \beta_{density_top} \cdot bulk_density_top$ $+ \beta_{aspect_cos} \cdot aspect_cos$ $+ \beta_{slope} \cdot slope_scaled$	$ \beta_{\text{air}} \sim \text{Normal}(0, 1) $ $ \beta_{\text{depth}} \sim \text{Normal}(0, 2) $ $ \beta_{\text{density_top}} \sim \text{Normal}(0, 10) $ $ \beta_{\text{aspect_cos}} \sim \text{Normal}(0, 1) $ $ \beta_{\text{slope}} \sim \text{Normal}(0, 1) $ $ \sigma_{\text{snow}} \sim \text{Exponential}(1.0) $
$T_surface \sim offset_surface \\ + \beta_{snow_to_surface} \cdot T_snow \\ + \beta_{density_bottom} \cdot bulk_density_bottom$	$ \beta_{\text{snow_to_surface}} \sim \text{Normal}(1, 0.5) $ $ \beta_{\text{density_bottom}} \sim \text{Normal}(0, 10) $ offset_surface $\sim \text{Normal}(0, 1)$ $ \sigma_{\text{surface}} \sim \text{Exponential}(1.0) $
$T_{soil} \sim offset_{soil} + \beta_{surface_{to_{soil}}} \cdot T_{surface}$	$ \beta_{\text{surface_to_soil}} \sim \text{Normal}(1, 0.5) $ offset_soil $\sim \text{Normal}(0, 1)$ $\sigma_{\text{soil}} \sim \text{Exponential}(1.0)$

Table A.6: Snow-Soil Temperature model formulas and prior specifications. This table shows the structure and priors for the pooled model, which does not include group-level effects. In the vegetation and geomorphon models, additional varying intercepts are added to account for hierarchical structure, allowing either vegetation type or geomorphon class to influence the intercepts of the temperature models.

Level	All Priors
$T_surface \sim offset_surface \\ + \beta_{snow \rightarrow surface} \cdot T_snow, obs \\ + \beta_{density_bottom} \cdot density_bottom$	$\beta_{\text{density_bottom}} \sim \text{Normal}(0, 10)$ $\beta_{\text{snow} \to \text{surface}} \sim \text{Normal}(1, 1)$ offset_surface $\sim \text{Normal}(0, 1)$
$T_{soil} \sim offset_{soil} + \beta_{surface \rightarrow soil} \cdot T_{surface}$	$\beta_{\text{surface} \to \text{soil}} \sim \text{Normal}(1, 1)$ offset_soil $\sim \text{Normal}(0, 1)$
Residual Standard Deviations:	$\sigma_{ m surface} \sim { m Exponential}(1.0)$ $\sigma_{ m soil} \sim { m Exponential}(1.0)$

B Extended results

In the following, I provide further information on my results including complementing figures of the study site, its meteorology, model set ups and tables of the model outputs.

B.1 Winter conditions

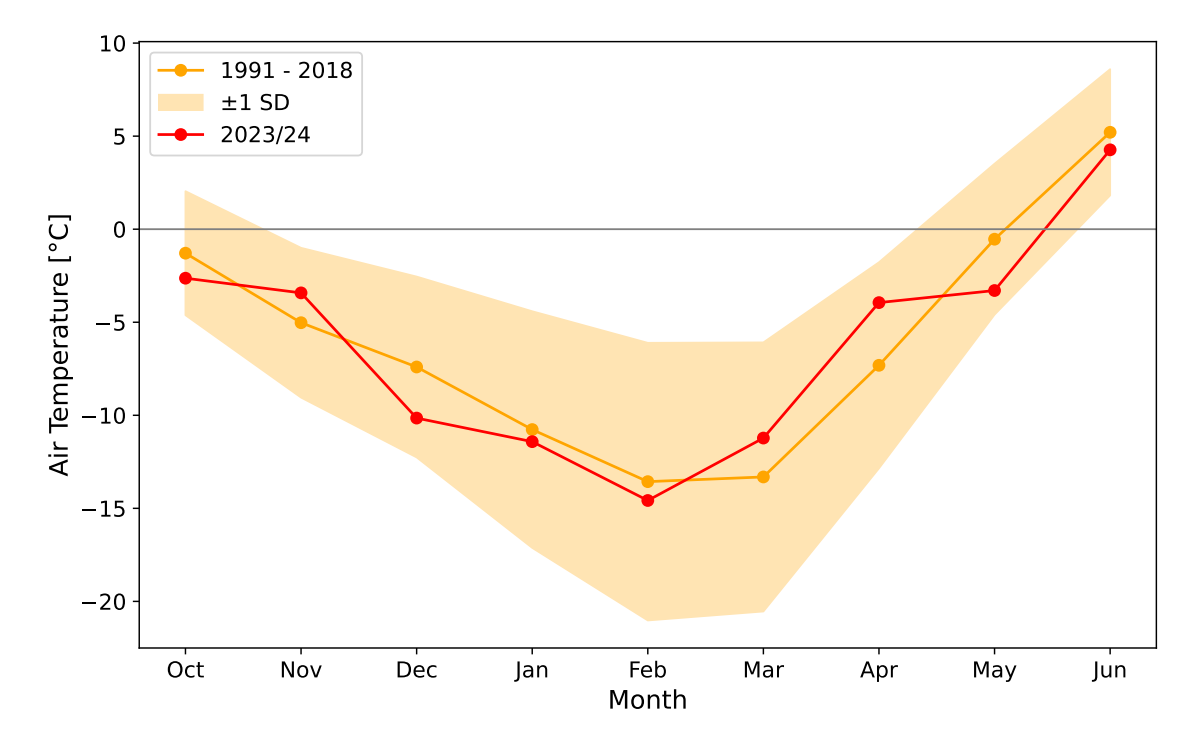


Figure A.7: Winter air temperatures. Monthly temperatures of winters from October to June between 1991 and 2018 (orange) and Winter 23/24 (red). Shaded areas represent the standard deviation of the long term averages.

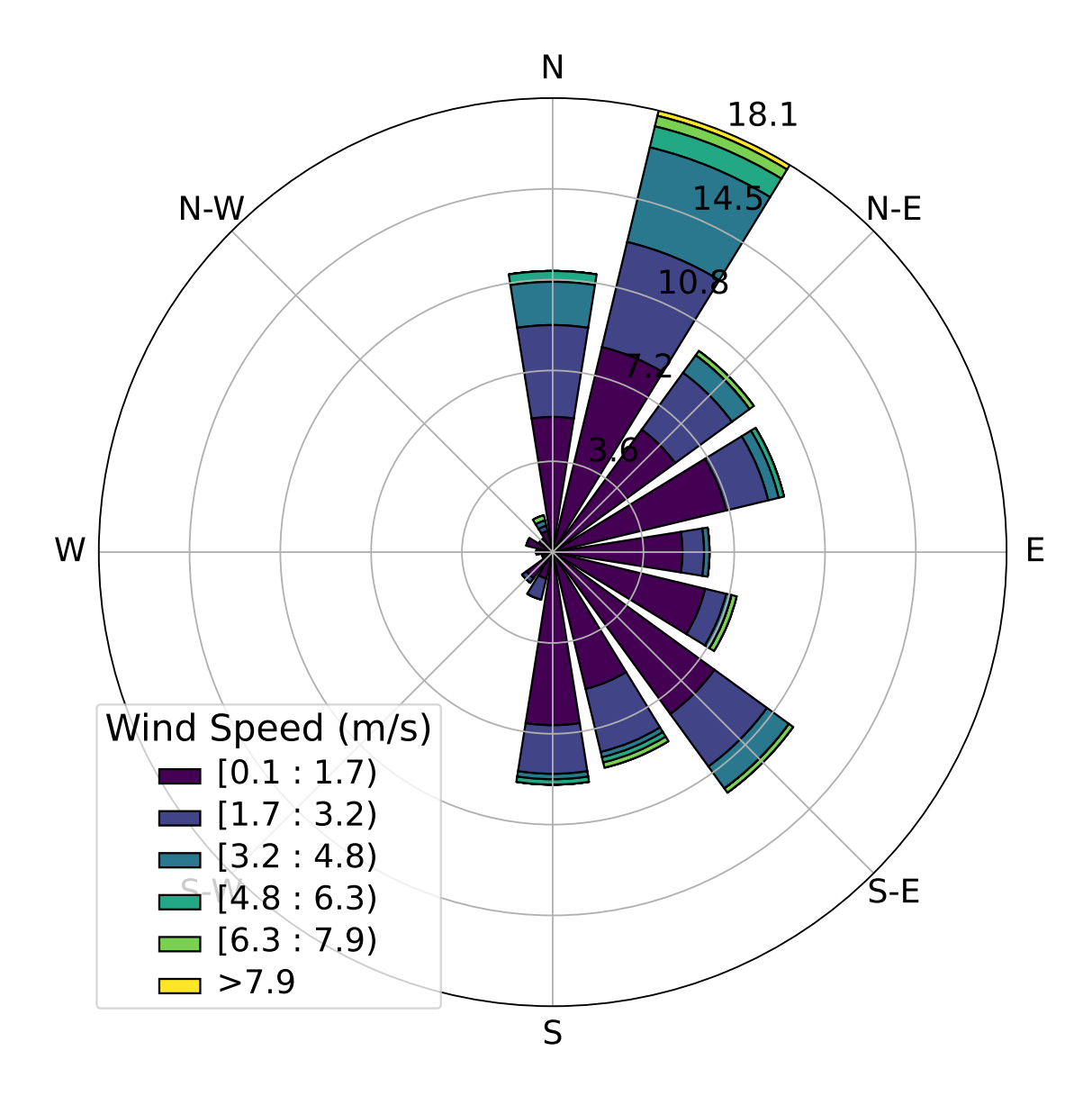


Figure A.8: Wind direction. Hourly wind direction derived from u and v wind components measured at AWS2 during the winter of 2023/2024.

B.2 Spatial variability

Table A.7: Snow depth and density measurements across sampling locations. Measurements including respective TMS, SMP profile, coordinates, snow depth, average snow density and standard deviation.

TMS SMP profile Lat Lon Depth (kg/m³) Avg Density SD Density A 1 69.27862568 -53.47877289 0.88 294 61 A 2 69.27862505 -53.47876705 0.87 289 77 A 3 69.27863077 -53.47872824 0.90 309 77 A 4 69.27863688 -53.47855965 0.81 330 91 A 5 69.2786502 -53.47855965 0.59 314 106 B 15 69.2786502 -53.47783208 0.60 304 113 B 16 69.2786562 -53.47781112 0.55 302 104 B 17 69.27865238 -53.4771072 0.61 285 73 C 25 69.27864073 -53.4771072 0.64 286 92 D 48 69.27856329 -53.47500329 1.09 332 89 D 49	Loc	ation	Coordinates		Snow properties		
A 1 69.27862568 -53.47877289 0.88 294 61 A 2 69.27862505 -53.47876705 0.87 289 77 A 3 69.27863077 -53.47872824 0.90 309 77 A 4 69.27863868 -53.47854655 0.81 330 91 A 5 69.27865622 -53.47783208 0.60 304 113 B 16 69.2786507 -53.47783208 0.60 304 113 B 16 69.2786523 -53.47778320 0.61 285 73 C 25 69.27865238 -53.47775932 0.61 285 73 C 25 69.27864004 -53.4771052 0.79 272 66 C 26 69.27862769 -53.4771072 0.64 286 92 D 48 69.27857632 -53.47493736 1.10 409 96 D 50 69.27857952	TMS	SMP	Lat	Lon	Depth	Avg Density	SD
A 2 69.27862505 -53.47876705 0.87 289 77 A 3 69.27863077 -53.47872824 0.90 309 77 A 4 69.27863868 -53.47864465 0.81 330 91 A 5 69.27862622 -53.47855965 0.59 314 106 B 15 69.2786507 -53.47783208 0.60 304 113 B 16 69.2786562 -53.47781112 0.55 302 104 B 17 69.27865238 -53.47775932 0.61 285 73 C 25 69.27864073 -53.47717692 0.79 300 77 C 26 69.27862769 -53.4771072 0.64 286 92 D 48 69.2786529 -53.47500329 1.09 332 89 D 49 69.27857068 -53.47500329 1.09 332 89 D 49 69.27857068 -53.47493736 1.10 409 96 D 50 69.27857068 -53.47493736 1.10 409 96 D 50 69.27859035 -53.4745002 1.09 316 57 D 53 69.27860308 -53.47452524 0.44 272 54 E 57 69.27862343 -53.474387 0.41 298 112 E 58 69.27862343 -53.474387 0.41 298 112 E 58 69.27862761 -53.47436199 0.17 247 155 E 59 69.27862455 -53.47431125 0.40 273 64 E 60 69.27864745 -53.47449362 0.48 272 87 F 68 69.26997184 -53.46994687 0.17 352 136 F 69 69.26997184 -53.4698467 0.24 312 67 G 110 69.27101946 -53.46847495 0.61 285 71 G 111 69.27103038 -53.46845644 0.51 291 93 G 112 69.27103622 -53.4684687 0.68 290 90 G 114 69.27104952 -53.46842689 0.49 292 66 G 115 69.2710545 -53.46841545 0.48 283 71 H 191 69.2676718 -53.46667398 0.60 290 94		profile			(m)	$({\rm kg/m^3})$	Density
A 3 69.27863077 -53.47872824 0.90 309 77 A 4 69.27863868 -53.47864465 0.81 330 91 A 5 69.27862622 -53.47855965 0.59 314 106 B 15 69.2786567 -53.47783208 0.60 304 113 B 16 69.2786562 -53.47781112 0.55 302 104 B 17 69.27865238 -53.47775932 0.61 285 73 C 25 69.27864073 -53.4771692 0.79 272 66 C 26 69.27864004 -53.47717692 0.79 300 77 C 27 69.27862769 -53.4771072 0.64 286 92 D 48 69.27856329 -53.47500329 1.09 332 89 D 49 69.27857068 -53.47493736 1.10 409 96 D 50 69.27857068 -53.4745092 1.09 316 57 D 52 69.27860308 -53.4745092 1.09 316 57 D 53 69.27860308 -53.47452524 0.44 272 54 E 57 69.27862343 -53.474387 0.41 298 112 E 58 69.27862343 -53.47436199 0.17 247 155 E 59 69.2786271 -53.47436199 0.17 247 155 E 59 69.27864745 -53.4743694 0.48 272 87 F 68 69.2698314 -53.4694687 0.17 352 136 F 69 69.26997184 -53.4694687 0.17 352 136 F 69 69.27101946 -53.46847495 0.61 285 71 G 111 69.27103038 -53.46845644 0.51 291 93 G 112 69.27105545 -53.4684467 0.68 290 90 G 114 69.27104952 -53.4684689 0.49 292 66 G 115 69.27105545 -53.46841545 0.48 283 71 H 191 69.2676718 -53.46847545 0.48 283 71 H 191 69.2676718 -53.46847545 0.48 283 71 H 191 69.2676718 -53.46867536 0.55 296 96 H 194 69.26769353 -53.46667398 0.60 290 94	A	1	69.27862568	-53.47877289	0.88	294	61
A 4 69.27863868 -53.47864465 0.81 330 91 A 5 69.27862622 -53.47855965 0.59 314 106 B 15 69.2786507 -53.47783208 0.60 304 113 B 16 69.2786502 -53.47781112 0.55 302 104 B 17 69.27865238 -53.47775932 0.61 285 73 C 25 69.27864073 -53.47710720 0.61 285 73 C 26 69.27864004 -53.4771072 0.64 286 92 D 48 69.27856329 -53.47500329 1.09 332 89 D 49 69.27857068 -53.47493736 1.10 409 96 D 50 69.27857952 -53.47481456 1.09 385 87 D 52 69.27860308 -53.4745902 1.09 316 57 D 53 69.27862343 -53.474387 0.41 298 112 E 59	A	2	69.27862505	-53.47876705	0.87	289	77
A 5 69.27862622 -53.47855965 0.59 314 106 B 15 69.2786507 -53.47783208 0.60 304 113 B 16 69.2786562 -53.47781112 0.55 302 104 B 17 69.27865238 -53.47775932 0.61 285 73 C 25 69.27864073 -53.47710726 0.79 272 66 C 26 69.27864004 -53.4771072 0.64 286 92 D 48 69.27856329 -53.47500329 1.09 332 89 D 49 69.27857068 -53.47493736 1.10 409 96 D 50 69.27857952 -53.47481456 1.09 385 87 D 52 69.27860308 -53.4745902 1.09 316 57 D 53 69.27862343 -53.474387 0.41 298 112 E 59 69.2786	A	3	69.27863077	-53.47872824	0.90	309	77
B 15 69.2786507 -53.47783208 0.60 304 113 B 16 69.2786562 -53.47781112 0.55 302 104 B 17 69.27865238 -53.47775932 0.61 285 73 C 25 69.27864073 -53.4772056 0.79 272 66 C 26 69.27864004 -53.4771072 0.64 286 92 D 48 69.27856329 -53.47500329 1.09 332 89 D 49 69.27857068 -53.47493736 1.10 409 96 D 50 69.27857068 -53.47481456 1.09 385 87 D 50 69.27857952 -53.4745902 1.09 316 57 D 53 69.27860308 -53.4745902 1.09 316 57 D 53 69.27862343 -53.474387 0.41 298 112 E 59 69.278624	A	4	69.27863868	-53.47864465	0.81	330	91
B 16 69.2786562 -53.47781112 0.55 302 104 B 17 69.27865238 -53.47775932 0.61 285 73 C 25 69.27864073 -53.4772056 0.79 272 66 C 26 69.27864004 -53.4771072 0.64 286 92 D 48 69.27856329 -53.47500329 1.09 332 89 D 49 69.27857068 -53.47493736 1.10 409 96 D 50 69.27857952 -53.47481456 1.09 385 87 D 52 69.27859035 -53.4745902 1.09 316 57 D 53 69.27860308 -53.4745902 1.09 316 57 D 53 69.27862343 -53.474387 0.41 298 112 E 57 69.27862571 -53.474387 0.41 298 112 E 59 69.2786474	A	5	69.27862622	-53.47855965	0.59	314	106
B 17 69.27865238 -53.47775932 0.61 285 73 C 25 69.27864073 -53.4772056 0.79 272 66 C 26 69.27864004 -53.4771072 0.64 286 92 D 48 69.27856329 -53.47500329 1.09 332 89 D 49 69.27857068 -53.47493736 1.10 409 96 D 50 69.27857952 -53.47481456 1.09 385 87 D 52 69.27859035 -53.4745902 1.09 316 57 D 53 69.27860308 -53.4745902 1.09 316 57 D 53 69.27862343 -53.474387 0.41 298 112 E 57 69.27862455 -53.47431125 0.40 273 64 E 59 69.27864745 -53.47431125 0.40 273 64 E 60 69.269931	В	15	69.2786507	-53.47783208	0.60	304	113
C 25 69.27864073 -53.4772056 0.79 272 66 C 26 69.27864004 -53.47717692 0.79 300 77 C 27 69.27862769 -53.4771072 0.64 286 92 D 48 69.27856329 -53.47500329 1.09 332 89 D 49 69.27857068 -53.47493736 1.10 409 96 D 50 69.27857952 -53.47449736 1.09 385 87 D 52 69.27859035 -53.4745902 1.09 316 57 D 53 69.27860308 -53.4745902 1.09 316 57 D 53 69.27862343 -53.474387 0.41 298 112 E 59 69.27862455 -53.47436199 0.17 247 155 E 59 69.27862455 -53.47431125 0.40 273 64 E 59 69.27864	В	16	69.2786562	-53.47781112	0.55	302	104
C 26 69.27864004 -53.47717692 0.79 300 77 C 27 69.27862769 -53.4771072 0.64 286 92 D 48 69.27856329 -53.47500329 1.09 332 89 D 49 69.27857068 -53.47493736 1.10 409 96 D 50 69.27857952 -53.47481456 1.09 385 87 D 52 69.27859035 -53.4745902 1.09 316 57 D 53 69.27860308 -53.4745902 1.09 316 57 D 53 69.27860308 -53.4745902 1.09 316 57 E 57 69.27862343 -53.474387 0.41 298 112 E 58 69.27862455 -53.474381125 0.40 273 64 E 59 69.27862455 -53.47431125 0.40 273 64 E 60 69.27864	В	17	69.27865238	-53.47775932	0.61	285	73
C 27 69.27862769 -53.4771072 0.64 286 92 D 48 69.27856329 -53.47500329 1.09 332 89 D 49 69.27857068 -53.47493736 1.10 409 96 D 50 69.27857952 -53.47481456 1.09 385 87 D 52 69.27859035 -53.4745902 1.09 316 57 D 53 69.27860308 -53.47452524 0.44 272 54 E 57 69.27862343 -53.474387 0.41 298 112 E 58 69.27862343 -53.47436199 0.17 247 155 E 59 69.27862455 -53.47431125 0.40 273 64 E 59 69.27864745 -53.47449362 0.48 272 87 F 68 69.26997184 -53.46994687 0.17 352 136 F 69 69.26	\overline{C}	25	69.27864073	-53.4772056	0.79	272	66
D 48 69.27856329 -53.47500329 1.09 332 89 D 49 69.27857068 -53.47493736 1.10 409 96 D 50 69.27857952 -53.47481456 1.09 385 87 D 52 69.27859035 -53.4745902 1.09 316 57 D 53 69.27860308 -53.47452524 0.44 272 54 E 57 69.27862343 -53.474387 0.41 298 112 E 58 69.27862571 -53.47436199 0.17 247 155 E 59 69.27862455 -53.47431125 0.40 273 64 E 60 69.27862455 -53.47449362 0.48 272 87 F 68 69.26998314 -53.46994687 0.17 352 136 F 69 69.26997184 -53.46988947 0.24 312 67 G 110 69.27103038 -53.46847495 0.61 285 71 G 112 </td <td>\mathbf{C}</td> <td>26</td> <td>69.27864004</td> <td>-53.47717692</td> <td>0.79</td> <td>300</td> <td>77</td>	\mathbf{C}	26	69.27864004	-53.47717692	0.79	300	77
D 49 69.27857068 -53.47493736 1.10 409 96 D 50 69.27857952 -53.47481456 1.09 385 87 D 52 69.27859035 -53.4745902 1.09 316 57 D 53 69.27860308 -53.47452524 0.44 272 54 E 57 69.27862343 -53.474387 0.41 298 112 E 58 69.27862571 -53.47436199 0.17 247 155 E 59 69.27862455 -53.47431125 0.40 273 64 E 60 69.27864745 -53.47449362 0.48 272 87 F 68 69.26998314 -53.46994687 0.17 352 136 F 69 69.26997184 -53.46988947 0.24 312 67 G 110 69.27103038 -53.46845644 0.51 291 93 G 112 69.27103622 -53.46845644 0.51 291 93 G 114<	\mathbf{C}	27	69.27862769	-53.4771072	0.64	286	92
D 50 69.27857952 -53.47481456 1.09 385 87 D 52 69.27859035 -53.4745902 1.09 316 57 D 53 69.27860308 -53.47452524 0.44 272 54 E 57 69.27862343 -53.474387 0.41 298 112 E 58 69.27862571 -53.47436199 0.17 247 155 E 59 69.27862455 -53.47431125 0.40 273 64 E 60 69.27864745 -53.47449362 0.48 272 87 F 68 69.26998314 -53.46994687 0.17 352 136 F 69 69.26997184 -53.46988947 0.24 312 67 G 110 69.27101946 -53.46847495 0.61 285 71 G 111 69.27103038 -53.4684644 0.51 291 93 G 112 69.27103622 -53.46846467 0.68 290 90 G 114<	D	48	69.27856329	-53.47500329	1.09	332	89
D 52 69.27859035 -53.4745902 1.09 316 57 D 53 69.27860308 -53.47452524 0.44 272 54 E 57 69.27862343 -53.474387 0.41 298 112 E 58 69.27862571 -53.47436199 0.17 247 155 E 59 69.27862455 -53.474431125 0.40 273 64 E 60 69.27864745 -53.47449362 0.48 272 87 F 68 69.26998314 -53.46994687 0.17 352 136 F 69 69.26997184 -53.46988947 0.24 312 67 G 110 69.27101946 -53.46847495 0.61 285 71 G 111 69.27103038 -53.46845644 0.51 291 93 G 112 69.27103622 -53.4684467 0.68 290 90 G 114 69.27104952 -53.46841545 0.48 283 71 H 19	D	49	69.27857068	-53.47493736	1.10	409	96
D 53 69.27860308 -53.47452524 0.44 272 54 E 57 69.27862343 -53.474387 0.41 298 112 E 58 69.27862571 -53.47436199 0.17 247 155 E 59 69.27862455 -53.47431125 0.40 273 64 E 60 69.27864745 -53.47449362 0.48 272 87 F 68 69.26998314 -53.46994687 0.17 352 136 F 69 69.26997184 -53.46988947 0.24 312 67 G 110 69.27101946 -53.46847495 0.61 285 71 G 111 69.27103038 -53.46845644 0.51 291 93 G 112 69.27103622 -53.4684467 0.68 290 90 G 114 69.27104952 -53.46842689 0.49 292 66 G 115 69.27105545 -53.466677536 0.55 296 96 H	D	50	69.27857952	-53.47481456	1.09	385	87
E 57 69.27862343 -53.474387 0.41 298 112 E 58 69.27862571 -53.47436199 0.17 247 155 E 59 69.27862455 -53.47431125 0.40 273 64 E 60 69.27864745 -53.47449362 0.48 272 87 F 68 69.26998314 -53.46994687 0.17 352 136 F 69 69.26997184 -53.46988947 0.24 312 67 G 110 69.27101946 -53.46847495 0.61 285 71 G 111 69.27103038 -53.46845644 0.51 291 93 G 112 69.27103622 -53.4684467 0.68 290 90 G 114 69.27104952 -53.46842689 0.49 292 66 G 115 69.27105545 -53.4687536 0.55 296 96 H 194 69.26769353 -53.46667398 0.60 290 94	D	52	69.27859035	-53.4745902	1.09	316	57
E 58 69.27862571 -53.47436199 0.17 247 155 E 59 69.27862455 -53.47431125 0.40 273 64 E 60 69.27864745 -53.47449362 0.48 272 87 F 68 69.26998314 -53.46994687 0.17 352 136 F 69 69.26997184 -53.46988947 0.24 312 67 G 110 69.27101946 -53.46847495 0.61 285 71 G 111 69.27103038 -53.46845644 0.51 291 93 G 112 69.27103622 -53.4684467 0.68 290 90 G 114 69.27104952 -53.46842689 0.49 292 66 G 115 69.27105545 -53.46841545 0.48 283 71 H 191 69.2676718 -53.46677536 0.55 296 96 H 194 69.26769353 -53.46667398 0.60 290 94	D	53	69.27860308	-53.47452524	0.44	272	54
E 59 69.27862455 -53.47431125 0.40 273 64 E 60 69.27864745 -53.47449362 0.48 272 87 F 68 69.26998314 -53.46994687 0.17 352 136 F 69 69.26997184 -53.46988947 0.24 312 67 G 110 69.27101946 -53.46847495 0.61 285 71 G 111 69.27103038 -53.46845644 0.51 291 93 G 112 69.27103622 -53.4684467 0.68 290 90 G 114 69.27104952 -53.46842689 0.49 292 66 G 115 69.27105545 -53.46841545 0.48 283 71 H 191 69.2676718 -53.46677536 0.55 296 96 H 194 69.26769353 -53.46667398 0.60 290 94	E	57	69.27862343	-53.474387	0.41	298	112
E 60 69.27864745 -53.47449362 0.48 272 87 F 68 69.26998314 -53.46994687 0.17 352 136 F 69 69.26997184 -53.46988947 0.24 312 67 G 110 69.27101946 -53.46847495 0.61 285 71 G 111 69.27103038 -53.46845644 0.51 291 93 G 112 69.27103622 -53.4684467 0.68 290 90 G 114 69.27104952 -53.46842689 0.49 292 66 G 115 69.27105545 -53.46841545 0.48 283 71 H 191 69.2676718 -53.46677536 0.55 296 96 H 194 69.26769353 -53.46667398 0.60 290 94	\mathbf{E}	58	69.27862571	-53.47436199	0.17	247	155
F 68 69.26998314 -53.46994687 0.17 352 136 F 69 69.26997184 -53.46988947 0.24 312 67 G 110 69.27101946 -53.46847495 0.61 285 71 G 111 69.27103038 -53.46845644 0.51 291 93 G 112 69.27103622 -53.4684467 0.68 290 90 G 114 69.27104952 -53.46842689 0.49 292 66 G 115 69.27105545 -53.46841545 0.48 283 71 H 191 69.2676718 -53.46677536 0.55 296 96 H 194 69.26769353 -53.46667398 0.60 290 94	\mathbf{E}	59	69.27862455	-53.47431125	0.40	273	64
F 69 69.26997184 -53.46988947 0.24 312 67 G 110 69.27101946 -53.46847495 0.61 285 71 G 111 69.27103038 -53.46845644 0.51 291 93 G 112 69.27103622 -53.4684467 0.68 290 90 G 114 69.27104952 -53.46842689 0.49 292 66 G 115 69.27105545 -53.46841545 0.48 283 71 H 191 69.2676718 -53.46677536 0.55 296 96 H 194 69.26769353 -53.46667398 0.60 290 94	\mathbf{E}	60	69.27864745	-53.47449362	0.48	272	87
G 110 69.27101946 -53.46847495 0.61 285 71 G 111 69.27103038 -53.46845644 0.51 291 93 G 112 69.27103622 -53.4684467 0.68 290 90 G 114 69.27104952 -53.46842689 0.49 292 66 G 115 69.27105545 -53.46841545 0.48 283 71 H 191 69.2676718 -53.46677536 0.55 296 96 H 194 69.26769353 -53.46667398 0.60 290 94	F	68	69.26998314	-53.46994687	0.17	352	136
G 111 69.27103038 -53.46845644 0.51 291 93 G 112 69.27103622 -53.4684467 0.68 290 90 G 114 69.27104952 -53.46842689 0.49 292 66 G 115 69.27105545 -53.46841545 0.48 283 71 H 191 69.2676718 -53.46677536 0.55 296 96 H 194 69.26769353 -53.46667398 0.60 290 94	F	69	69.26997184	-53.46988947	0.24	312	67
G 112 69.27103622 -53.4684467 0.68 290 90 G 114 69.27104952 -53.46842689 0.49 292 66 G 115 69.27105545 -53.46841545 0.48 283 71 H 191 69.2676718 -53.46677536 0.55 296 96 H 194 69.26769353 -53.46667398 0.60 290 94	G	110	69.27101946	-53.46847495	0.61	285	71
G 114 69.27104952 -53.46842689 0.49 292 66 G 115 69.27105545 -53.46841545 0.48 283 71 H 191 69.2676718 -53.46677536 0.55 296 96 H 194 69.26769353 -53.46667398 0.60 290 94	\mathbf{G}	111	69.27103038	-53.46845644	0.51	291	93
G 115 69.27105545 -53.46841545 0.48 283 71 H 191 69.2676718 -53.46677536 0.55 296 96 H 194 69.26769353 -53.46667398 0.60 290 94	G	112	69.27103622	-53.4684467	0.68	290	90
H 191 69.2676718 -53.46677536 0.55 296 96 H 194 69.26769353 -53.46667398 0.60 290 94	G	114	69.27104952	-53.46842689	0.49	292	66
H 194 69.26769353 -53.46667398 0.60 290 94	G	115	69.27105545	-53.46841545	0.48	283	71
	H	191	69.2676718	-53.46677536	0.55	296	96
H 195 69.26770514 -53.46664313 0.56 281 99	Η	194	69.26769353	-53.46667398	0.60	290	94
201	Η	195	69.26770514	-53.46664313	0.56	281	99

Continued on next page

Table A.7 continued from previous page

Loc	ation	Coord	dinates	Snow properties		
TMS	SMP	Lat Lon		Depth	Avg Density	SD
	profile			(m)	(kg/m^3)	Density
I	224	69.26790057	-53.46593019	0.49	318	115
I	225	69.26791663	-53.46589791	0.71	283	84
I	226	69.26794237	-53.46578396	0.84	284	69
J	204	69.26782024	-53.46624638	0.51	293	96
J	207	69.26784907	-53.46616708	0.55	275	88
J	208	69.26785983	-53.46613246	0.58	269	94
J	209	69.2678662	-53.46609865	0.49	268	86
J	210	69.2678685	-53.46607898	0.44	287	100
J	211	69.26786331	-53.46606759	0.54	302	96
J	212	69.2678543	-53.46604897	0.55	289	98
J	213	69.26784633	-53.46603139	0.42	278	95
J	214	69.26784172	-53.46601645	0.46	292	105
J	215	69.26783754	-53.46599636	0.40	299	85
J	216	69.26783234	-53.46598553	0.43	295	88
J	217	69.26782895	-53.46597267	0.35	323	101
K	234	69.26816819	-53.46488751	0.48	284	123
K	235	69.26820738	-53.46478164	0.66	298	124
K	236	69.26823673	-53.46465205	0.65	278	72
L	251	69.26877319	-53.46248167	0.46	288	59
${ m L}$	252	69.26876664	-53.46243988	0.56	297	77
L	253	69.26876051	-53.46240625	0.62	286	53
L	254	69.26875348	-53.46238008	0.66	304	93
L	257	69.26874112	-53.46229166	0.66	307	99
L	258	69.26873469	-53.46228772	0.41	314	89
M	246	69.26870657	-53.46274333	0.89	308	84
M	262	69.2686984	-53.4622556	0.21	274	100
M	263	69.26869444	-53.46224385	0.39	333	128
N	247	69.26874708	-53.46265237	0.60	302	63
N	248	69.26875731	-53.462611	0.55	295	67
N	249	69.26877667	-53.46257024	0.41	280	65

Table A.8: Soil temperature and snow properties for each TMS. Mean soil temperature from October 2023 to June 2024 per TMS, and snow properties averaged from surrounding SMP profiles conducted in April 2024.

TMS	Soil temperature (°C)	Snow	depth (m)	Snow d	ensity (kg/m ⁻³)
		Avg	SD	Avg	SD
A	-2.3	0.8	0.13	307	17
В	-1.2	0.6	0.03	297	10
\mathbf{C}	-1.7	0.7	0.09	286	14
D	-0.3	1.0	0.29	343	55
E	-3.7	0.4	0.14	272	21
F	-3.8	0.2	0.06	332	28
G	-2.3	0.6	0.09	288	4
Η	-0.5	0.6	0.03	289	8
Ι	-1.2	0.7	0.17	295	20
J	-1.9	0.5	0.07	289	16
K	-1.3	0.6	0.10	286	10
L	-1.6	0.6	0.11	299	11
M	-1.8	0.5	0.35	305	30
N	-2.1	0.5	0.10	292	11

B.3 Bayesian linear regression models

Table A.9: Posterior summary statistics of linear regression models on snow depth. Each subsection shows the posterior means, standard deviations (SD) and 94% highest density interval (HDI) for the pooled model, vegetation-group model, and geomorphon-group model. Monte Carlo standard errors (MCSE) for the mean and SD are omitted from this table because, for all parameters except alpha, elevation, and slope (where MCSE values are up to about 2% of the posterior SD), MCSE values are less than 1% of the corresponding posterior standard deviation. For the snow depth models, the mean ESS bulk and mean ESS tail are as follows: the pooled model has a mean ESS bulk of 3300 and a mean ESS tail of 2832; the vegetation-grouped model has a mean ESS bulk of 2158 and a mean ESS tail of 2557; and the geomorphon-grouped model has a mean ESS bulk of 3586 and a mean ESS tail of 2853. These values indicate strong sampling efficiency and reliable posterior estimates for all three models. \hat{R} is below 1.05 for all variables.

	Pooled model				
Parameter	Mean	SD	3% HDI	$97\%~\mathrm{HDI}$	
alpha	6.93	3.11	1.76	12.56	
Intercept	-0.04	1.15	-2.20	2.12	
slope	0.14	0.19	-0.23	0.51	
elevation	-6.92	12.74	-30.98	17.07	
$\mathtt{aspect_sin}$	-0.18	0.21	-0.58	0.22	
${\tt aspect_cos}$	0.04	0.18	-0.29	0.41	

Vegetation-group model Parameter Mean SD3% HDI 97% HDI alpha 2.90 0.911.41 4.70vegetation_sigma 0.110.070.000.24-0.10 -0.390.12 [dry tundra] 0.14[moist tundra] -0.0850.14-0.370.130.17

[wet tundra] -0.040.13 -0.33Geomorphon-group model

Parameter	Mean	SD	3% HDI	97% HDI
alpha	2.280	0.63	1.17	3.48
Intercept	-0.53	0.88	-2.23	1.12
slope	0.10	0.26	-0.37	0.61
elevation	-1.07	9.32	-18.04	17.14
$aspect_sin$	-0.12	0.31	-0.68	0.49
aspect_cos	0.07	0.25	-0.40	0.58
${\tt geomorphon_sigma}$	0.08	0.06	0.00	0.18
[hollow/footslope]	0.03	0.09	-0.17	0.21
[slope]	-0.012	0.093	-0.215	0.155
[valley/depression]	-0.01	0.10	-0.24	0.16

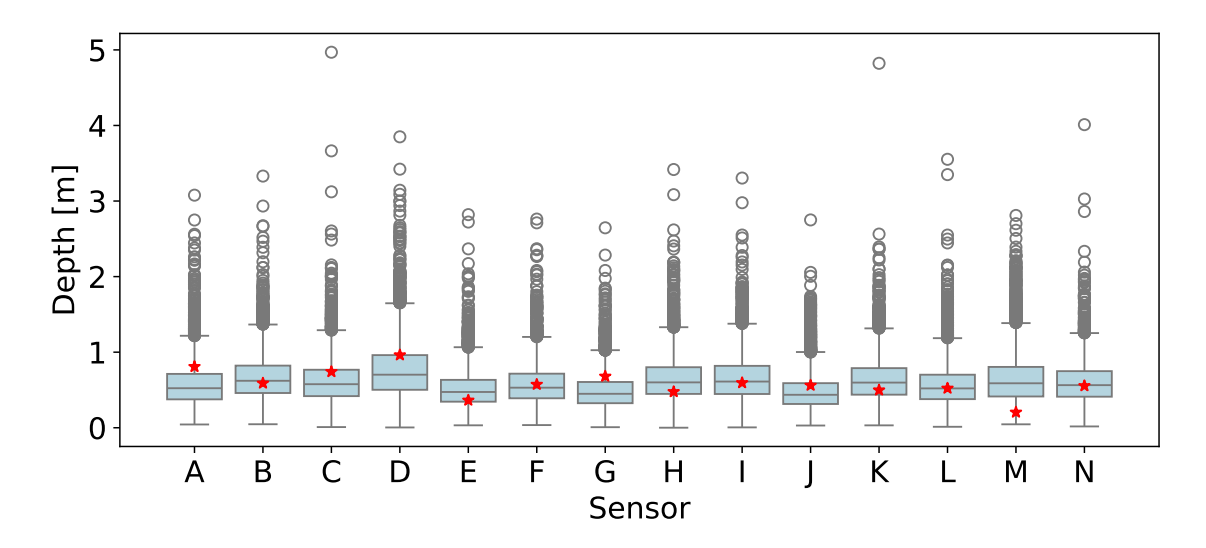


Figure A.9: Posterior predictive distributions for snow depth. Boxplots show the predicted distribution from the posterior predictive samples of the linear regression on snow depth across the TMS. Red stars indicate the observed values.

Table A.10: Posterior summary statistics of linear regression models on relative snow density. Each subsection shows the posterior means, standard deviations (SD) and 94% highest density interval (HDI) for the pooled model, vegetation-group model, and geomorphon-group model. MCSE (Mean) and MCSE (SD) columns are omitted as all values are below 1% of the posterior SD for all parameters except kappa (where they are about 2%). All reported ESS values for the pooled, vegetation-group, and geomorphon-group models are reliable, with mean ESS bulk values around 2631, 2296, and 4558 respectively, and mean ESS tail values around 2329, 1896, and 2973 respectively. \hat{R} is below 1.05 for all variables.

Daa	เกล	model
ГОО	ıecı	moder

Parameter	Mean	SD	3% HDI	97% HDI
kappa	939.08	466.23	195.03	1816.95
Intercept	-0.86	0.20	-1.26	-0.49
slope	0.10	0.04	0.03	0.19
elevation	-0.29	2.25	-4.45	4.02
$aspect_sin$	0.04	0.05	-0.05	0.12
aspect_cos	0.08	0.04	0.01	0.15

Vegetation-group model

Parameter	Mean	SD	$3\%~\mathrm{HDI}$	97% HDI
kappa	861.96	447.75	154.65	1692.93
Intercept	-0.87	0.21	-1.26	-0.46
slope	0.10	0.04	0.01	0.18
elevation	-0.14	2.34	-4.74	4.08
$aspect_sin$	0.04	0.05	-0.06	0.12
$aspect_cos$	0.08	0.04	-0.00	0.16
${\tt vegetation_sigma}$	0.04	0.04	0.00	0.11
[dry tundra]	-0.01	0.04	-0.10	0.05
[moist tundra]	-0.01	0.04	-0.08	0.08
[wet tundra]	-0.00	0.04	-0.09	0.08

${\bf Geomorphon\text{-}group\ model}$

Parameter	Mean	SD	3% HDI	97% HDI
kappa	2.88	0.65	1.68	4.12
Intercept	-0.71	0.38	-1.40	0.03
slope	0.01	0.15	-0.27	0.27
elevation	0.06	2.97	-5.67	5.47
$aspect_sin$	-0.00	0.26	-0.48	0.49
aspect_cos	0.03	0.24	-0.43	0.48
${\tt geomorphon_sigma}$	0.08	0.06	0.00	0.18
[hollow/footslope]	0.01	0.09	-0.16	0.20
[slope]	0.00	0.10	-0.19	0.20
[valley/depression]	0.00	0.10	-0.19	0.20

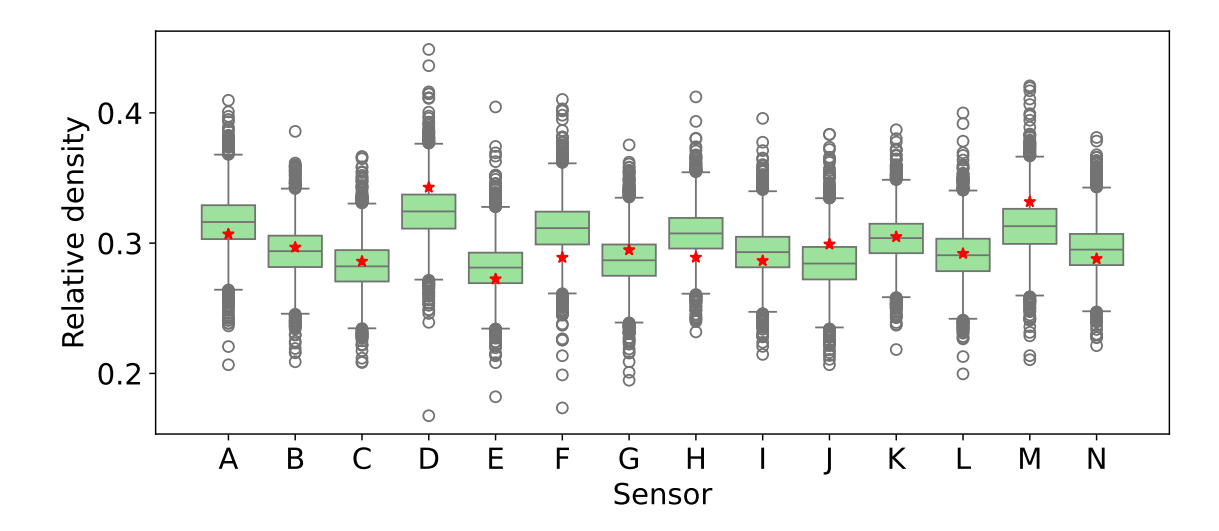


Figure A.10: Posterior predictive distributions for snow density. Boxplots show the predicted distribution from the posterior predictive samples of the pooled linear regression on snow density across the TMS. Red stars indicate the observed values.

Table A.11: Posterior summary statistics of linear regression models on snow temperature. Each subsection shows the posterior means, standard deviations (SD) and 94% highest density interval (HDI) for the pooled model, vegetation-group model, and geomorphon-group model. For most parameters, MCSE mean and SD values are below 4% of the corresponding posterior standard deviation. However, for the group-level parameters sigma, hollow/footslope, slope, valley/depression, and geomorphon_sigma in the geomorphon-group model, MCSE values reach up to 18% of SD, and ESS values are as low as 22, reflecting less precise posterior estimates for those parameters. The pooled model has a mean ESS bulk of 3711 and a mean ESS tail of 2848. The vegetation-group model has a mean ESS bulk of 1827 and a mean ESS tail of 1686. In contrast, the geomorphon-group model shows much lower sampling efficiency, with a mean ESS bulk of 727 and a mean ESS tail of 1036, mainly due to some parameters (sigma and geomorphon groups) with very low (22) ESS values. \hat{R} is below 1.05 for all variables.

Pooled model								
Parameter	Mean	SD	3% HDI	$97\%~\mathrm{HDI}$				
sigma	1.12	0.27	0.68	1.60				
Intercept	-1.16	3.34	-7.59	4.84				
slope	1.08	0.55	0.05	2.13				
elevation	-37.86	36.66	-105.94	31.41				
$aspect_sin$	-0.28	0.40	-1.01	0.49				
aspect cos	0.15	0.35	-0.50	0.83				

Vegetation-group model						
Parameter	Mean	SD	3% HDI	97% HDI		
sigma	1.04	0.26	0.62	1.53		
Intercept	-3.01	3.56	-9.46	3.95		
slope	0.97	0.52	-0.02	1.92		
elevation	-19.70	38.45	-91.52	52.69		
$aspect_sin$	-0.38	0.39	-1.09	0.38		
$aspect_cos$	0.08	0.35	-0.59	0.72		
${\tt vegetation_sigma}$	1.0	0.77	0.00	2.355		
[dry tundra]	-0.26	0.73	-1.79	1.04		
[moist tundra]	0.628	0.82	-0.73	2.24		
[wet tundra]	0.26	0.78	-1.10	1.90		

Parameter Mean SD 3% HDI 97% HDI sigma 1.05 0.28 0.57 1.53 Intercept -3.60 4.17 -10.90 4.30 slope 1.05 0.52 0.03 1.96 elevation -17.76 43.22 -101.70 59.45 aspect_sin -0.24 0.38 -0.97 0.46 aspect_cos 0.21 0.34 -0.43 0.86
Intercept -3.60 4.17 -10.90 4.30 slope 1.05 0.52 0.03 1.96 elevation -17.76 43.22 -101.70 59.45 aspect_sin -0.24 0.38 -0.97 0.46 aspect_cos 0.21 0.34 -0.43 0.86
slope 1.05 0.52 0.03 1.96 elevation -17.76 43.22 -101.70 59.45 aspect_sin -0.24 0.38 -0.97 0.46 aspect_cos 0.21 0.34 -0.43 0.86
elevation
aspect_sin
aspect_cos 0.21 0.34 -0.43 0.86
$\texttt{geomorphon_sigma} \qquad \qquad 1.06 \qquad 0.77 \qquad \qquad 0.00 \qquad \qquad 2.39$
$[\verb hollow/footslope] \qquad 0.84 \qquad 1.05 \qquad -0.33 \qquad \qquad 3.49$
[slope] $0.18 0.93 -1.46 2.12$
$[valley/depression] \qquad 0.03 \qquad 1.00 \qquad -1.81 \qquad \qquad 2.11$

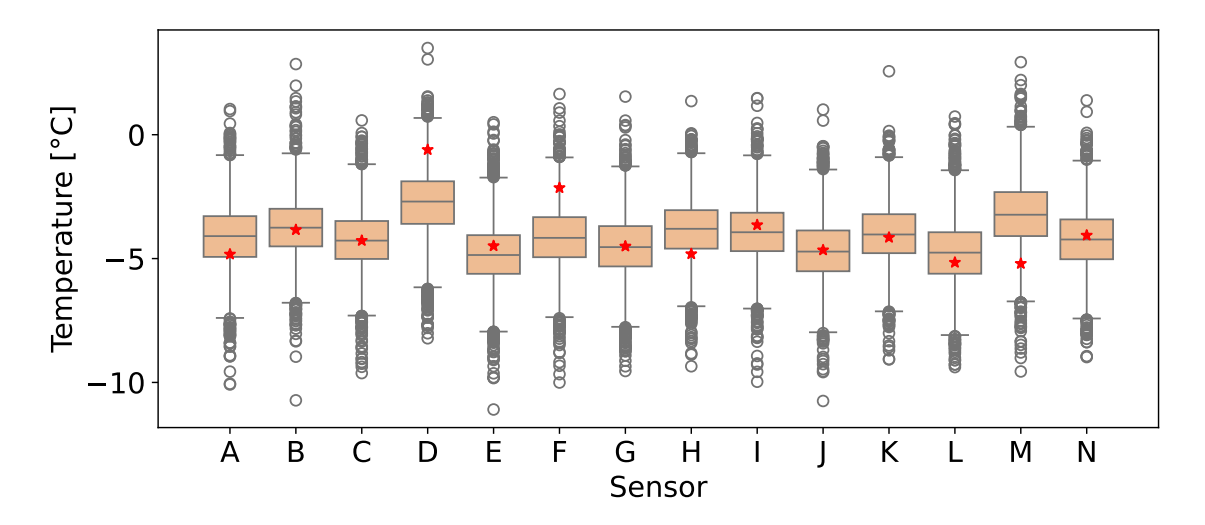


Figure A.11: Posterior predictive distributions for snow temperature. Boxplots show the predicted distribution from the posterior predictive samples of the pooled linear regression on snow temperature across the TMS. Red stars indicate the observed values.

B.4 Bayesian hierarchical models

Table A.12: Posterior summary statistics for Air-Soil Temperature model. Each subsection shows posterior means, standard deviations (SD), and 94% highest density intervals (HDI) for the pooled model, the vegetation-group model, and the geomorphon-group model. Monte Carlo standard errors (MCSE) are omitted because they are mostly below 1% of the posterior SD, except for two parameters (beta_density_top and beta_density_bottom) where MCSE is up to about 2% of the SD. Effective sample sizes (ESS) are greater than 2000, and \hat{R} is below 1.01 for all variables.

Pooled model						
Parameter	Mean	SD	3% HDI	97% HDI		
beta_air	0.65	0.31	0.11	1.26		
$beta_depth$	1.77	1.37	-0.93	4.21		
$beta_density_top$	-1.96	7.68	-16.45	12.48		
${\tt beta_density_bottom}$	3.98	3.53	-2.43	11.01		
beta_aspect_cos	0.37	0.47	-0.52	1.26		
beta_slope	0.82	0.53	-0.25	1.78		
${\tt beta_snow_to_surface}$	1.24	0.18	0.91	1.60		
beta_surface_to_soil	1.04	0.05	0.95	1.15		
$offset_surface$	0.24	0.91	-1.46	2.00		
$offset_soil$	0.20	0.21	-0.18	0.61		
$sigma_snow$	1.13	0.30	0.69	1.66		
$sigma_surface$	0.66	0.15	0.42	0.94		
sigma_soil	0.26	0.61	0.16	0.36		

Vegetation-group model						
Parameter	Mean	SD	3% HDI	97% HDI		
beta_air	0.50	0.29	-0.04	1.04		
beta_depth	2.69	1.22	0.34	4.89		
${\tt beta_density_top}$	-6.65	7.13	-20.14	6.70		
${\tt beta_density_bottom}$	4.32	3.77	-2.72	11.53		
beta_aspect_cos	0.24	0.38	-0.48	0.93		
beta_slope	1.00	0.42	0.15	1.72		
${\tt beta_snow_to_surface}$	1.27	0.20	0.91	1.65		
$beta_surface_to_soil$	1.05	0.05	0.94	1.14		
$offset_surface$	0.25	0.95	-1.45	2.05		
$offset_soil$	0.21	0.21	-0.18	0.61		
$sigma_snow$	0.80	0.25	0.42	1.23		
$sigma_surface$	0.66	0.15	0.42	0.92		
$sigma_soil$	0.26	0.06	0.16	0.37		
[dry tundra]	-0.78	0.67	-1.99	0.50		
[wet tundra]	0.57	0.68	-0.69	1.85		
[moist tundra]	0.08	0.70	-1.26	1.33		

Parameter	Mean	SD	3% HDI	97% HDI
beta_air	0.58	0.32	-0.04	1.19
$beta_depth$	0.94	1.51	-1.74	3.87
$beta_density_top$	-3.23	7.92	-18.78	11.08
$\verb beta_density_bottom $	4.40	3.75	-2.42	11.44
beta_aspect_cos	0.44	0.46	-0.40	1.29
beta_slope	1.02	0.54	0.07	2.07
beta_snow_to_surface	1.27	0.20	0.89	1.65
beta_surface_to_soil	1.04	0.05	0.95	1.15
$offset_surface$	0.24	0.94	-1.58	1.92
offset_soil	0.20	0.21	-0.19	0.60
sigma_snow	1.08	0.29	0.64	1.62
$sigma_surface$	0.66	0.15	0.42	0.93
$sigma_soil$	0.25	0.06	0.15	0.36
[hollow/footslope]	0.48	0.74	-0.90	1.87
[slope]	-0.30	0.72	-1.57	1.12
[valley/depression]	-0.25	0.87	-1.89	1.30

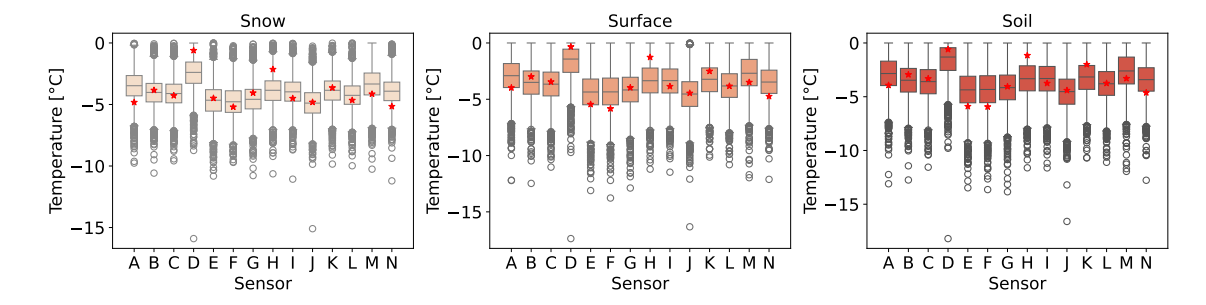


Figure A.12: Posterior predictive distributions for TMS temperatures. Boxplots show the distribution of posterior predictions of the pooled hierarchical Air-Soil Temperature Model for snow, surface, and soil temperatures across the TMS. Red stars indicate observed temperature values.

Table A.13: Posterior summary statistics for Snow-Soil Temperature model. Each subsection shows posterior means, standard deviations (SD) and 94% highest density intervals (HDI) for the pooled model, the vegetation-group model, and the geomorphon-group model. Monte Carlo standard errors (MCSE) for the mean and SD w are less than 1% of the corresponding posterior standard deviation. Effective sample sizes (ESS, bulk and tail) are always greater than 1700, and \hat{R} is below 1.01 for all variables.

Pooled	mod	lel
--------	-----	----------------------

Parameter	Mean	SD	3% HDI	97% HDI
beta_density_bottom	4.36	3.78	-2.61	11.55
$offset_surface$	0.25	0.94	-1.49	2.02
beta_snow_to_surface	1.27	0.20	0.90	1.63
$offset_soil$	0.20	0.21	-0.17	0.60
beta_surface_to_soil	1.04	0.05	0.94	1.14
$sigma_surface$	0.65	0.14	0.43	0.92
$sigma_soil$	0.25	0.06	0.16	0.36

Vegetation-group model

Parameter	Mean	SD	3% HDI	97% HDI
beta_density_bottom	5.16	4.29	-2.32	13.39
$offset_surface$	0.20	0.95	-1.59	1.90
beta_snow_to_surface	1.34	0.24	0.91	1.82
$offset_soil$	0.20	0.20	-0.17	0.58
beta_surface_to_soil	1.04	0.05	0.94	1.13
sigma_surface	0.70	0.18	0.42	1.02
sigma_soil	0.25	0.06	0.16	0.36
[dry tundra]	0.24	0.63	-0.97	1.40
[wet tundra]	-0.04	0.65	-1.21	1.22
[moist tundra]	0.00	0.66	-1.22	1.21

${\bf Geomorphon\text{-}group\ model}$

Parameter	Mean	SD	3% HDI	97% HDI
beta_density_bottom	3.51	4.02	-3.94	11.13
offset_surface	0.00	0.97	-1.76	1.86
beta_snow_to_surface	1.20	0.21	0.81	1.58
$offset_soil$	0.20	0.21	-0.19	0.57
beta_surface_to_soil	1.04	0.05	0.95	1.14
$sigma_surface$	0.63	0.16	0.37	0.91
sigma_soil	0.25	0.06	0.16	0.37
[hollow/footslope]	0.36	0.61	-0.79	1.52
[slope]	0.21	0.62	-0.95	1.35
[valley/depression]	-0.56	0.72	-1.87	0.83

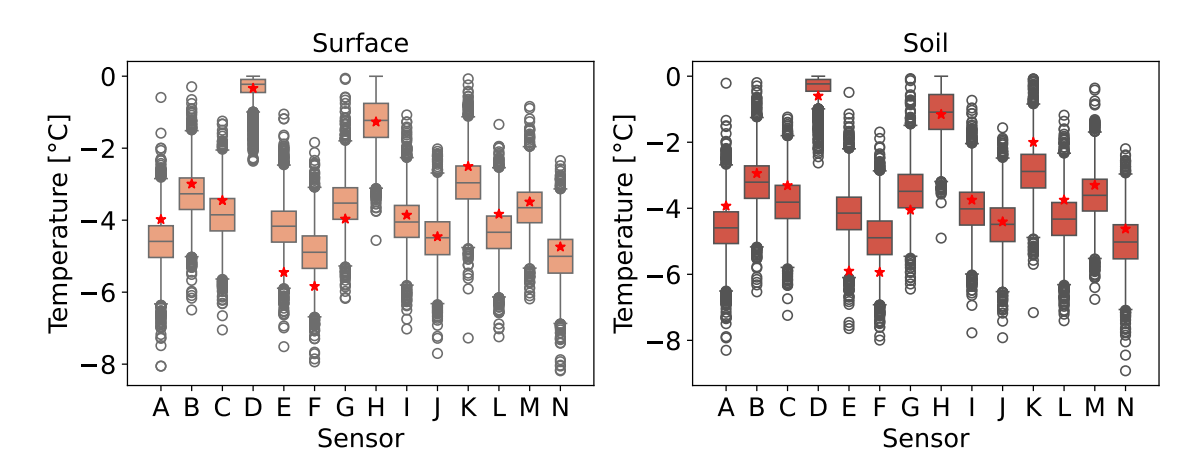


Figure A.13: Posterior predictive distributions for TMS temperatures. Boxplots show the distribution of posterior predictions of the pooled hierarchical Snow-Soil Temperature Model for surface (left), and soil temperatures (right) across the TMS. Red stars indicate observed temperature values.

Declaration

I hereby declare that I have not submitted this thesis, or any part of it, for any other examination or academic purpose. I affirm that I have completed the work independently, using only the sources and tools listed. All online sources, graphics, tables, and images that I have used are clearly identified as such. I confirm that I have worked independently throughout the preparation of this thesis. I am aware that violations of these principles will be treated as attempted or actual deception.

I further assure that I have fully documented the use of artificial intelligence tools in the preparation of this work (see table below). I am solely responsible for the inclusion of any machine-generated text, code, or suggestions. I acknowledge that I bear full responsibility for any inaccuracies, distorted content, incorrect references, or violations of copyright and data protection laws arising from the use of such tools. I also affirm that my own creative input and academic judgment are the predominant contributions to this thesis.

AI Tool	Type of use	Affected work	Comments
ChatGPT, Gemini	Code generation in Python	Data analysis and modeling	Used for coding help and debugging
Perplexity	Literature re- search	Literature review and general research process	Used for finding sources and clarifying topics
ChatGPT	LaTeX formatting	Tables in Overleaf	Used to generate LaTeX table syntax
ChatGPT	Explanation of Brian's feedback	Bayesian Modeling	Used to understand his input
ChatGPT	Restructuring and reformulating text	Text	Assisted with improving narrative flow